

Fusion hierarchies, T -systems and Y -systems of logarithmic minimal models

February 28, 2022

Alexi Morin-Duchesne*, Paul A. Pearce†, Jørgen Rasmussen*

**School of Mathematics and Physics, University of Queensland
St Lucia, Brisbane, Queensland 4072, Australia*

*†Department of Mathematics and Statistics, University of Melbourne
Parkville, Victoria 3010, Australia*

alexi.morin.duchesne@gmail.com p.pearce@ms.unimelb.edu.au j.rasmussen@uq.edu.au

Abstract

A Temperley-Lieb (TL) loop model is a Yang-Baxter integrable lattice model with nonlocal degrees of freedom. On a strip of width $N \in \mathbb{N}$, the evolution operator is the double-row transfer tangle $\mathbf{D}(u)$, an element of the TL algebra $TL_N(\beta)$ with loop fugacity $\beta = 2 \cos \lambda$, $\lambda \in \mathbb{R}$. Similarly on a cylinder, the single-row transfer tangle $\mathbf{T}(u)$ is an element of the so-called enlarged periodic TL algebra. The logarithmic minimal models $\mathcal{LM}(p, p')$ comprise a subfamily of the TL loop models for which the crossing parameter $\lambda = (p' - p)\pi/p'$ is a rational multiple of π parameterised by coprime integers $1 \leq p < p'$. For these special values, additional symmetries allow for particular degeneracies in the spectra that account for the logarithmic nature of these theories. For critical dense polymers $\mathcal{LM}(1, 2)$, with $\beta = 0$, $\mathbf{D}(u)$ and $\mathbf{T}(u)$ satisfy inversion identities that have led to the exact determination of the eigenvalues in any representation and for arbitrary finite system size N . The generalisation for $p' > 2$ takes the form of functional relations for $\mathbf{D}(u)$ and $\mathbf{T}(u)$ of polynomial degree p' . These derive from fusion hierarchies of commuting transfer tangles $\mathbf{D}^{m,n}(u)$ and $\mathbf{T}^{m,n}(u)$ where $\mathbf{D}(u) = \mathbf{D}^{1,1}(u)$ and $\mathbf{T}(u) = \mathbf{T}^{1,1}(u)$. The fused transfer tangles are constructed from (m, n) -fused face operators involving Wenzl-Jones projectors P_k on $k = m$ or $k = n$ nodes. Some projectors P_k are singular for $k \geq p'$, but we argue that $\mathbf{D}^{m,n}(u)$ and $\mathbf{T}^{m,n}(u)$ are nonsingular for every $m, n \in \mathbb{N}$ in certain cabled link state representations. For generic λ , we derive the fusion hierarchies and the associated T - and Y -systems. For the logarithmic theories, the closure of the fusion hierarchies at $n = p'$ translates into functional relations of polynomial degree p' for $\mathbf{D}^{m,1}(u)$ and $\mathbf{T}^{m,1}(u)$. We also derive the closure of the Y -systems for the logarithmic theories. The T - and Y -systems are the key to exact integrability and we observe that the underlying structure of these functional equations relate to Dynkin diagrams of affine Lie algebras.

Contents

1	Introduction	3
1.1	Notation	6
2	Temperley-Lieb loop models	6
3	Fused Temperley-Lieb loop models	14
3.1	Fused face operators	14
3.2	Yang-Baxter equations	16
3.3	Crossing symmetry	17
4	Transfer tangles	18
4.1	Fused transfer tangles for generic λ	18
4.2	Effective projectors and fused transfer tangles for fractional λ	20
4.3	Braid transfer tangles	22
5	Matrix representations	23
6	Fusion hierarchies and T- and Y-systems	27
6.1	Fusion hierarchy on the strip	27
6.2	Fusion hierarchy on the cylinder	28
6.3	T -systems	28
6.4	Y -systems	29
7	Functional relations in logarithmic minimal models	30
7.1	Closure of the fusion hierarchy on the strip	30
7.2	Closure of the fusion hierarchy on the cylinder	33
7.3	Closure of the Y -systems	35
8	Comparison with rational models	37
9	Conclusion	38
A	Decomposition of fused face operators	39
B	Boundary Yang-Baxter equations for fused face operators	41
C	Effective projectors	43
D	Cabled link states and lattice paths	45
E	Fusion hierarchies	48
E.1	On the strip	48
E.2	On the cylinder	53
F	Closure of the fusion hierarchies	54
F.1	Preliminaries	54
F.2	On the strip	56
F.3	On the cylinder	71

1 Introduction

The logarithmic minimal models $\mathcal{LM}(p, p')$ [1], where p, p' are coprime integers, are a family of Yang-Baxter integrable models built on the square lattice using the planar Temperley-Lieb (TL) algebra [2, 3]. These models are loop models that admit nonlocal degrees of freedom in the form of polymers or connectivities. The first members of this series include critical dense polymers $\mathcal{LM}(1, 2)$ [4–7] and critical (bond) percolation $\mathcal{LM}(2, 3)$ [8]. The motivation for introducing these models was (i) to initiate a lattice approach to the study of logarithmic Conformal Field Theory (CFT) from the continuum scaling limit of a Yang-Baxter integrable model, and (ii) to demonstrate that the Jordan blocks associated with reducible yet indecomposable representations of these theories are accessible through finite-size lattice calculations. The *logarithmic* minimal models are the simplest family of logarithmic CFTs (without extended symmetries) and are expected to play the same role for logarithmic CFTs that the *rational* minimal models [9] play for rational CFTs. Recent reviews on logarithmic CFT can be found in [10].

Although logarithmic minimal models are not rational and not unitary, they have many similarities with the rational minimal models $\mathcal{M}(m, m')$ where m, m' are coprime integers. The rational minimal models are realised as the continuum scaling limit of the Yang-Baxter integrable Restricted-Solid-on-Solid (RSOS) lattice models [11, 12]. For the *unitary* minimal models $\mathcal{M}(m, m+1)$ [11], a fusion hierarchy of functional equations satisfied by the periodic single-row transfer matrices of the level $n \in \mathbb{N}$ fused RSOS models $\mathcal{M}(m, m+1)_{n \times n}$ was obtained by Bazhanov and Reshetikhin [13]. Working within a lattice approach, it was shown, by Klümper and Pearce [14–16] and in subsequent work, that T - and Y -systems are the key to the analytic solution of these theories. The T -system is solved for the *non-universal* properties of the statistical system such as bulk free energies [17], boundary and seam free energies [18] and correlation lengths [19]. The Y -system is solved, in the continuum scaling limit, for the *universal* conformal quantities such as central charges, conformal dimensions and characters.

To put T - and Y -systems into historical perspective, it was in the context of the $su(2)$ unitary minimal models [14–16] that the first T -system appeared allowing the associated Y -system and non-linear integral equations to be systematically derived and solved for all excitations. For integrable quantum systems, the T -systems take the form of discrete classical bilinear Hirota equations [20]. The first Y -systems appeared earlier in the work of Zamolodchikov [21, 22] in relation to thermodynamic Bethe ansatz equations for massive scattering theories. T - and Y -systems for theories associated with Lie algebras other than $su(2)$ were obtained in [23–26]. T - and Y -systems appear in many contexts. Recently, they have been used to study integrable aspects of the AdS/CFT correspondence. A general review article on T - and Y -systems appears in [27]. Historically, T - and Y -systems were first obtained for periodic single-row transfer matrices $\mathbf{T}^{m,n}(u)$. Later it was realised, at least for rational CFTs, that Y -systems are *universal* [28] in the sense that precisely the same Y -system of equations holds for all topologies and all boundary conditions. This *miracle*, the fact that you are solving the same equations, explains why the same central charge and the same set of conformal weights appear in each topology with various boundary conditions. For unitary minimal models on the strip in the presence of boundary conditions, the T - and Y -systems were obtained [29] by working with double-row transfer matrices $\mathbf{D}^{m,n}(u)$. In the case of the tricritical Ising model on the strip, the functional equations have been solved [30] for all conformal boundary conditions and all excitations, underscoring the power of these methods.

The fused minimal models $\mathcal{M}(m, m')_{n \times n}$ have a long history of being described, as CFTs, by models $\mathcal{M}(M, M'; n)$ admitting diagonal GKO coset descriptions [31–33], where $M = M(m, m')$ and $M' = M'(m, m')$ are integers satisfying $2 \leq M < M'$. It has recently been argued [34] that general logarithmic minimal models at higher fusion level can similarly be described as diagonal $su(2)$ GKO cosets

$$\mathcal{LM}(P, P'; n) \simeq \text{COSET}\left(\frac{nP}{P'-P} - 2, n\right), \quad \gcd\left(P, \frac{P'-P}{n}\right) = 1, \quad 1 \leq P < P', \quad n, P, P' \in \mathbb{N} \quad (1.1)$$

where n is the integer fusion level. The diagonal GKO coset [31–33] takes the form

$$\text{COSET}(k, n) : \frac{(A_1^{(1)})_k \oplus (A_1^{(1)})_n}{(A_1^{(1)})_{k+n}}, \quad k = \frac{\hat{p}}{\hat{p}'} - 2, \quad \gcd(\hat{p}, \hat{p}') = 1, \quad n, \hat{p}, \hat{p}' \in \mathbb{N} \quad (1.2)$$

where k is a fractional fusion level and the subscripts on the affine $su(2)$ current algebra $A_1^{(1)}$ denote the respective levels k , n and $k + n$. The central charges of the logarithmic minimal models $\mathcal{LM}(P, P'; n)$ are

$$c^{P, P'; n} = \frac{3n}{n+2} \left[1 - \frac{2(n+2)(P' - P)^2}{n^2 P P'} \right]. \quad (1.3)$$

In [1], the non-fused lattice loop model $\mathcal{LM}(p, p')_{1 \times 1}$ and the corresponding CFT $\mathcal{LM}(P, P'; 1)$ were studied and both referred to as the logarithmic minimal model $\mathcal{LM}(p, p')$. To emphasise the strong relation between the lattice model and the corresponding CFT, here we write

$$\mathcal{LM}(p, p')_{1 \times 1} \equiv \mathcal{LM}(P, P'; 1), \quad P = p, \quad P' = p'. \quad (1.4)$$

For $n > 1$, it has been conjectured in [35] that the theories $\mathcal{LM}(P, P'; n)$ are realised on the lattice by $n \times n$ fusions built from the elementary logarithmic minimal models $\mathcal{LM}(p, p')$, that is

$$\mathcal{LM}(p, p')_{n \times n} \equiv \mathcal{LM}(P, P'; n) \quad (1.5)$$

for some $P = P(p, p')$, $P' = P'(p, p')$. In particular, for $n = 2$, the theories are logarithmic superconformal field theories [35]

$$\mathcal{LM}(p, p')_{2 \times 2} \equiv \mathcal{LM}(P, P'; 2), \quad P = |2p - p'|, \quad P' = p' \quad (1.6)$$

also denoted by $\mathcal{LSM}(p, p')$. The first members of the superconformal series include superconformal dense polymers $\mathcal{LSM}(2, 3)$ and superconformal percolation $\mathcal{LSM}(3, 4)$ which are lattice models that are expected to be of independent interest in statistical mechanics. At present, it is not known what relation between P, P' and p, p' is required to make the identification (1.5) valid in general. This is also the case for the fused minimal models.

According to [34], the coset construction of the general logarithmic minimal models $\mathcal{LM}(P, P'; n)$ is completely analogous to the coset construction of the rational minimal models $\mathcal{M}(M, M'; n)$, but based on more complicated representation theories. Furthermore, the chiral logarithmic minimal models can be described [34] as the logarithmic limit [36, 37] of the rational minimal models

$$\mathcal{LM}(P, P'; n) = \lim_{\substack{M, M' \rightarrow \infty \\ M/M' \rightarrow P/P'}} \mathcal{M}(M, M'; n) \quad (1.7)$$

where the limit is taken through a sequence of M, M' values satisfying

$$\gcd\left(M, \frac{M' - M}{n}\right) = 1, \quad 2 \leq M < M', \quad M, M' \in \mathbb{N}. \quad (1.8)$$

It follows that the central charges (1.3) of the logarithmic minimal models are given as limits of the central charges of the rational minimal models

$$c^{P, P'; n} = \lim_{\substack{M, M' \rightarrow \infty \\ M/M' \rightarrow P/P'}} c^{M, M'; n}. \quad (1.9)$$

The coset construction (1.1), along with the logarithmic limit (1.7), makes precise the sense in which the logarithmic minimal models $\mathcal{LM}(P, P'; n)$ are extensions of the rational minimal models $\mathcal{M}(M, M'; n)$.

The goal of this paper is to extend the fusion hierarchy and the T - and Y -systems to the commuting double-row and single-row transfer matrices of the fused logarithmic minimal models $\mathcal{LM}(p, p')_{n \times n}$.

For the case of the double-row transfer matrices on the strip, we only consider the simplest vacuum boundary conditions conjugate to the identity operator. These transfer matrices are not actually matrices but rather diagrammatic objects (tangles [38, 39]) defined in the corresponding planar TL algebra [2, 3]. Matrix representations are obtained by acting with these tangles on suitable vector spaces of link states [1, 35]. Our results mirror the results obtained in [16] for the corresponding rational RSOS models [11, 12], but here they are established directly in the planar algebra. Crucially, this ensures that the results are valid for *all* matrix representations of the transfer tangles. Since the logarithmic minimal models are $su(2)$ theories, we work throughout with T - and Y -systems of the same form as in [16]. Remarkably, we find that these functional equations hold for arbitrary coprime integers p, p' and that the underlying structures are related to the Dynkin diagrams of the affine Lie algebras $A_{p'-1}^{(1)}$. Indeed, the determinantal structure of the polynomial functional equations of degree p' is the same [40] as for the Cyclic Solid-on-Solid (CSOS) models [41–43]. In contrast, the structure of the T - and Y -systems of rational minimal models are related to the Dynkin diagrams of classical Lie algebras.

The layout of the paper is as follows. Section 1.1 contains notation and functions used repeatedly throughout the paper. In Section 2, we present a brief review of the ordinary (non-fused) TL loop models. As computations are later carried out in the planar TL algebras, we first discuss this framework, its relation with linear TL algebras and the construction of link state modules for these algebras. We then write down some fundamental planar identities and define the transfer tangles on the strip and cylinder. The definition and key properties of Wenzl-Jones projectors are also reviewed.

In Section 3, we introduce (m, n) -fused face operators and study their decomposition in terms of generalised monoids. (The fusion index m should not be confused with the minimal model label m used above.) The explicit decomposition coefficients generalise results of [44, 45] for (n, n) -fusion and their computation is deferred to Appendix A. Planar identities similar to the ones in the non-fused case are obtained for the fused faces. The generalisation of the boundary Yang-Baxter equation to the fused setting is nontrivial and a proof is presented in Appendix B, following ideas developed in [29].

In Section 4, we introduce fused transfer tangles. The projectors and fused faces are well defined for λ generic, but in general not for $\frac{\lambda}{\pi}$ rational. However, we show that the expression for the transfer tangles can alternatively be given by replacing the P_n projectors by effective projectors Q_n which are well defined for all $\beta \in \mathbb{C}^*$. From this, we argue that singularities of the P_n projectors can be eliminated from the transfer tangles. A key property of the effective projectors is established in Appendix C.

In Section 5, we argue that singularities of the P_m projectors can also be ignored by studying representations of the fused TL algebra built from cabled link states explored in Appendix D. These representations are defined for generic λ and we show that, in certain quotient representations, the limit to rational $\frac{\lambda}{\pi}$ is well defined. The corresponding transfer matrix representations are therefore nonsingular and well defined.

In Section 6, we derive the fusion hierarchies satisfied by the transfer tangles on the strip and cylinder, with lengthy diagrammatic proofs deferred to Appendix E. The corresponding T - and Y -systems are subsequently worked out algebraically.

In Section 7, we focus on fractional $\lambda = \frac{(p'-p)\pi}{p'}$. For $m = n$, this corresponds to the higher-level logarithmic minimal model $\mathcal{LM}(p, p')_{n \times n}$. For general n , the fusion hierarchies close and we prove this diagrammatically in Appendix F. The closure translates into functional relations of polynomial degree p' for the transfer tangles. In the cylinder case, the closure and functional relations are expressed in terms of the so-called braid transfer tangle. The closure of the Y -systems is also worked out explicitly.

In Section 8, we compare our results for the fusion hierarchies, T -systems and Y -systems of the logarithmic minimal models with those obtained previously for rational models. We find that the fusion hierarchies and T -systems coincide with those of the critical A - D - E models, as described in [28], but observe that the closure mechanisms of the fusion hierarchy and Y -systems differ significantly.

Finally, Section 9 contains some concluding remarks.

1.1 Notation

For ease of reference, definitions and conventions used repeatedly in the paper are listed below.

Weight function and shifted spectral parameter:

$$s_k(u) := \frac{\sin(u + k\lambda)}{\sin \lambda} = s_0(u_k), \quad u_k := u + k\lambda. \quad (1.10)$$

Coefficient functions arising from half-arc propagation:

$$q^m(u) := \prod_{i=0}^{m-1} s_{-i}(u) s_{2+i}(-u). \quad (1.11)$$

Fused transfer tangles with shifted arguments:

$$\mathbf{D}_k^{m,n} := \mathbf{D}^{m,n}(u + k\lambda), \quad \mathbf{T}_k^{m,n} := \mathbf{T}^{m,n}(u + k\lambda). \quad (1.12)$$

Renormalised double-row transfer tangles:

$$\hat{\mathbf{D}}_k^{m,n} := s_{2k+n-1}(2u-\mu) \left(\prod_{j=k}^{n+k-2} s_{2j+1}(2u-\mu) \right) \mathbf{D}_k^{m,n}. \quad (1.13)$$

Collapsed transfer and braid transfer tangles:

$$\mathbf{D}^{m,0}(u) \equiv \mathbf{F}^{m,0} \equiv \mathbf{I}^m, \quad \mathbf{T}^{m,0}(u) \equiv \tilde{\mathbf{F}}^{m,0} \equiv \mathbf{I}^m, \quad (1.14)$$

$$\hat{\mathbf{D}}^{m,-1}(u) \equiv \mathbf{F}^{m,-1} \equiv 0, \quad \mathbf{T}^{m,-1}(u) \equiv \tilde{\mathbf{F}}^{m,-1} \equiv 0. \quad (1.15)$$

Fusion hierarchy coefficient functions:

$$f_k^m := s_{2k+1}(2u-\mu) \left(\prod_{i=0}^{m-1} s_{k-i}(u) s_{k+m-i}(u-\mu) \right)^N, \quad h_k^m := \left(\prod_{j=0}^{m-1} (-i) s_{k-j}(u) \right)^N. \quad (1.16)$$

T -system coefficient functions:

$$\nu_k^{(n)} := \prod_{j=k}^{n+k-1} f_{j-1}^m f_{j+1}^m, \quad \tilde{\nu}_k^{(n)} := \prod_{j=k}^{n+k-1} h_{j-1}^m h_{j+1}^m. \quad (1.17)$$

Fusion closure coefficient functions:

$$a := \prod_{j=0}^{p'-1} f_j^m, \quad \tilde{a} := e^{i\theta} \prod_{j=0}^{p'-1} h_j^m, \quad \theta := \frac{1}{2} N m (p' - p) \pi. \quad (1.18)$$

2 Temperley-Lieb loop models

Elementary face operators The dense loop model with crossing parameter λ can be described by the planar TL algebra [1–3] generated by the elementary face operators

$$\boxed{u} := s_1(-u) \boxed{\text{diag 1}} + s_0(u) \boxed{\text{diag 2}} \quad (2.1)$$

This decomposition is in terms of the two possible internal connectivities with the coefficients indicating the corresponding (local Boltzmann) weights. The small quarter arc in the lower-left corner is a marker

indicating the orientation of the diagrams in the decomposition. The weights are given in terms of the spectral parameter u where the chosen normalisation in (1.10) requires a real crossing parameter to be of the form

$$\lambda \in \pi(\mathbb{R} \setminus \mathbb{Z}). \quad (2.2)$$

The corresponding loop fugacity

$$\beta = 2 \cos \lambda = s_2(0) \quad (2.3)$$

is the (nonlocal Boltzmann) weight assigned to a (closed) contractible loop. We note that

$$s_k(0) = U_{k-1}\left(\frac{\beta}{2}\right), \quad k \in \mathbb{N}_0 \quad (2.4)$$

where $U_k(x)$ is the k -th Chebyshev polynomial of the second kind.

The elements of the planar TL algebra are called tangles [38, 39] and are diagrammatic objects formed by adding or linking together a number of elementary face operators. Noting that

$$\begin{array}{|c|} \hline \text{Diagram with two blue arcs in a square} \\ \hline \end{array} = \begin{array}{|c|} \hline 0 \\ \hline \end{array}, \quad \begin{array}{|c|} \hline \text{Diagram with two blue arcs in a square} \\ \hline \end{array} = \begin{array}{|c|} \hline \lambda \\ \hline \end{array}, \quad (2.5)$$

we stress that individual connectivity diagrams are themselves tangles. Tangles are linear combinations of planar connectivity diagrams with an even number of free nodes connected by non-intersecting loop segments. Here a node refers to the midpoint of an edge of an elementary face operator, and it is said to be free if it is not linked to any other node via the outside of the corresponding box. In the decomposition of a tangle in terms of connectivity diagrams, closed loops may be formed but every one of them is replaced by a multiplicative factor of β , the loop fugacity. Two tangles are equal if their decompositions in terms of connectivity diagrams are identical. A tangle with $2n$ free nodes is called an n -tangle and is a (possibly trivial) linear combination of connectivity diagrams containing exactly $2n$ free nodes.

Multiplication of tangles is performed diagrammatically by linking or gluing together the tangles using non-intersecting loop segments. Here is an example of a 4-tangle, with its free nodes indicated by black dots, obtained as the product of two 3-tangles:


(2.6)

where the extra free nodes of the two 3-tangles are indicated in blue. In the decomposition of this 4-tangle, the particular connectivity diagram


(2.7)

appears with decomposition coefficient

$$s_0(2\lambda)s_0(u)s_0(w)s_1(-v)s_0(u+\lambda)s_0(v-\lambda) = -\beta s_0(u)s_1(u)[s_1(-v)]^2 s_0(w). \quad (2.8)$$

The removal of the three closed loops introduces an additional factor of β^3 .

If the $2n$ free nodes of an n -tangle can be linked without intersections to $2n$ distinct points on a circle encircling the tangle, a direction of transfer can be defined by selecting n of the free nodes, linked to n consecutive points on the circle, to represent an instate direction. In this case, the remaining n (likewise consecutive) nodes represent the corresponding outstate direction. As tangles can also be defined on more complicated geometries such as annuli and cylinders, the notion of a direction of transfer has to be adjusted in some cases.

Linear Temperley-Lieb algebras With the direction of transfer fixed, a planar N -tangle can be expressed in terms of words of the ordinary (linear) TL algebra

$$TL_N(\beta) = \langle I, e_j; j = 1, \dots, N-1 \rangle, \quad I = \begin{array}{c} | \\ 1 \end{array} \begin{array}{c} | \\ 2 \end{array} \begin{array}{c} | \\ 3 \end{array} \cdots \begin{array}{c} | \\ N \end{array}, \quad e_j = \begin{array}{c} | \\ 1 \end{array} \cdots \begin{array}{c} | \\ j \end{array} \begin{array}{c} \cup \\ j+1 \end{array} \begin{array}{c} | \\ N \end{array} \quad (2.9)$$

whose defining relations are

$$IA = AI = A, \quad e_j^2 = \beta e_j, \quad e_j e_{j\pm 1} e_j = e_j, \quad e_i e_j = e_j e_i \quad (|i - j| > 1), \quad (2.10)$$

where A is any element of $TL_N(\beta)$. Multiplication in the diagrammatic realisation is by vertical concatenation placing e_j atop e_i to form the product $e_i e_j$, for example. The diagrammatic realisation is faithful in the sense that the ensuing diagrammatic algebra is isomorphic to the TL algebra.

In the cylinder case, the relevant algebra is the enlarged periodic TL algebra,

$$\mathcal{EPTL}_N(\alpha, \beta) = \langle I, \Omega, \Omega^{-1}, e_j; j = 1, \dots, N \rangle, \quad (2.11)$$

where the three new generators are realised as

$$e_N = \begin{array}{c} \cup \\ 1 \end{array} \begin{array}{c} | \\ 2 \end{array} \begin{array}{c} | \\ 3 \end{array} \cdots \begin{array}{c} | \\ N \end{array} \begin{array}{c} \cup \\ N \end{array}, \quad \Omega = \begin{array}{c} \diagup \\ 1 \end{array} \begin{array}{c} \diagup \\ 2 \end{array} \begin{array}{c} \diagup \\ 3 \end{array} \cdots \begin{array}{c} \diagup \\ N \end{array}, \quad \Omega^{-1} = \begin{array}{c} \diagdown \\ 1 \end{array} \begin{array}{c} \diagdown \\ 2 \end{array} \begin{array}{c} \diagdown \\ 3 \end{array} \cdots \begin{array}{c} \diagdown \\ N \end{array} \quad (2.12)$$

with periodic boundary conditions identifying the matching left and right nodes, thereby forming connectivity diagrams on the surface of a cylinder. The vertical line along which the identification is taking place is referred to as the *virtual boundary*. The defining relations of $\mathcal{EPTL}_N(\alpha, \beta)$ are given by (2.10) supplemented by

$$\begin{aligned} \Omega e_i \Omega^{-1} &= e_{i-1}, \\ \Omega \Omega^{-1} &= \Omega^{-1} \Omega = I, \\ (\Omega^{\pm 1} e_N)^{N-1} &= \Omega^{\pm N} (\Omega^{\pm 1} e_N), \\ \Omega^{\pm N} e_N \Omega^{\mp N} &= e_N, \\ E \Omega^{\pm 1} E &= \alpha E, \quad E := e_2 e_4 \dots e_{N-2} e_N \quad (N \text{ even}), \end{aligned} \quad (2.13)$$


where the subscripts are defined modulo N . The parameter α is seen to be the (nonlocal Boltzmann) weight assigned to non-contractible loops formed around the cylinder. Note that such loops can only appear for N even. As for the linear TL algebra above, the diagrammatic realisation is faithful in the sense that the ensuing diagrammatic algebra is isomorphic to the enlarged periodic TL algebra. The enlarged periodic TL algebra is the quotient of the affine TL algebra [46–49] by the last relation in (2.13).

Even though vertical can be chosen as the natural direction of transfer in many of our considerations, see (2.25) and (2.26) for example, it is often more convenient to work in the planar or cylindrical setting without reference to any particular direction of transfer.

Link states A natural way to produce matrix representations of TL algebras is to let the tangles act on a suitable vector space of link states.

A planar link state on N nodes is a planar diagram that encodes connectivities between N nodes equally spaced on a horizontal line. It consists of $d \in \{0, \dots, N\}$ vertical loop segments (called defects) attached to individual nodes and $\frac{N-d}{2}$ half-arcs, where $N - d = 0 \bmod 2$, connecting nodes pairwise by loop segments that live above the horizontal line and cannot over-arch defects.

We distinguish between planar link states and cylindrical link states. An example of a planar link state on $N = 10$ nodes with $d = 2$ defects is given by


(2.14)

while an example of a cylindrical link state on $N = 10$ nodes with $d = 4$ defects is given by


(2.15)

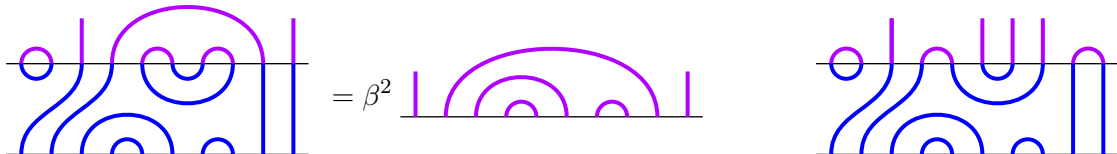
Letting V_N^d and \tilde{V}_N^d respectively denote the linear spans of planar and cylindrical link states on N nodes with d defects, we have

$$\dim V_N^d = \binom{N}{\frac{N-d}{2}} - \binom{N}{\frac{N-d-2}{2}}, \quad \dim \tilde{V}_N^d = \binom{N}{\frac{N-d}{2}}. \quad (2.16)$$

We say that the planar and cylindrical link states form *canonical bases* of V_N^d and \tilde{V}_N^d , respectively. To obtain concrete matrix representations, one still has to identify the subset of link states the tangles are meant to act on and specify the action itself. A particularly simple prescription yields the so-called standard modules reviewed in the following.

Standard modules Both on the strip and cylinder, the simplest nontrivial modules are the *standard modules*. For N fixed, they yield representations of $TL_N(\beta)$ and $\mathcal{EPTL}_N(\alpha, \beta)$ on $\text{End}(V_N^d)$ and $\text{End}(\tilde{V}_N^d)$, respectively, with $d = 0, \dots, N$ subject to $d = N \bmod 2$.

For the strip case, let c be a connectivity (diagrammatic realisation of a word) in $TL_N(\beta)$ and w be a link state in the canonical basis of V_N^d . Viewing w as the instate (see the discussion following (2.8)), the action of c on w is computed from the composition diagram obtained by placing w atop c and linking the nodes of w to the N free nodes on the upper edge of c . If the result is not in V_N^d , it is readily set to zero. Otherwise, the result cw is a multiple scalar of a link state in the basis of V_N^d , called the outstate, and the scalar is given by $\beta^\#$ where $\#$ is the number of (closed) loops in the composition diagram. By construction, this action preserves the number of defects. It is linearly extended to any tangle in $TL_N(\beta)$ and any element of V_N^d , and it is well known that it generates a representation of $TL_N(\beta)$, see [50, 51], for example. The matrix representative of $c \in TL_N(\beta)$ on the standard module with d defects is denoted by $\rho_N^d(c)$. We illustrate the action of connectivities on link states in the definition of standard modules on the strip for $N = 10$ with the two examples


(2.17)

For standard modules on the cylinder, the action of a connectivity $c \in \mathcal{EPTL}_N(\alpha, \beta)$ on an element w of the canonical basis of \tilde{V}_N^d is likewise computed by the connection procedure described above for the strip case. The result cw is a basis link state in \tilde{V}_N^d multiplied by $\alpha^{\#(\alpha)} \beta^{\#(\beta)}$, where $\#(\alpha)$ and

$\#(\beta)$ are the respective numbers of non-contractible and contractible loops in the ensuing composition diagram, whereas it is zero if defects have been annihilated in the diagram. As an illustration, we have

$$\text{Complex loop diagram} = \alpha^2 \beta \text{Simpler loop diagram} \quad (2.18)$$

This action defines a representation of $\mathcal{EPTL}_N(\alpha, \beta)$. The matrix representative of $c \in \mathcal{EPTL}_N(\alpha, \beta)$ on the standard module with d defects is denoted by $\tilde{\rho}_N^d(c)$.

Fundamental tangle relations The face operators enjoy the crossing relations

$$\boxed{u} = \boxed{\lambda-u} = \boxed{u} = \boxed{\lambda-u}, \quad (2.19)$$

commute in the sense that

$$\text{Diamond } u \text{ crossing Diamond } v = \text{Diamond } v \text{ crossing Diamond } u \quad (2.20)$$

and satisfy the local inversion relation

$$\text{Diamond } u \text{ crossing Diamond } -u = s_1(u)s_1(-u) \text{Diamond with arcs} \quad (2.21)$$

the Yang-Baxter equation (YBE)

$$\text{Diamond } u-v \text{ crossing Square } v, u = \text{Square } u, v \text{ crossing Diamond } u-v \quad (2.22)$$

and the boundary Yang-Baxter equations (BYBEs)

$$\text{Boundary relation 1} = \text{Boundary relation 2} \quad (2.23)$$

Because only vacuum boundary conditions are considered, the two relations in (2.23) are simplified versions of the usual BYBE, see for example [1]. In fact, the BYBEs (2.23) are equivalent to the commutation relation (2.20). The face operators also have the push-through properties

$$\text{Push-through 1} = s_0(u)s_2(-u) \text{Push-through 2} = s_1(u)s_1(-u) \text{Push-through 3} \quad (2.24)$$

which one can regard as rewritings of the local inversion relation (2.21).

Transfer tangles On a strip of width N and with trivial boundary conditions, the *double-row transfer tangle* $\mathbf{D}(u)$ is defined by

$$\mathbf{D}(u) := \begin{array}{|c|c|c|c|c|} \hline \lambda-u & \lambda-u & \cdots & \cdots & \lambda-u \\ \hline u & u & \cdots & \cdots & u \\ \hline \end{array} \quad (2.25)$$

$\underbrace{\hspace{10em}}_N$

Similarly on a cylinder, the *single-row transfer tangle* $\mathbf{T}(u)$ is defined as

$$\mathbf{T}(u) := \begin{array}{|c|c|c|c|c|} \hline u & u & \cdots & \cdots & u \\ \hline \end{array} \quad (2.26)$$

$\underbrace{\hspace{10em}}_N$

where the periodic boundary conditions identify the left and right edges of $\mathbf{T}(u)$ thereby forming a band of length N around the cylinder. Strictly speaking, $\mathbf{T}(u)$ is only *locally planar* as it is defined on the surface of a cylinder. Transfer matrices on the strip and cylinder are obtained by fixing a representation of $TL_N(\beta)$ and $\mathcal{EPTL}_N(\alpha, \beta)$. For example, in the standard representations, the transfer matrices are $\rho_N^d(\mathbf{D}(u))$ and $\tilde{\rho}_N^d(\mathbf{T}(u))$.

From (2.21), (2.22) and (2.23), these tangles can be shown to form distinct commuting families of tangles [29, 52], in the sense that

$$[\mathbf{D}(u), \mathbf{D}(v)] = 0, \quad [\mathbf{T}(u), \mathbf{T}(v)] = 0, \quad u, v \in \mathbb{C} \quad (2.27)$$

where multiplication is by concatenation of diagrams placing $\mathbf{D}(v)$ atop $\mathbf{D}(u)$ in the product $\mathbf{D}(u)\mathbf{D}(v)$, for example. Even though $\mathbf{D}(u)$ and $\mathbf{T}(u)$ are planar tangles and hence not matrices, they are occasionally referred to as transfer matrices in the literature.

Crossing symmetry Following arguments in [29], it can be shown that $\mathbf{D}(u)$ is crossing symmetric in the sense that

$$\mathbf{D}(u) = \mathbf{D}(\lambda - u). \quad (2.28)$$

The manifestation of crossing symmetry of the cylinder transfer tangle $\mathbf{T}(u)$ requires the extension of $\mathcal{EPTL}_N(\alpha, \beta)$ by a reflection generator R . Due to the periodicity of the cylinder, we can choose $R = R_j$ for any $j = 1, \dots, N$ where R_j is defined by the relations

$$R_j e_j R_j = e_j, \quad R_j \Omega R_j = \Omega^{-1}, \quad R_j^2 = I. \quad (2.29)$$

Using relations such as $e_5 = \Omega^{-3} e_2 \Omega^3$, it follows that $R_2 e_5 R_2 = e_{-1} \equiv e_{N-1}$ and more generally

$$R_i e_j R_i = e_{2i-j}, \quad i, j = 1, \dots, N \quad (2.30)$$

where it is recalled that $e_k \equiv e_\ell$ if $k \equiv \ell \pmod{N}$. The crossing symmetry then reads

$$R \mathbf{T}(u) R = \mathbf{T}(\lambda - u). \quad (2.31)$$

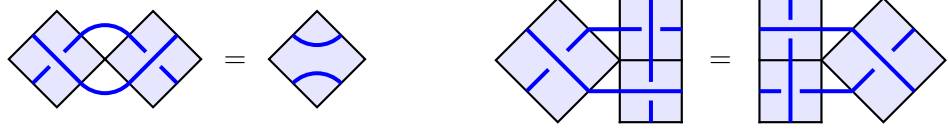
Braid transfer tangles and braid limits The *elementary braid tangles* are 2-tangles defined by

$$\begin{array}{|c|} \hline | \\ \hline | \\ \hline \end{array} := e^{-i\frac{\pi-\lambda}{2}} \begin{array}{|c|} \hline \swarrow \\ \hline \end{array} + e^{i\frac{\pi-\lambda}{2}} \begin{array}{|c|} \hline \searrow \\ \hline \end{array} \quad \begin{array}{|c|} \hline - \\ \hline - \\ \hline \end{array} = e^{i\frac{\pi-\lambda}{2}} \begin{array}{|c|} \hline \swarrow \\ \hline \end{array} + e^{-i\frac{\pi-\lambda}{2}} \begin{array}{|c|} \hline \searrow \\ \hline \end{array} \quad (2.32)$$

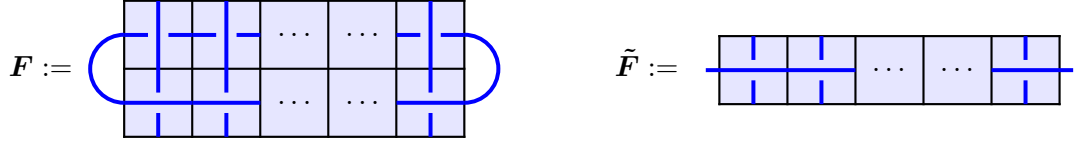
These can be obtained in the *braid limit* of the face operators as

$$\begin{array}{|c|} \hline | \\ \hline | \\ \hline \end{array} = \lim_{u \rightarrow i\infty} \left(\frac{e^{i\frac{\pi-\lambda}{2}}}{s_k(u)} \begin{array}{|c|} \hline u_k \\ \hline \end{array} \right), \quad \begin{array}{|c|} \hline - \\ \hline - \\ \hline \end{array} = \lim_{u \rightarrow i\infty} \left(\frac{e^{i\frac{\pi-\lambda}{2}}}{s_k(u)} \begin{array}{|c|} \hline u_k \\ \hline \end{array} \right), \quad k \in \mathbb{Z}, \quad (2.33)$$

and satisfy planar relations obtained as braid limits of usual planar identities, such as


(2.34)

We define the *braid transfer tangles* in terms of these braid 2-tangles as


(2.35)

The braid transfer tangles are central elements of $TL_N(\beta)$ and $\mathcal{EPTL}_N(\alpha, \beta)$, respectively [57, 58], and can be obtained as braid limits of the corresponding transfer tangles as

$$\mathbf{F} = \lim_{u \rightarrow i\infty} \left(\left(\frac{e^{i\frac{\pi-\lambda}{2}}}{s_0(u)} \right)^{2N} \mathbf{D}(u) \right), \quad \tilde{\mathbf{F}} = \lim_{u \rightarrow i\infty} \left(\left(\frac{e^{i\frac{\pi-\lambda}{2}}}{s_0(u)} \right)^N \mathbf{T}(u) \right). \quad (2.36)$$

On standard modules, the braid transfer tangles \mathbf{F} and $\tilde{\mathbf{F}}$ act as scalar multiples of the identity, that is

$$\rho_N^d(\mathbf{F}) = \mathcal{U}_1^d I, \quad \tilde{\rho}_N^d(\tilde{\mathbf{F}}) = \tilde{\mathcal{U}}_1^d I, \quad (2.37)$$

where

$$\mathcal{U}_1^d = 2(-1)^d \cos((d+1)\lambda), \quad \tilde{\mathcal{U}}_1^d = 2 \cos\left(\frac{d}{2}(\pi - \lambda)\right) \quad (2.38)$$

are special cases of the expressions in (5.29), while I is the identity matrix of dimension $\dim V_N^d$ or $\dim \tilde{V}_N^d$, respectively.

Characterisation of λ values A primary goal of this paper is to find functional relations satisfied by the transfer tangles $\mathbf{D}(u)$ and $\mathbf{T}(u)$ in the case the crossing parameter is a non-integer *rational multiple* of π . In this case, we write

$$\lambda = \lambda_{p,p'} := \frac{(p' - p)\pi}{p'}, \quad \gcd(p, p') = 1, \quad p \in \mathbb{N}, \quad p' \in \mathbb{N}_{\geq 2}, \quad (2.39)$$

and we refer to these λ values as *fractional*. Accordingly, the values $\lambda \in \pi(\mathbb{R} \setminus \mathbb{Q})$ are referred to as *generic*. The *logarithmic minimal models* $\mathcal{LM}(p, p')$ [1] are defined for fractional $\lambda = \lambda_{p,p'}$ for which $1 \leq p < p'$ and are the focus of Section 7, in particular.

For $\lambda = \lambda_{p,1} \in \pi\mathbb{Z}$, the weights in (2.2) diverge. After these divergencies are removed by a renormalisation of the face operator, the relative weight of the two connectivity diagrams in (2.1) is simply ± 1 since $s_0(u)$ and $s_1(-u)$ are equal up to a sign for $\lambda \in \pi\mathbb{Z}$. In this case, one can show that $\mathbf{D}(u)$ is merely a scalar multiple of the *identity tangle*

$$\mathbf{I} := \begin{array}{c} | \\ | \\ | \\ | \\ \dots \\ | \end{array} \quad (2.40)$$

while the periodic transfer tangle $\mathbf{T}(u)$ is a scalar multiple of the single-row braid transfer tangle $\tilde{\mathbf{F}}$. We view these as trivial functional relations of degree $p' = 1$. As already indicated in (2.2), crossing parameters of the form $\lambda \in \pi\mathbb{Z}$ are therefore excluded in the remainder of this paper.

Wenzl-Jones projectors Let λ be generic. The Wenzl-Jones (WJ) projector P_n [39, 53, 54] is an n -tangle

$$P_n = \boxed{n}, \quad n \in \mathbb{N} \quad (2.41)$$

defined recursively by

$$\boxed{n} = \boxed{n-1} \mid - \frac{s_{n-1}(0)}{s_n(0)} \begin{array}{c} \boxed{n-1} \\ \vdots \\ \boxed{n-1} \end{array} \text{ (with } n-1 \text{ boxes)}, \quad \boxed{1} = \mid. \quad (2.42)$$

The first nontrivial examples are

$$\boxed{2} = \text{||} - \frac{1}{s_2(0)} \text{ } \begin{array}{c} \text{ } \\ \text{ } \end{array} \quad (2.43)$$

and

$$\boxed{3} = \begin{array}{|c|} \hline | \\ \hline \end{array} \begin{array}{|c|} \hline | \\ \hline \end{array} \begin{array}{|c|} \hline | \\ \hline \end{array} - \frac{s_2(0)}{s_3(0)} \left(\begin{array}{|c|} \hline \text{ } \\ \hline \end{array} \begin{array}{|c|} \hline \text{ } \\ \hline \end{array} \begin{array}{|c|} \hline \text{ } \\ \hline \end{array} + \begin{array}{|c|} \hline \text{ } \\ \hline \end{array} \begin{array}{|c|} \hline \text{ } \\ \hline \end{array} \begin{array}{|c|} \hline \text{ } \\ \hline \end{array} \right) + \frac{1}{s_3(0)} \left(\begin{array}{|c|} \hline \text{ } \\ \hline \end{array} \begin{array}{|c|} \hline \text{ } \\ \hline \end{array} \begin{array}{|c|} \hline \text{ } \\ \hline \end{array} + \begin{array}{|c|} \hline \text{ } \\ \hline \end{array} \begin{array}{|c|} \hline \text{ } \\ \hline \end{array} \begin{array}{|c|} \hline \text{ } \\ \hline \end{array} \right). \quad (2.44)$$

The WJ projectors have many remarkable properties. In particular, as an element of $TL_n(\beta)$, P_n is indeed a projector, that is

$$\begin{array}{|c|} \hline n \\ \hline n \\ \hline \end{array} = \boxed{n} . \quad (2.45)$$

Second, P_n is a half-arc annihilator in the sense that if two adjacent nodes from the top edge (or bottom edge) are connected by a half-arc, the resulting diagram vanishes as

$$\boxed{n}^{\circ} = \boxed{n}_{\circ} = 0. \quad (2.46)$$

These two properties are used in the definition of fused loop models in Section 3 and repeatedly in the planar computations of Appendix E and F. Moreover, P_n is the unique n -tangle with properties (2.45) and (2.46). Two other important properties of WJ projectors are

$$\begin{array}{c} m \\ \hline n \end{array} = \begin{array}{c} n \\ \hline m \end{array} = \boxed{n}, \quad m \leq n \quad (2.47)$$

and

$$\boxed{n} \text{ with a blue loop on the right} = \frac{s_{n+1}(0)}{s_n(0)} \boxed{n-1}. \quad (2.48)$$

Finally, P_n can be realised in terms of face operators as

$$P_n = \begin{array}{c} \text{Diagram 1: A diamond shape with } n \text{ rows. The top row has 1 cell labeled 1. The next row has 2 cells labeled 2. The next row has } \dots \text{ cells labeled } \dots. \text{ The next row has } n-2 \text{ cells labeled } n-2. \text{ The next row has } n-1 \text{ cells labeled } n-1. \text{ The next row has } n-2 \text{ cells labeled } n-2. \text{ The next row has } \dots \text{ cells labeled } \dots. \text{ The next row has 2 cells labeled 2. The bottom row has 1 cell labeled 1.} \end{array}$$

For $\lambda = \lambda_{p,p'}$, the recursive definition (2.42) of P_n is well defined for $n \in \{1, \dots, p' - 1\}$, but breaks down for $n = p'$ since $s_{p'}(0) = 0$. In certain contexts, one can circumvent the non-existence of WJ projectors and still perform the corresponding projection operations. For example, the general construction of boundary conditions in logarithmic minimal models [1] involves projection operations which can be handled by so-called generalised TL projectors [6]. In the remainder of this section, we only consider λ for which the participating projectors exist. Later, we will need to handle situations where some projectors do not exist. Thus, in Sections 4 and 5, we will discuss how to implement the relevant properties of certain projectors for general λ and, following [6], why we may ignore certain other projectors in our analyses.

3 Fused Temperley-Lieb loop models

In this section, we construct fused face operators and write down the generalised planar identities. The parameter λ is taken to be generic, so that the projectors P_m and P_n exist for all m and n .

3.1 Fused face operators

Definition of fusion Fusion of $m \times n$ blocks of loop faces is implemented diagrammatically by (i) forming a rectangular array of m by n elementary face operators with spectral parameters as in (3.1), and (ii) applying P_m and P_n projectors along the horizontal and vertical edges, respectively. The ensuing (m, n) -fused face operator is thus the $(m + n)$ -tangle given by

$$\begin{array}{|c|} \hline (m,n) \\ \hline u \\ \hline \end{array} := \begin{array}{|c|} \hline m \\ \hline \begin{array}{|c|} \hline u_{n-m} \quad \dots \quad u_{n-2} \quad u_{n-1} \\ \hline \vdots \quad \quad \quad \vdots \quad \vdots \\ \hline u_{2-m} \quad \dots \quad u_0 \quad u_1 \\ \hline u_{1-m} \quad \dots \quad u_{-1} \quad u_0 \\ \hline m \\ \hline \end{array} \\ \hline n \end{array} \quad (3.1)$$

A fused face with the small orientation-indicating quarter circle drawn in the lower-right, upper-right or upper-left corner corresponds to a counterclockwise rotation by 90° , 180° or 270° , respectively, of the diagram in (3.1).

We mention that fused face operators can be scaled by a factor $\eta^{m,n}$ that removes overall poles and zeroes, see for example [28]. However, the absence of such normalisation factors makes the planar computations in Appendix E and F slightly less cumbersome. A discussion of our results with the factors included is presented in Section 8.

If an internal arc beginning and ending on the *same* edge appears in a configuration in the decomposition of the mn elementary face operators in (3.1), then there must be a small half-arc connecting neighbouring nodes somewhere along that edge and the configuration has weight zero due to property (2.46) of the WJ projectors. The fusion procedure thus projects out all faces with an internal arc attached to a single projector along the edges.

A simplified albeit asymmetric realisation of the (m, n) -fused face is obtained by removing the P_n projector acting on the right and the P_m projector acting on the top of the fused block. Indeed, if these projectors are expanded in terms of connectivity diagrams, every one of these diagrams but I (which is always present in the decomposition of a WJ projector) contains one or more half-arcs that propagate through the fused face (because of the push-through properties (2.24)) to eventually be annihilated by the projectors at the bottom or to the left, by property (2.46). The only remaining connectivity diagram is I and, from property (2.45) or (2.49) of the projector, it readily follows that its weight is 1.

This implies that the original and simplified realisations are in fact equal as tangles,

$$(3.2)$$

Monoid decomposition An (m, n) -fused face can be written as a linear combination of $\min(m, n) + 1$ *generalised monoids* labeled by $a \in \{0, 1, \dots, \min(m, n)\}$ and given by

$$X_a^{m,n} = \quad (m \geq n) \quad (3.3)$$

where the diagram $X_a^{m,n}$ for $m < n$ is obtained by performing a left-right reflection of the diagram in (3.3) and interchanging m and n in the reflected diagram. The details of this decomposition is the content of the following proposition whose proof is presented in Appendix A.

PROPOSITION 3.1 *The decomposition of an (m, n) -fused face in terms of generalised monoids is given by*

$$u^{(m,n)} = \sum_{a=0}^r \alpha_a^{m,n} X_a^{m,n}, \quad r := \min(m, n) \quad (3.4)$$

where

$$\frac{\alpha_a^{m,n}}{\alpha_0^{m,n}} = (-1)^{(m+n)a} \left(\prod_{j=1}^a \frac{s_{r-j+1}(0)}{s_j(0)} \right) \left(\prod_{i=0}^{a-1} \frac{s_{n-r+i}(u)}{s_{m-i}(-u)} \right), \quad \alpha_0^{m,n} = \prod_{i=0}^{m-1} \prod_{j=0}^{n-1} s_{i-j+1}(-u). \quad (3.5)$$

For example, in the non-fused case where $m = n = 1$, we simply have

$$X_0^{1,1} = \quad X_1^{1,1} = \quad \alpha_0^{1,1} = s_1(-u), \quad \alpha_1^{1,1} = s_0(u), \quad (3.6)$$

corresponding to the decomposition (2.1) of the elementary face operators, while in the case of $(2, 2)$ -fused faces, the decomposition reads

$$u^{(2,2)} = s_{-1}(u)s_0(u) \left(s_{-2}(u)s_{-1}(u)X_0^{2,2} - \beta s_{-1}(u)s_0(u)X_1^{2,2} + s_0(u)s_1(u)X_2^{2,2} \right) \quad (3.7)$$

and involves the three generalised monoids

$$X_0^{2,2} = \text{diagram}, \quad X_1^{2,2} = \text{diagram}, \quad X_2^{2,2} = \text{diagram} \quad (3.8)$$

Along with the corresponding coefficients $\alpha_a^{2,2}$, diagrams similar to (3.8) were introduced in [44] and later generalised to the $n \times n$ case in [45]. The $(2, 2)$ -fused loop model and its conformal properties are investigated in [35].

Fused planar identities The $(m + n)$ -tangle

$$I^{m,n} = \text{diagram} \quad (3.9)$$

acts from below as the identity on the generalised monoid $X_a^{m,n}$, while $I^{n,m}$ acts as the identity from above, that is

$$I^{m,n} X_a^{m,n} = X_a^{m,n} I^{n,m} = X_a^{m,n}, \quad a = 0, 1, \dots, r. \quad (3.10)$$

In the case $m = n$, we have $X_0^{n,n} = I^{n,n}$.

The fused face operators satisfy generalised versions of the various identities for the elementary 1×1 boxes discussed in Section 2. The generalised YBEs and crossing relations are thus discussed in Sections 3.2 and 3.3, while here we note the local inversion relation

$$\text{diagram} = g^{m,n}(u) \text{diagram}, \quad g^{m,n}(u) := \prod_{i=0}^{m-1} \prod_{j=0}^{n-1} s_{j-i+1}(u) s_{i-j+1}(-u), \quad (3.11)$$

where the diagram to the right represents the identity tangle $I^{m,n}$ in (3.9) rotated by 90° in the counterclockwise direction. Pairs of half-arcs as in the diagram to the left in (3.11) will be used to indicate that *multiple half-arcs* connect the fused faces. In the concrete example in (3.11), the upper and lower pairs represent m and n nested half-arcs, respectively. Another example of multiple half-arcs is given by comparing equations (4.3) and (4.10) below.

The extension of the push-through properties (2.24) to the $(m, 1)$ -fused faces is given by

$$\text{diagram} = q^m(u) \text{diagram} = q^m(u) \text{diagram}, \quad \text{diagram} = q^m(u_1) \text{diagram} = q^m(u_1) \text{diagram} \quad (3.12)$$

where $q^m(u)$ is defined in (1.11).

3.2 Yang-Baxter equations

The YBE for fused face operators is

$$\text{diagram} = \text{diagram} \quad (3.13)$$

For general $\ell, m, n \in \mathbb{N}$, this identity follows readily from the YBE (2.22) for the elementary 1×1 face operators and properties of the projectors. The fused face operators also satisfy [29] the left and right BYBEs

$$(3.14)$$

As in the non-fused case (2.23), the simplicity of the BYBE (3.14) is due to the fact that we are only considering vacuum boundary conditions. Proofs of (3.14), adapted from [29] to the present loop model context, are given in Appendix B.

3.3 Crossing symmetry

Fused faces of the form $(1, n)$ or $(m, 1)$ decompose in terms of two generalised monoids only. This is merely a special case of the more general situation where a vertical array of elementary faces sandwiched between two P_n projectors decomposes as

$$(3.15)$$

It readily follows that fusion of single columns or rows yields fully symmetric functions of the spectral parameters,

$$(3.16)$$

where the face weights are related by a permutation operator \mathcal{P}_n on n items. Similar relations obviously hold for horizontal arrays of elementary faces. As an immediate consequence, we have the crossing relation

$$(3.17)$$

Generally, the fused faces enjoy the crossing relations

$$(3.18)$$

To prove the crossing relations for $m > 1$, extra projectors are inserted inside the fused faces. This is made possible because of the push-through properties (2.24) and property (2.46) of the WJ projectors. The proof then uses the crossing property already established for $(1, n)$, from which the similar results for $(m, 1)$ follow. For example, for $(m, n) = (2, 3)$,

Diagrammatic equation (3.19) showing the decomposition of a $(2,3)$ transfer matrix into a product of three 3×3 matrices and then into a single $(3,2)$ matrix. The first row shows the $(2,3)$ matrix as a 3×3 matrix with entries u_{-1}, u_0, u_1, u_2 and red strands labeled 2 and 3. This is equal to the product of three 3×3 matrices, which is then equal to a single $(3,2)$ matrix with entry $\lambda - u$.

This is readily extended from $(2,3)$ to general (m,n) , and the remaining equalities in (3.18) are proved using similar arguments.

4 Transfer tangles

For λ generic, a set of m cabled strands is obtained by inserting a P_m projector acting on these m strands,

Diagrammatic equation (4.1) showing the transformation of m free strands into m cabled strands. On the left, m free strands are shown as vertical blue lines. On the right, m cabled strands are shown as vertical blue lines with a red horizontal bar labeled m representing the projector P_m .

As discussed at the end of Section 2, some projectors fail to exist for fractional λ and in this case, an alternative scheme must be used to project out unwanted connections. This is described in Section 5. For now, we keep λ generic and note that on an array of N sets of m -cabled strands as in (4.1), the identity tangle is given by

Diagrammatic equation (4.2) showing the identity tangle I^m as a sequence of projectors P_m acting on m -cabled strands. The diagram consists of a sequence of red horizontal bars labeled m connected by vertical blue lines.

where the number of P_m projectors is N . For $m = 1$, this reduces to the identity tangle in (2.40) as $I^1 = I$. For $m > 1$, on the other hand, I^m does not act as the identity on free strands. Instead, it is the identity of the subalgebras $F\mathcal{T}L_{N,m}(\beta) \subset \mathcal{T}L_{Nm}(\beta)$ and $F\mathcal{EPT}L_{N,m}(\alpha, \beta) \subset \mathcal{EPT}L_{Nm}(\alpha, \beta)$ defined in Section 5.

4.1 Fused transfer tangles for generic λ

For λ generic, the *multi-row transfer tangles* are defined by

Diagrammatic equation (4.3) defining the multi-row transfer tangle $D^{m,n}(u)$ as a sequence of N transfer matrices. The diagram shows a sequence of (m,n) transfer matrices with entries u and $\mu - u_{n-1}$, connected by blue strands.

and

$$\mathbf{T}^{m,n}(u) := \underbrace{\begin{array}{|c|c|c|c|c|} \hline \textcolor{blue}{(m,n)} & \textcolor{blue}{(m,n)} & \dots & \dots & \textcolor{blue}{(m,n)} \\ \hline u & u & & & u \\ \hline \end{array}}_N \quad (4.4)$$

On the strip, the construction of fused transfer tangles involves an additional *fused crossing parameter* $\mu \in \mathbb{C}$. One should note that (i) μ only enters in the weight of the face operators in the top multi-row of $\mathbf{D}^{m,n}(u)$, and (ii) the transfer tangle still depends on λ through the fugacity of closed loops $\beta = 2 \cos \lambda$ and the definition (2.1) of the face operators. This mimics the analogous construction for rational models [29]. For $m = 1$ and $n = 1$, the logarithmic minimal models $\mathcal{LM}(p, p')$ correspond to $\mu = \lambda$, but in general, μ may depend on the fusion indices. For example, the infinite family of higher-level logarithmic minimal models [34] are believed to correspond to $m = n$ and $\mu = n\lambda$. In the case $m = n = 2$, in particular, setting $\mu = 2\lambda$ indeed gives rise to logarithmic superconformal minimal models [35].

It is occasionally convenient to indicate explicitly the dependence on the crossing parameter λ by writing

$$\mathbf{D}^{m,n}(u) = \mathbf{D}^{m,n}(u, \lambda), \quad \mathbf{T}^{m,n}(u) = \mathbf{T}^{m,n}(u, \lambda). \quad (4.5)$$

It is also observed that $\mathbf{D}^{m,n}(u)$ and $\mathbf{T}^{m,n}(u)$ have the crossing and periodicity properties

$$\mathbf{D}^{m,n}(\mu - u_{n-1}) = \mathbf{D}^{m,n}(u), \quad R \mathbf{T}^{m,n}(\lambda - u) R = \mathbf{T}^{m,n}(u) \quad (4.6)$$

and

$$\mathbf{D}^{m,n}(u + \pi) = \mathbf{D}^{m,n}(u), \quad \mathbf{T}^{m,n}(u + \pi) = (-1)^{Nmn} \mathbf{T}^{m,n}(u), \quad (4.7)$$

where R is the reflection generator appearing in (2.31). For convenience, we recall the shorthand notations (1.12)

$$\mathbf{D}_k^{m,n} := \mathbf{D}^{m,n}(u + k\lambda), \quad \mathbf{T}_k^{m,n} := \mathbf{T}^{m,n}(u + k\lambda). \quad (4.8)$$

Crucially, the transfer tangles (4.3) and (4.4) form two separate *commuting families*,

$$[\mathbf{D}^{m,n}(u), \mathbf{D}^{m,n'}(v)] = 0, \quad [\mathbf{T}^{m,n}(u), \mathbf{T}^{m,n'}(v)] = 0. \quad (4.9)$$

Using diagrammatic arguments as in [29], this commutativity property follows from equations (3.11), (3.13) and (3.14).

As a consequence of the crossing relations (2.19) and the push-through properties (2.24), the multi-row transfer tangles $\mathbf{D}^{m,n}(u)$ and $\mathbf{T}^{m,n}(u)$ can be written in terms of $(m, 1)$ - and $(1, m)$ -fused face operators and a *single* P_n projector,

$$\begin{aligned} \mathbf{D}_0^{m,n} = & \begin{array}{c} \begin{array}{|c|c|c|c|c|} \hline \textcolor{blue}{(1,m)} & \textcolor{blue}{(1,m)} & \dots & \dots & \textcolor{blue}{(1,m)} \\ \hline u_{n-\mu} & u_{n-\mu} & & & u_{n-\mu} \\ \hline \vdots & \vdots & & & \vdots \\ \hline \textcolor{blue}{(1,m)} & \textcolor{blue}{(1,m)} & \dots & \dots & \textcolor{blue}{(1,m)} \\ \hline u_{2-\mu} & u_{2-\mu} & & & u_{2-\mu} \\ \hline \textcolor{blue}{(1,m)} & \textcolor{blue}{(1,m)} & \dots & \dots & \textcolor{blue}{(1,m)} \\ \hline u_{1-\mu} & u_{1-\mu} & & & u_{1-\mu} \\ \hline \textcolor{blue}{(m,1)} & \textcolor{blue}{(m,1)} & \dots & \dots & \textcolor{blue}{(m,1)} \\ \hline u_{n-1} & u_{n-1} & & & u_{n-1} \\ \hline \vdots & \vdots & & & \vdots \\ \hline \textcolor{blue}{(m,1)} & \textcolor{blue}{(m,1)} & \dots & \dots & \textcolor{blue}{(m,1)} \\ \hline u_1 & u_1 & & & u_1 \\ \hline \textcolor{blue}{(m,1)} & \textcolor{blue}{(m,1)} & \dots & \dots & \textcolor{blue}{(m,1)} \\ \hline u_0 & u_0 & & & u_0 \\ \hline \end{array} \\ \textcolor{red}{\text{---}} \textcolor{red}{n} \textcolor{red}{\text{---}} \end{array} \quad \mathbf{T}_0^{m,n} = \begin{array}{c} \begin{array}{|c|c|c|c|c|} \hline \textcolor{blue}{(m,1)} & \textcolor{blue}{(m,1)} & \dots & \dots & \textcolor{blue}{(m,1)} \\ \hline u_{n-1} & u_{n-1} & & & u_{n-1} \\ \hline \vdots & \vdots & & & \vdots \\ \hline \textcolor{blue}{(m,1)} & \textcolor{blue}{(m,1)} & \dots & \dots & \textcolor{blue}{(m,1)} \\ \hline u_1 & u_1 & & & u_1 \\ \hline \textcolor{blue}{(m,1)} & \textcolor{blue}{(m,1)} & \dots & \dots & \textcolor{blue}{(m,1)} \\ \hline u_0 & u_0 & & & u_0 \\ \hline \end{array} \\ \textcolor{red}{\text{---}} \textcolor{red}{n} \textcolor{red}{\text{---}} \end{array} \end{array} \quad (4.10)$$

It is noted that the connections indicated in blue are all single (not multiple) connections. Using the definition (3.1) in (4.3), push-through properties allow half-arc propagation towards the left both in the top n and bottom n layers of $\mathbf{D}^{m,n}(u)$ (\Leftarrow), whereas in (4.10), half-arcs propagate towards the right in the top fused faces, but towards the left in the bottom faces (\Rightarrow).

4.2 Effective projectors and fused transfer tangles for fractional λ

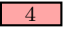
It is recalled from Section 2 that the WJ projectors fail to exist for some fractional λ . However, there is an important distinction between the roles of the WJ projectors P_n and P_m located along the vertical and horizontal interfaces (and edges), respectively, of the multi-row transfer tangles. We can actually ignore the projectors P_m along the horizontal interfaces and edges due to the push-through properties and because the transfer tangles are ultimately meant to act on so-called cabled link states whose characterisation will implement the projection offered by P_m , see Section 5. We will therefore not be concerned with questions about the existence of P_m until Section 5.

Regarding P_n , the above constructions of the multi-row transfer tangles $\mathbf{D}^{m,n}(u, \lambda)$ and $\mathbf{T}^{m,n}(u, \lambda)$ are ill-defined for some fractional λ . However, as we will discuss below, there exist alternative expressions for $\mathbf{D}^{m,n}(u, \lambda)$ and $\mathbf{T}^{m,n}(u, \lambda)$ which are manifestly equivalent to our original definition for generic λ , but are well defined for fractional λ as well (modulo potential issues with P_m). We view these alternative expressions as suitable starting points for generalisations to fractional λ . Alternatively, we could have taken any of these expressions and used it as our definition of the corresponding strip or cylinder transfer tangle. In doing so, however, many features and manipulations of the transfer tangles would become more involved and less transparent. This is why we prefer to work with the projector dependent constructions of Section 4.1.

To appreciate that we can avoid the projector P_n in (4.10), we consider the transfer tangle $\mathbf{D}^{m,n}(u)$ in the case $\mu = \lambda$, $m = 1$ and $n = 4$, where it readily follows from (2.42) and the push-through properties that

$$\begin{aligned}
\mathbf{D}_0^{1,4} = & \left(\begin{array}{|c|c|c|} \hline u_3 & \cdots & u_3 \\ \hline u_2 & \cdots & u_2 \\ \hline u_1 & \cdots & u_1 \\ \hline u_0 & \cdots & u_0 \\ \hline u_3 & \cdots & u_3 \\ \hline u_2 & \cdots & u_2 \\ \hline u_1 & \cdots & u_1 \\ \hline u_0 & \cdots & u_0 \\ \hline \end{array} \right) - [q^1(u_2)q^1(-u_0)]^N \left(\begin{array}{|c|c|c|} \hline u_3 & \cdots & u_3 \\ \hline u_0 & \cdots & u_0 \\ \hline u_3 & \cdots & u_3 \\ \hline u_0 & \cdots & u_0 \\ \hline \end{array} \right) \\
& - [q^1(u_3)q^1(-u_{-1})]^N \left(\begin{array}{|c|c|c|} \hline u_3 & \cdots & u_3 \\ \hline u_2 & \cdots & u_2 \\ \hline u_1 & \cdots & u_1 \\ \hline u_0 & \cdots & u_0 \\ \hline \end{array} \right) - [q^1(u_1)q^1(-u_1)]^N \left(\begin{array}{|c|c|c|} \hline u_1 & \cdots & u_1 \\ \hline u_0 & \cdots & u_0 \\ \hline u_3 & \cdots & u_3 \\ \hline u_2 & \cdots & u_2 \\ \hline \end{array} \right) \\
& + [q^1(u_1)q^1(u_3)q^1(-u_{-1})q^1(-u_1)]^N \mathbf{I}.
\end{aligned} \tag{4.11}$$

It is emphasized that this expression is *independent* of WJ projectors and thus well defined for all $N \in \mathbb{N}$ and $\beta \in \mathbb{C}$. It can therefore serve as a definition of $\mathbf{D}_0^{1,4}$ for all $\lambda \in \pi(\mathbb{R} \setminus \mathbb{Z})$, in particular for fractional λ .

Effective projectors For $\beta \neq 0$, there is a neat way to encode the above result for $D_0^{1,4}$. In the definition (4.10) of $D_0^{1,4}$, one can replace the P_4 projector, , by the 4-tangle

$$\text{orange box with } 4 := \begin{array}{|c|} \hline \text{four vertical lines} \\ \hline \end{array} - \frac{1}{\beta} \left(\begin{array}{|c|} \hline \text{two crossings} \\ \hline \end{array} + \begin{array}{|c|} \hline \text{two crossings} \\ \hline \end{array} + \begin{array}{|c|} \hline \text{two crossings} \\ \hline \end{array} \right) + \frac{1}{\beta^2} \begin{array}{|c|} \hline \text{two crossings} \\ \hline \end{array} \quad (4.12)$$

Indeed, it is readily verified that this prescription correctly reproduces the decomposition (4.11).

For $\beta \neq 0$, this construction extends to general $n \in \mathbb{N}$, replacing the WJ projector P_n by the *effective projector*

$$Q_n = \text{orange box with } n, \quad n \in \mathbb{N} \quad (4.13)$$

defined recursively as

$$\text{orange box with } n = \text{orange box with } n-1 \text{ followed by a vertical line} - \frac{1}{\beta} \text{orange box with } n-2 \text{ followed by a crossing}, \quad \text{orange box with } 1 := \text{vertical line}, \quad \text{orange box with } 2 := \text{two vertical lines} - \frac{1}{\beta} \text{crossing} \quad (4.14)$$

Written in terms of elements of $TL_n(\beta)$, Q_n is simply given by

$$Q_n = I + \sum_{k=1}^{\lfloor \frac{n}{2} \rfloor} \sum_{1 \leq j_1 \ll j_2 \ll \dots \ll j_k \leq n-1} \left(-\frac{1}{\beta}\right)^k e_{j_1} e_{j_2} \dots e_{j_k} \quad (4.15)$$

where $a \ll b$ here means that $a \leq b-2$.

It is emphasised that, for $n > 2$, Q_n is not a projector as it violates the condition for property (2.45) of the WJ projectors. It likewise does not have the fundamental properties (2.46) and (2.47) of the WJ projectors. However, the following proposition, which we prove in Appendix C, states that the expressions (4.10) for $D_0^{m,n}$ and $T_0^{m,n}$ are equal to the corresponding tangles with the projectors P_n replaced by Q_n . This result thus explains why we refer to the n -tangle Q_n as an effective projector.

PROPOSITION 4.1 *For λ generic, the transfer tangles can be expressed in terms of effective projectors as*

$$D_0^{m,n} = \begin{array}{c} \text{Diagram of } D_0^{m,n} \text{ with } n \text{ vertical lines and } m \text{ horizontal lines, with blue loops on the left and right sides.} \end{array} \quad T_0^{m,n} = \begin{array}{c} \text{Diagram of } T_0^{m,n} \text{ with } n \text{ vertical lines and } m \text{ horizontal lines, with blue lines on the left and right sides.} \end{array} \quad (4.16)$$

Since the expressions (4.16) are based on the effective projector Q_n , they are well defined for all $\beta \in \mathbb{C}^*$ and can therefore serve as definitions of the transfer tangles for fractional λ for which $2 \cos \lambda \neq 0$. The argument extends to $\beta = 0$ in the following way. For each tangle in the decomposition (4.15) applied to (4.16), the factor $(\frac{1}{\beta})^k$ is exactly cancelled by a factor β^k coming from closed loops that appear

in the simplification of the tangle. As in (4.11), the decomposition coefficients are thereby rendered nonsingular at $\beta = 0$.

As we will discuss in Sections 6.1 and 6.2, there exists yet another way, valid for all $\lambda \in \pi(\mathbb{R} \setminus \mathbb{Z})$, to write $\mathbf{D}^{m,n}(u)$ and $\mathbf{T}^{m,n}(u)$ without the use of P_n , namely the determinant forms in (6.4) and (6.7).

Having established that $\mathbf{D}^{m,n}(u)$ in (4.3) and $\mathbf{T}^{m,n}(u)$ in (4.4) for generic λ can be rewritten in a form independent of the projector P_n , we may view the transfer tangles for fractional $\lambda = \lambda_{p,p'}$ and $m < p'$ as

$$\mathbf{D}^{m,n}(u, \lambda_{p,p'}) = \lim_{\lambda \rightarrow \lambda_{p,p'}} \mathbf{D}^{m,n}(u, \lambda), \quad \mathbf{T}^{m,n}(u, \lambda_{p,p'}) = \lim_{\lambda \rightarrow \lambda_{p,p'}} \mathbf{T}^{m,n}(u, \lambda), \quad 1 \leq m \leq p' - 1, \quad n \in \mathbb{N}. \quad (4.17)$$

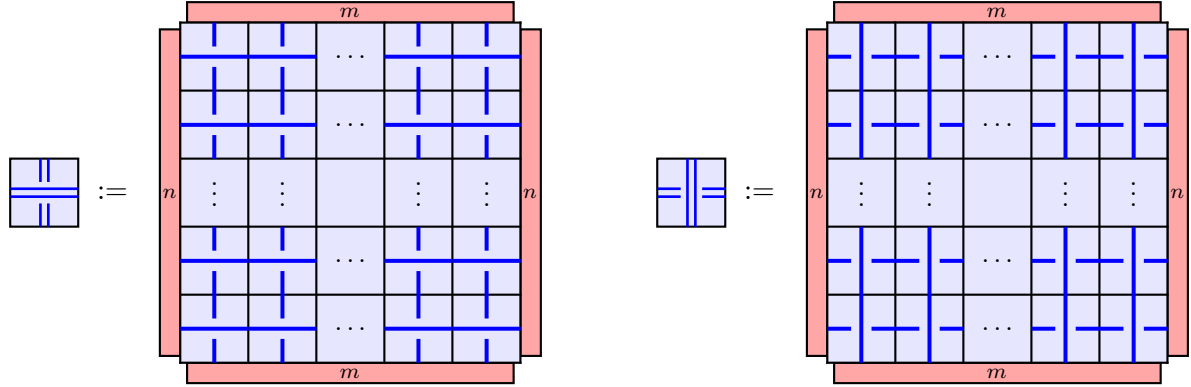
We note that the arguments of these limits are given by projector *dependent* transfer tangles. The existence of the limits implies that every coefficient in the decomposition of these tangles in elementary connectivity diagrams is nonsingular at $\lambda = \lambda_{p,p'}$. As already indicated, potential issues with the projectors along the horizontal edges disappear for the fused link states representations $\rho_{N,m}^d$ and $\tilde{\rho}_{N,m}^d$ introduced in Section 5, so the limits

$$\begin{aligned} \rho_{N,m}^d[\mathbf{D}^{m,n}(u, \lambda_{p,p'})] &= \lim_{\lambda \rightarrow \lambda_{p,p'}} \rho_{N,m}^d[\mathbf{D}^{m,n}(u, \lambda)], \\ \tilde{\rho}_{N,m}^d[\mathbf{T}^{m,n}(u, \lambda_{p,p'})] &= \lim_{\lambda \rightarrow \lambda_{p,p'}} \tilde{\rho}_{N,m}^d[\mathbf{T}^{m,n}(u, \lambda)], \end{aligned} \quad m, n \in \mathbb{N} \quad (4.18)$$

for the corresponding *transfer matrices* are well defined for all $m, n \in \mathbb{N}$. This further implies that relations between transfer *tangles* obtained by diagrammatic manipulations for λ generic are valid for the transfer *matrices* in the $\lambda \rightarrow \lambda_{p,p'}$ limit. As we will discuss in Section 7, additional special relations hold for fractional λ .

4.3 Braid transfer tangles

(m, n) -fused braid operators are defined by

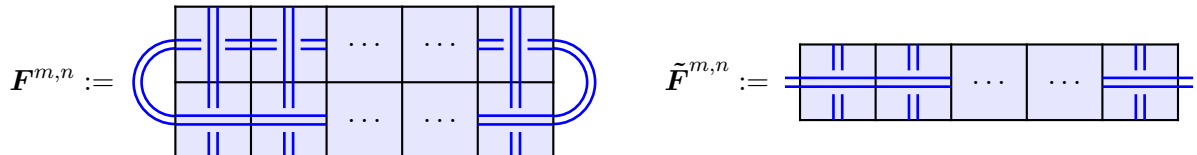


$$\begin{aligned} \begin{array}{|c|} \hline \text{---} \\ \hline \text{---} \\ \hline \end{array} &:= \begin{array}{|c|} \hline \text{---} \\ \hline \text{---} \\ \hline \end{array} \\ \begin{array}{|c|} \hline \text{---} \\ \hline \text{---} \\ \hline \end{array} &:= \begin{array}{|c|} \hline \text{---} \\ \hline \text{---} \\ \hline \end{array} \end{aligned} \quad (4.19)$$

and appear in the braid limit of (m, n) -fused faces,

$$\begin{aligned} \begin{array}{|c|} \hline \text{---} \\ \hline \text{---} \\ \hline \end{array} &= \lim_{u \rightarrow i\infty} \left(\prod_{i=0}^{m-1} \prod_{j=0}^{n-1} \frac{e^{i\frac{\pi-\lambda}{2}}}{s_{j-i}(u_k)} \begin{array}{|c|} \hline \text{---} \\ \hline \text{---} \\ \hline \end{array} \right), & \begin{array}{|c|} \hline \text{---} \\ \hline \text{---} \\ \hline \end{array} &= \lim_{u \rightarrow i\infty} \left(\prod_{i=0}^{m-1} \prod_{j=0}^{n-1} \frac{e^{i\frac{\pi-\lambda}{2}}}{s_{i-j}(u_k)} \begin{array}{|c|} \hline \text{---} \\ \hline \text{---} \\ \hline \end{array} \right). \end{aligned} \quad (4.20)$$

In terms of these, the *fused braid transfer tangles* are defined as



$$\mathbf{F}^{m,n} := \begin{array}{|c|} \hline \text{---} \\ \hline \text{---} \\ \hline \end{array} \quad \tilde{\mathbf{F}}^{m,n} := \begin{array}{|c|} \hline \text{---} \\ \hline \text{---} \\ \hline \end{array} \quad (4.21)$$

and appear in the braid limit as

$$\mathbf{F}^{m,n} = \lim_{u \rightarrow i\infty} \left(\left(\prod_{i=0}^{m-1} \prod_{j=0}^{n-1} \frac{e^{i(\pi-\lambda)}}{s_{j-i}(u) s_{i-j}(u_n - \mu)} \right)^N \mathbf{D}_0^{m,n} \right), \quad \tilde{\mathbf{F}}^{m,n} = \lim_{u \rightarrow i\infty} \left(\left(\prod_{i=0}^{m-1} \prod_{j=0}^{n-1} \frac{e^{i\frac{\pi-\lambda}{2}}}{s_{j-i}(u)} \right)^N \mathbf{T}_0^{m,n} \right). \quad (4.22)$$

5 Matrix representations

In this section, we identify states and modules on which the fused transfer tangles can act. A primary goal is to resolve the issue with the non-existence of some P_m projectors for fractional λ . Initially, we let λ be generic and we commence by making some algebraic observations before discussing the construction of states and representations. To build these for $m > 1$ and generic λ , we adopt the defect preserving diagrammatic action of tangles on link states used in the construction of standard modules for $m = 1$ in Section 2. We conclude by turning our attention to fractional λ , by showing that the P_m projectors play no role in the matrix representations for the transfer tangles.

Transfer tangles without P_m projectors The push-through properties allow us to write

$$\mathbf{D}^{m,n}(u) = \mathbf{I}^m \bar{\mathbf{D}}^{m,n}(u) \mathbf{I}^m, \quad \mathbf{T}^{m,n}(u) = \mathbf{I}^m \bar{\mathbf{T}}^{m,n}(u) \mathbf{I}^m, \quad (5.1)$$

where $\bar{\mathbf{D}}^{m,n}(u)$ and $\bar{\mathbf{T}}^{m,n}(u)$ are identical to (4.3) and (4.4), but with all P_m projectors removed. That is,

$$\bar{\mathbf{D}}^{m,n}(u) := \begin{array}{|c|c|c|c|c|} \hline \begin{array}{c} (m,n) \\ \mu - u_{n-1} \end{array} & \begin{array}{c} (m,n) \\ \mu - u_{n-1} \end{array} & \cdots & \cdots & \begin{array}{c} (m,n) \\ \mu - u_{n-1} \end{array} \\ \hline \begin{array}{c} (m,n) \\ u \end{array} & \begin{array}{c} (m,n) \\ u \end{array} & \cdots & \cdots & \begin{array}{c} (m,n) \\ u \end{array} \\ \hline \end{array} \quad (5.2)$$

and

$$\bar{\mathbf{T}}^{m,n}(u) := \begin{array}{|c|c|c|c|c|} \hline \begin{array}{c} (m,n) \\ u \end{array} & \begin{array}{c} (m,n) \\ u \end{array} & \cdots & \cdots & \begin{array}{c} (m,n) \\ u \end{array} \\ \hline \end{array} \quad (5.3)$$

where

$$\begin{array}{|c|} \hline \begin{array}{c} (m,n) \\ u \end{array} \\ \hline \end{array} := \begin{array}{|c|c|c|c|c|} \hline u_{n-m} & \cdots & \cdots & u_{n-2} & u_{n-1} \\ \hline \vdots & & & \vdots & \vdots \\ \hline \vdots & & & \vdots & \vdots \\ \hline u_{2-m} & \cdots & \cdots & u_0 & u_1 \\ \hline u_{1-m} & \cdots & \cdots & u_{-1} & u_0 \\ \hline \end{array} \quad (5.4)$$

To distinguish these fused faces with projectors only on the left and right, we indicate the orientation with a small square instead of the usual small arc. In fact, the push-through properties allow us to simplify (5.1) and write

$$\mathbf{D}^{m,n}(u) = \mathbf{I}^m \bar{\mathbf{D}}^{m,n}(u), \quad \mathbf{T}^{m,n}(u) = \mathbf{I}^m \bar{\mathbf{T}}^{m,n}(u). \quad (5.5)$$

We also note that

$$\bar{\mathbf{I}}^m = \mathbf{I} \quad (5.6)$$

and that we can elevate the limit (4.18) from matrices to tangles as

$$\bar{\mathbf{D}}^{m,n}(u, \lambda_{p,p'}) = \lim_{\lambda \rightarrow \lambda_{p,p'}} \bar{\mathbf{D}}^{m,n}(u, \lambda), \quad \bar{\mathbf{T}}^{m,n}(u, \lambda_{p,p'}) = \lim_{\lambda \rightarrow \lambda_{p,p'}} \bar{\mathbf{T}}^{m,n}(u, \lambda), \quad m, n \in \mathbb{N}. \quad (5.7)$$

Fused Temperley-Lieb algebra Focusing on the situation on the strip, we introduce

$$FTL_{N,m}(\beta) := \left\langle x \in TL_{Nm}(\beta) \mid \exists \bar{x} \in TL_{Nm}(\beta) \text{ such that } x = \mathbf{I}^m \bar{x} \mathbf{I}^m = \mathbf{I}^m \bar{x} \right\rangle \quad (5.8)$$

which is a subalgebra of $TL_{Nm}(\beta)$ since

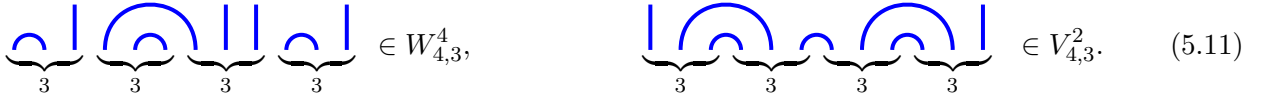
$$x_1, x_2 \in FTL_{N,m}(\beta) \Rightarrow \begin{cases} x_1 + x_2 = \mathbf{I}^m(\bar{x}_1 + \bar{x}_2)\mathbf{I}^m = \mathbf{I}^m(\bar{x}_1 + \bar{x}_2) & \in FTL_{N,m}(\beta), \\ x_1 x_2 = \begin{cases} (\mathbf{I}^m \bar{x}_1 \mathbf{I}^m)(\mathbf{I}^m \bar{x}_2 \mathbf{I}^m) = \mathbf{I}^m(\bar{x}_1 \bar{x}_2)\mathbf{I}^m \\ (\mathbf{I}^m \bar{x}_1)(\mathbf{I}^m \bar{x}_2) = \mathbf{I}^m(\bar{x}_1 \bar{x}_2) \end{cases} & \in FTL_{N,m}(\beta). \end{cases} \quad (5.9)$$

Tacitly assuming that the direction of transfer is vertical, the transfer tangle $\mathbf{D}^{m,n}(u)$ is an element of $FTL_{N,m}(\beta)$. It is also noted that \mathbf{I}^m is in the algebra $FTL_{N,m}(\beta)$ and that it plays the role of the identity. On the cylinder, we similarly introduce

$$F\mathcal{EPTL}_{N,m}(\alpha, \beta) := \left\langle x \in \mathcal{EPTL}_{Nm}(\alpha, \beta) \mid \exists \bar{x} \in \mathcal{EPTL}_{Nm}(\alpha, \beta) \text{ such that } x = \mathbf{I}^m \bar{x} \mathbf{I}^m = \mathbf{I}^m \bar{x} \right\rangle \quad (5.10)$$

which is a subalgebra of $\mathcal{EPTL}_{Nm}(\alpha, \beta)$ and includes $\mathbf{T}^{m,n}(u)$ as one of its elements.

Cabled link states On the strip, we define an m -cabled link state on Nm nodes with d defects as a (canonical basis) link state in $V_{N \times m}^d$ that does not have a half-arc linking a pair of nodes located between positions $\ell m + 1$ and $(\ell + 1)m$ for any $\ell \in \{0, \dots, N - 1\}$. This generalises the construction for $m = 2$ in [35]. The linear span of m -cabled link states is denoted by $V_{N,m}^d$ and its complement $W_{N,m}^d$ in $V_{N \times m}^d$ is generated by the link states having at least one half-arc linking a pair of nodes located between positions $\ell m + 1$ and $(\ell + 1)m$ for some $\ell \in \{0, \dots, N - 1\}$. We illustrate this characterisation of link states with a link state in $V_{4 \times 3}^4$ and one in $V_{4 \times 3}^2$, namely

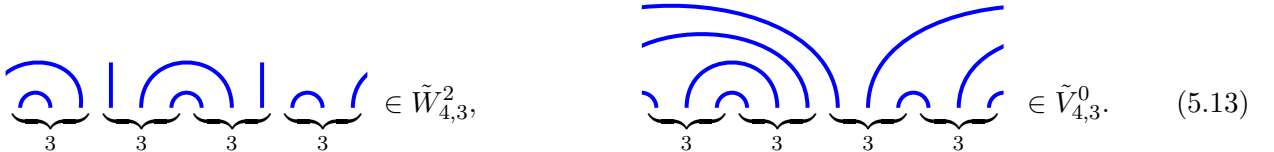


$$\underbrace{\quad}_3 \underbrace{\quad}_3 \underbrace{\quad}_3 \underbrace{\quad}_3 \in W_{4,3}^4, \quad \underbrace{\quad}_3 \underbrace{\quad}_3 \underbrace{\quad}_3 \underbrace{\quad}_3 \in V_{4,3}^2. \quad (5.11)$$

As indicated, only the second of these is a 3-cabled link state. It is also noted that the defect number d is subject to the constraints

$$0 \leq d \leq Nm, \quad Nm - d = 0 \pmod{2}. \quad (5.12)$$

Similarly on the cylinder, an m -cabled link state on Nm nodes with d defects is defined as a link state in the canonical basis of $\tilde{V}_{N \times m}^d$ with no half-arc linking, via the front of the cylinder, two nodes located between positions $\ell m + 1$ and $(\ell + 1)m$ for any $\ell \in \{0, \dots, N - 1\}$. The linear span of these m -cabled link states is denoted by $\tilde{V}_{N,m}^d$ and its complement $\tilde{W}_{N,m}^d$ in $\tilde{V}_{N \times m}^d$ is generated by the link states having at least one half-arc linking, via the front of the cylinder, a pair of nodes located between positions $\ell m + 1$ and $(\ell + 1)m$ for some $\ell \in \{0, \dots, N - 1\}$. Examples are



$$\underbrace{\quad}_3 \underbrace{\quad}_3 \underbrace{\quad}_3 \underbrace{\quad}_3 \in \tilde{W}_{4,3}^2, \quad \underbrace{\quad}_3 \underbrace{\quad}_3 \underbrace{\quad}_3 \underbrace{\quad}_3 \in \tilde{V}_{4,3}^0. \quad (5.13)$$

The spaces $V_{N \times m}^d$ and $\tilde{V}_{N \times m}^d$ thus decompose as

$$V_{N \times m}^d = V_{N,m}^d \oplus W_{N,m}^d, \quad \tilde{V}_{N \times m}^d = \tilde{V}_{N,m}^d \oplus \tilde{W}_{N,m}^d, \quad (5.14)$$

and we let $\mathcal{P}_{N,m}^d$ and $\tilde{\mathcal{P}}_{N,m}^d$ be the corresponding matrix projectors from $V_{N \times m}^d$ and $\tilde{V}_{N \times m}^d$ onto $V_{N,m}^d$ and $\tilde{V}_{N,m}^d$, respectively. With respect to the decompositions (5.14), these matrices are of the form

$$\mathcal{P}_{N,m}^d = \begin{pmatrix} I & 0 \\ 0 & 0 \end{pmatrix}, \quad \tilde{\mathcal{P}}_{N,m}^d = \begin{pmatrix} I & 0 \\ 0 & 0 \end{pmatrix}. \quad (5.15)$$

It is stressed that the decompositions (5.14) and the matrix projectors are well defined for all $m \in \mathbb{N}$, independently of λ .

In Appendix D, we prove that the numbers of m -cabled link states on the strip and cylinder, respectively, for N and d subject to (5.12) are given by

$$\dim V_{N,m}^d = \binom{N}{\frac{Nm-d}{2}}_m - \binom{N}{\frac{Nm-d-2}{2}}_m, \quad \dim \tilde{V}_{N,m}^d = \binom{N}{\frac{Nm-d}{2}}_m, \quad (5.16)$$

see Propositions D.1 and D.2. Here the $(m+1)$ -nomial coefficients $\binom{N}{k}_m$, with $k \in \{0, \dots, Nm\}$, are defined as the expansion coefficients of the generating function

$$\left[\sum_{i=0}^m z^i \right]^N = \sum_{k=0}^{Nm} \binom{N}{k}_m z^k, \quad N, m \in \mathbb{N}_0. \quad (5.17)$$

For $m = 1, 2$, these coefficients are recognised as the usual binomial and trinomial coefficients, respectively. In Appendix D, we also discuss how these sets of link states are related to certain classes of lattice paths.

Generalised standard modules By construction of the link states in $W_{N,m}^d$, the diagrammatic action of $x \in FTL_{N,m}(\beta)$ on $w \in W_{N,m}^d$ yields $xw = 0$ due to the presence of \mathbf{I}^m in x . The space $W_{N,m}^d$ is therefore trivially stable under the action of $FTL_{N,m}(\beta)$. As a similar argument applies in the cylinder case, we can view the quotient spaces

$$V_{N,m}^d = V_{N \times m}^d / W_{N,m}^d, \quad \tilde{V}_{N,m}^d = \tilde{V}_{N \times m}^d / \tilde{W}_{N,m}^d \quad (5.18)$$

as vector spaces on which representations of $FTL_{N,m}(\beta)$ and its cylinder counterpart are built. Decomposing the matrix representative $\rho_{N \times m}^d(x)$ of an element $x \in FTL_{N,m}(\beta)$ on $V_{N \times m}^d$ with respect to (5.14) as

$$\rho_{N \times m}^d(x) = \begin{pmatrix} A_x & 0 \\ C_x & 0 \end{pmatrix}, \quad (5.19)$$

the corresponding representation $\rho_{N,m}^d$ of $FTL_{N,m}(\beta)$ on $V_{N,m}^d$ is obtained by using the matrix projector $\mathcal{P}_{N,m}^d$ introduced in (5.15), or equivalent by taking the upper-left matrix minor $M_{N,m}^d$ of the appropriate size,

$$\rho_{N,m}^d(x) := M_{N,m}^d [\rho_{N \times m}^d(x)] = A_x. \quad (5.20)$$

From

$$\rho_{N \times m}^d(x_1 x_2) = \begin{pmatrix} A_{x_1} A_{x_2} & 0 \\ C_{x_1} A_{x_2} & 0 \end{pmatrix}, \quad (5.21)$$

it readily follows that $\rho_{N,m}^d$ is a representation of $FTL_{N,m}(\beta)$, that is,

$$\rho_{N,m}^d(x_1 x_2) = A_{x_1} A_{x_2} = \rho_{N,m}^d(x_1) \rho_{N,m}^d(x_2). \quad (5.22)$$

In stark contrast, the matrices $M_{N,m}^d [\rho_{N \times m}^d(y)]$, $y \in T L_{Nm}(\beta)$, do not constitute representations of $T L_{N \times m}(\beta)$ for $m \geq 2$.

The construction of matrix representations $\tilde{\rho}_{N,m}^d$ of $F\mathcal{E}PTL_N(\alpha, \beta)$ is similar. Thus, for simplicity, the arguments are given for $\rho_{N,m}^d$ only.

Representations for fractional λ Let v be an element of $V_{N \times m}^d$ and decompose it as

$$v = v' + w, \quad v' \in V_{N,m}^d, \quad w \in W_{N,m}^d. \quad (5.23)$$

From the definition of \mathbf{I}^m , it satisfies

$$\mathbf{I}^m v = \mathbf{I}^m v' = v' + w', \quad w' \in W_{N,m}^d \quad (5.24)$$

from which it follows that

$$\rho_{N \times m}^d(\mathbf{I}^m) = \begin{pmatrix} I & 0 \\ S & 0 \end{pmatrix}, \quad \rho_{N,m}^d(\mathbf{I}^m) = I, \quad (5.25)$$

where I is the identity matrix of size $\dim V_{N,m}^d$ and S is a λ -dependent rectangular matrix that can have singularities for fractional λ . Then, for some $x \in FTL_{N,m}(\beta)$, the corresponding \bar{x} satisfies

$$\rho_{N \times m}^d(\bar{x}) = \begin{pmatrix} A_{\bar{x}} & B_{\bar{x}} \\ C_{\bar{x}} & D_{\bar{x}} \end{pmatrix} \quad (5.26)$$

and because $x = \mathbf{I}^m \bar{x}$,

$$A_x = \rho_{N,m}^d(x) = M_{N,m}^d \left[\begin{pmatrix} I & 0 \\ S & 0 \end{pmatrix} \begin{pmatrix} A_{\bar{x}} & B_{\bar{x}} \\ C_{\bar{x}} & D_{\bar{x}} \end{pmatrix} \right] = A_{\bar{x}}. \quad (5.27)$$

This shows that, for fractional λ , if \bar{x} exists, $\rho_{N,m}^d(x)$ is free of singularities. These arguments carry over to the cylinder case. We thus conclude that, for the action on cabled link states, it is equivalent to work with $\bar{\mathbf{D}}^{m,n}(u)$ and $\bar{\mathbf{T}}^{m,n}(u)$ instead of the transfer tangles $\mathbf{D}^{m,n}(u)$ and $\mathbf{T}^{m,n}(u)$. The expression on the righthand side of (5.27), in particular, does not involve any P_m projectors. Furthermore, recalling that the potential singularities arising from P_n projectors were dealt with using the corresponding effective projectors Q_n in Section 4.2, we see that we can compute matrix representations of the transfer tangles *without employing any projectors at all*. It follows that the proposed matrix representatives of $\mathbf{D}^{m,n}(u)$ and $\mathbf{T}^{m,n}(u)$ are well behaved for all $m, n \in \mathbb{N}$ and λ generic or fractional alike.

The modules built from the defect preserving diagrammatic action on $V_{N,m}^d$ or $\tilde{V}_{N,m}^d$ resemble the standard modules reviewed in Section 2. This class of modules is certainly not exhaustive, though, as more general modules and representations can be envisaged and are known to exist for $m = 1$. For example, representations of $TL_N(\beta)$ where defects can be annihilated in pairs appear naturally in the study of transfer tangles with nontrivial boundary conditions [1, 6, 55, 56]. The above construction of matrix representations without projectors can be extended to this larger class of modules.

As a final remark, we stress that we have defined the cabled link states *without* the use of projectors. Although it might seem natural a priori to include projectors in their definition by considering $\{\mathbf{I}^m v; v \in V_{N \times m}^d\}$ instead of $V_{N,m}^d$, and similarly on the cylinder, it is generally not appropriate in scenarios with $\lambda = \lambda_{p,p'}$ and $m \geq p'$. However, if one makes specific assumptions about $\lambda_{p,p'}$ (or β) to ensure the existence of the projector P_m , one can of course choose to work with cabled link states defined using these projectors. This is indeed the situation in [35], where the main focus is on the (2, 2)-fused case and β is assumed non-vanishing such that P_2 exists.

Braid transfer matrices Using arguments as in [57] and [58], one can show that the braid transfer tangles $\mathbf{F}^{m,n}$ and $\tilde{\mathbf{F}}^{m,n}$ are in the center of $FTL_{N,m}(\beta)$ and $F\mathcal{E}PTL_{N,m}(\alpha, \beta)$, respectively. They furthermore act as scalar multiples of the identity on $V_{N,m}^d$ and $\tilde{V}_{N,m}^d$, respectively, that is

$$\rho_{N,m}^d(\mathbf{F}^{m,n}) = \mathcal{U}_n^d I, \quad \tilde{\rho}_{N,m}^d(\tilde{\mathbf{F}}^{m,n}) = \tilde{\mathcal{U}}_n^d I \quad (5.28)$$

where I is the identity matrix of dimension $\dim V_{N,m}^d$ or $\dim \tilde{V}_{N,m}^d$, respectively, and the constants \mathcal{U}_n^d and $\tilde{\mathcal{U}}_n^d$ are real, independent of N and m and given by

$$\mathcal{U}_n^d = (-1)^{nd} \frac{\sin((n+1)(d+1)\lambda)}{\sin((d+1)\lambda)}, \quad \tilde{\mathcal{U}}_n^d = \frac{\sin((n+1)\frac{d}{2}(\pi - \lambda))}{\sin(\frac{d}{2}(\pi - \lambda))}. \quad (5.29)$$

6 Fusion hierarchies and T - and Y -systems

In this section, we show that for fixed m and λ , the commuting fused transfer tangles (4.10) with different vertical fusion index n are not all independent. Both on the strip and cylinder in Sections 6.1 and 6.2, we present a set of relations, the *fusion hierarchy*, relating transfer tangles with different vertical stacks of face operators. In Sections 6.3 and 6.4, we then show how the fusion hierarchy in each case translates into T - and Y -systems for the transfer tangles.

The proofs of Propositions 6.1 and 6.2 are provided in Appendices E.1 and E.2, respectively. There, the diagrammatic manipulations in the planar algebra are made for λ generic. However, it is recalled that the barred transfer tangles $\bar{\mathbf{D}}^{m,n}(u)$ and $\bar{\mathbf{T}}^{m,n}(u)$ are well defined for all $\lambda \in \pi(\mathbb{R} \setminus \mathbb{Z})$ (see Sections 4.2 and 5). The results presented in the five Propositions 6.1–6.5 for the transfer tangles $\mathbf{D}^{m,n}(u)$ and $\mathbf{T}^{m,n}(u)$ are therefore valid for the barred transfer tangles for λ generic and fractional alike. The results are likewise valid for the transfer tangles themselves for all fractional λ for which P_m exists. In all cases, the results are valid for the corresponding transfer matrices in the representations discussed in Section 5.

6.1 Fusion hierarchy on the strip

PROPOSITION 6.1 *On the strip, the fusion hierarchy for $m, n \in \mathbb{N}$ is given by*

$$\begin{aligned} \mathbf{D}_0^{m,n} \mathbf{D}_n^{m,1} &= \frac{s_n(2u - \mu)s_{2n-1}(2u - \mu)}{s_{n-1}(2u - \mu)s_{2n}(2u - \mu)} \mathbf{D}_0^{m,n+1} \\ &\quad + \frac{s_{n-2}(2u - \mu)s_{2n+1}(2u - \mu)}{s_{n-1}(2u - \mu)s_{2n}(2u - \mu)} [q^m(u_n)q^m(\mu - u_{n-1})]^N \mathbf{D}_0^{m,n-1} \end{aligned} \quad (6.1)$$

where $q^m(u)$ is defined in (1.11).

In terms of the renormalised transfer tangles $\hat{\mathbf{D}}_k^{m,n}$ defined in (1.13), equation (6.1) can be expressed as

$$\hat{\mathbf{D}}_0^{m,n} \hat{\mathbf{D}}_n^{m,1} = \hat{\mathbf{D}}_0^{m,n+1} + f_n^m f_{n-2}^m \hat{\mathbf{D}}_0^{m,n-1} \quad (6.2)$$

where f_k^m is defined in (1.16) and it is noted that

$$\hat{\mathbf{D}}_k^{m,n} = \hat{\mathbf{D}}_0^{m,n}(u + k\lambda), \quad f_k^m = f_0^m(u + k\lambda). \quad (6.3)$$

Equivalently, we have the determinant expression

$$\hat{\mathbf{D}}_0^{m,n+1} = \begin{vmatrix} \hat{\mathbf{D}}_0^{m,1} & f_{-1}^m & 0 & 0 & 0 \\ f_1^m & \hat{\mathbf{D}}_1^{m,1} & f_0^m & 0 & 0 \\ 0 & f_2^m & \ddots & \ddots & 0 \\ 0 & 0 & \ddots & \hat{\mathbf{D}}_{n-1}^{m,1} & f_{n-2}^m \\ 0 & 0 & 0 & f_n^m & \hat{\mathbf{D}}_n^{m,1} \end{vmatrix} \quad (6.4)$$

where non-tangle entries are understood to be multiplied by \mathbf{I}^m . Likewise, the braid transfer tangles satisfy

$$\mathbf{F}^{m,n+1} = \mathbf{F}^{m,n} \mathbf{F}^{m,1} - \mathbf{F}^{m,n-1} = U_{n+1} \left(\frac{1}{2} \mathbf{F}^{m,1} \right) = \begin{vmatrix} \mathbf{F}^{m,1} & 1 & 0 & 0 & 0 \\ 1 & \mathbf{F}^{m,1} & 1 & 0 & 0 \\ 0 & 1 & \ddots & \ddots & 0 \\ 0 & 0 & \ddots & \mathbf{F}^{m,1} & 1 \\ 0 & 0 & 0 & 1 & \mathbf{F}^{m,1} \end{vmatrix} \quad (6.5)$$

where $U_n(x)$ are Chebyshev polynomials of the second kind, and the matrix on the righthand side has dimension $n + 1$. This result for the braid transfer tangles can be shown either by the diagrammatic arguments underlying Proposition 6.1 in Appendix E.1, or by taking the appropriate braid limit of (6.1) and (6.4).

6.2 Fusion hierarchy on the cylinder

PROPOSITION 6.2 *On the cylinder, the fusion hierarchy for $m, n \in \mathbb{N}$ is given by*

$$\mathbf{T}_0^{m,n} \mathbf{T}_n^{m,1} = \mathbf{T}_0^{m,n+1} + h_n^m h_{n-2}^m \mathbf{T}_0^{m,n-1}, \quad (6.6)$$

where h_k^m is defined in (1.16).

The general fusion hierarchy can be rewritten in the determinant form

$$\mathbf{T}_0^{m,n+1} = \begin{vmatrix} \mathbf{T}_0^{m,1} & h_{-1}^m & 0 & 0 & 0 \\ h_1^m & \mathbf{T}_1^{m,1} & h_0^m & 0 & 0 \\ 0 & h_2^m & \ddots & \ddots & 0 \\ 0 & 0 & \ddots & \mathbf{T}_{n-1}^{m,1} & h_{n-2}^m \\ 0 & 0 & 0 & h_n^m & \mathbf{T}_n^{m,1} \end{vmatrix}. \quad (6.7)$$

The braid transfer tangles on the cylinder form a hierarchy identical to the one on the strip (6.5), namely

$$\tilde{\mathbf{F}}^{m,n+1} = \tilde{\mathbf{F}}^{m,n} \tilde{\mathbf{F}}^{m,1} - \tilde{\mathbf{F}}^{m,n-1} = U_{n+1}(\tfrac{1}{2} \tilde{\mathbf{F}}^{m,1}) = \begin{vmatrix} \tilde{\mathbf{F}}^{m,1} & 1 & 0 & 0 & 0 \\ 1 & \tilde{\mathbf{F}}^{m,1} & 1 & 0 & 0 \\ 0 & 1 & \ddots & \ddots & 0 \\ 0 & 0 & \ddots & \tilde{\mathbf{F}}^{m,1} & 1 \\ 0 & 0 & 0 & 1 & \tilde{\mathbf{F}}^{m,1} \end{vmatrix}. \quad (6.8)$$

6.3 T -systems

From the fusion hierarchy (6.2), we derive the T -system on the strip. This is the content of the following proposition.

PROPOSITION 6.3 *For $m, n \in \mathbb{N}$, the T -system on the strip is given by*

$$\hat{D}_0^{m,n} \hat{D}_1^{m,n} = \hat{D}_0^{m,n+1} \hat{D}_1^{m,n-1} + \nu_0^{(n)} \mathbf{I}^m, \quad (6.9)$$

where $\nu_0^{(n)}$ is defined in (1.17).

PROOF: For $n = 1$, equation (6.9) is trivially true as it coincides with (6.2). Following arguments given in [16], we prove (6.9) recursively. First, we use the commutativity of the transfer tangles and equation (6.2) to obtain

$$\begin{aligned} \hat{D}_0^{m,n} (\hat{D}_1^{m,n-1} \hat{D}_n^{m,1}) &= (\hat{D}_0^{m,n} \hat{D}_n^{m,1}) \hat{D}_1^{m,n-1}, \\ \hat{D}_0^{m,n} (\hat{D}_1^{m,n} + f_n^m f_{n-2}^m \hat{D}_1^{m,n-2}) &= (\hat{D}_0^{m,n+1} + f_n^m f_{n-2}^m \hat{D}_0^{m,n-1}) \hat{D}_1^{m,n-1}. \end{aligned} \quad (6.10)$$

Rearranging terms and assuming equation (6.9) for $n - 1$ subsequently gives

$$\begin{aligned} \hat{D}_0^{m,n} \hat{D}_1^{m,n} &= \hat{D}_0^{m,n+1} \hat{D}_1^{m,n-1} + f_n^m f_{n-2}^m (\hat{D}_0^{m,n-1} \hat{D}_1^{m,n-1} - \hat{D}_0^{m,n} \hat{D}_1^{m,n-2}) \\ &= \hat{D}_0^{m,n+1} \hat{D}_1^{m,n-1} + f_n^m f_{n-2}^m \nu_0^{(n-1)} \mathbf{I}^m = \hat{D}_0^{m,n+1} \hat{D}_1^{m,n-1} + \nu_0^{(n)} \mathbf{I}^m \end{aligned} \quad (6.11)$$

as required. \square

Taking the appropriate braid limit of the T -system in Proposition 6.3 yields the following T -system for the braid transfer tangles on the strip,

$$\mathbf{F}^{m,n} \mathbf{F}^{m,n} = \mathbf{F}^{m,n+1} \mathbf{F}^{m,n-1} + \mathbf{I}^m. \quad (6.12)$$

From the fusion hierarchy in Proposition 6.2, we derive the T -system on the cylinder. This is the content of the following proposition.

PROPOSITION 6.4 *For $m, n \in \mathbb{N}$, the T -system on the cylinder is given by*

$$\mathbf{T}_0^{m,n} \mathbf{T}_1^{m,n} = \mathbf{T}_0^{m,n+1} \mathbf{T}_1^{m,n-1} + \tilde{\nu}_0^{(n)} \mathbf{I}^m, \quad (6.13)$$

where $\tilde{\nu}_0^{(n)}$ is defined in (1.17).

PROOF: The proof is identical to the proof of Proposition 6.3. \square

The T -system for the braid transfer tangles on the cylinder is obtained by taking the appropriate braid limit of the T -system in Proposition 6.4 and is given by

$$\tilde{\mathbf{F}}^{m,n} \tilde{\mathbf{F}}^{m,n} = \tilde{\mathbf{F}}^{m,n+1} \tilde{\mathbf{F}}^{m,n-1} + \mathbf{I}^m. \quad (6.14)$$

This is seen to be identical to the T -system (6.12) for the braid transfer tangles on the strip.

6.4 Y -systems

For $m \in \mathbb{N}$ and $n \in \mathbb{N}_0$, we define

$$\mathbf{d}_k^{m,n} := \frac{\hat{\mathbf{D}}_{k+1}^{m,n-1} \hat{\mathbf{D}}_k^{m,n+1}}{\nu_k^{(n)}}, \quad \mathbf{t}_k^{m,n} := \frac{\mathbf{T}_{k+1}^{m,n-1} \mathbf{T}_k^{m,n+1}}{\tilde{\nu}_k^{(n)}}, \quad k \in \mathbb{Z}. \quad (6.15)$$

Since $\hat{\mathbf{D}}_{k+1}^{m,-1} \equiv 0$ and $\mathbf{T}_{k+1}^{m,-1} \equiv 0$, it follows that $\mathbf{d}_k^{m,0} \equiv 0$ and $\mathbf{t}_k^{m,0} \equiv 0$. As demonstrated in the following proposition, the infinite Y -system generated by (6.15) is *universal* in the sense that it is the same on the strip as on the cylinder.

PROPOSITION 6.5 *For $m, n \in \mathbb{N}$, the Y -system for $\mathbf{y} \in \{\mathbf{d}, \mathbf{t}\}$ is universally given by*

$$\mathbf{y}_0^{m,n} \mathbf{y}_1^{m,n} = (\mathbf{I}^m + \mathbf{y}_1^{m,n-1})(\mathbf{I}^m + \mathbf{y}_0^{m,n+1}). \quad (6.16)$$

PROOF: For $\mathbf{y} = \mathbf{d}$, we have

$$\begin{aligned} \mathbf{d}_0^{m,n} \mathbf{d}_1^{m,n} &= \frac{(\hat{\mathbf{D}}_1^{m,n-1} \hat{\mathbf{D}}_2^{m,n-1})(\hat{\mathbf{D}}_0^{m,n+1} \hat{\mathbf{D}}_1^{m,n+1})}{\nu_0^{(n)} \nu_1^{(n)}} \\ &= \frac{(\nu_1^{(n-1)} \mathbf{I}^m + \hat{\mathbf{D}}_2^{m,n-2} \hat{\mathbf{D}}_1^{m,n})(\nu_0^{(n+1)} \mathbf{I}^m + \hat{\mathbf{D}}_1^{m,n} \hat{\mathbf{D}}_0^{m,n+2})}{\nu_0^{(n)} \nu_1^{(n)}} \\ &= \left(\mathbf{I}^m + \frac{\hat{\mathbf{D}}_2^{m,n-2} \hat{\mathbf{D}}_1^{m,n}}{\nu_1^{(n-1)}} \right) \left(\mathbf{I}^m + \frac{\hat{\mathbf{D}}_1^{m,n} \hat{\mathbf{D}}_0^{m,n+2}}{\nu_0^{(n+1)}} \right) \\ &= (\mathbf{I}^m + \mathbf{d}_1^{m,n-1})(\mathbf{I}^m + \mathbf{d}_0^{m,n+1}) \end{aligned} \quad (6.17)$$

where the third equality follows from

$$\nu_1^{(n-1)} \nu_0^{(n+1)} = \nu_0^{(n)} \nu_1^{(n)}. \quad (6.18)$$

The proof for $\mathbf{y} = \mathbf{t}$ is identical to the proof for $\mathbf{y} = \mathbf{d}$. \square

It is noted that a shift in the spectral parameter u by a multiple of the crossing parameter λ readily yields

$$\mathbf{y}_k^{m,n} \mathbf{y}_{k+1}^{m,n} = (\mathbf{I}^m + \mathbf{y}_{k+1}^{m,n-1})(\mathbf{I}^m + \mathbf{y}_k^{m,n+1}). \quad (6.19)$$

The corresponding Y -system for the braid transfer tangles is given by

$$\mathbf{y}^{m,n} \mathbf{y}^{m,n} = (\mathbf{I}^m + \mathbf{y}^{m,n-1})(\mathbf{I}^m + \mathbf{y}^{m,n+1}), \quad \mathbf{y} \in \{\mathbf{f}, \tilde{\mathbf{f}}\} \quad (6.20)$$

where

$$\mathbf{f}^{m,n} := \mathbf{F}^{m,n-1} \mathbf{F}^{m,n+1}, \quad \tilde{\mathbf{f}}^{m,n} := \tilde{\mathbf{F}}^{m,n-1} \tilde{\mathbf{F}}^{m,n+1} \quad (6.21)$$

with $\mathbf{f}^{m,0} \equiv 0$ and $\tilde{\mathbf{f}}^{m,0} \equiv 0$ following from $\mathbf{F}^{m,-1} \equiv 0$ and $\tilde{\mathbf{F}}^{m,-1} \equiv 0$.

7 Functional relations in logarithmic minimal models

In this section, we consider fractional $\lambda = \lambda_{p,p'}$ with $1 \leq p < p'$. The corresponding TL loop model ($m = 1$) is referred to as the *logarithmic minimal model* $\mathcal{LM}(p, p')$ and, as argued in [1] and subsequent works, gives rise to logarithmic conformal field theories in the continuum scaling limit. Here we establish that the transfer tangles $\mathbf{D}(u)$ and $\mathbf{T}(u)$ satisfy certain functional relations of polynomial degree p' . More generally, we find that the transfer tangles $\mathbf{D}^{m,1}(u)$ and $\mathbf{T}^{m,1}(u)$ satisfy such relations for all $m \in \mathbb{N}$ for which P_m exists, and we emphasise that the derivation of these relations is performed in the planar algebra. If P_m does not exist, the relations are still valid provided the transfer tangles are replaced by their barred counterparts, see Section 5. For ease of presentation, however, the various results are given in terms of the transfer tangles themselves. The functional relations we obtain generalise the inversion identities (of polynomial degree $p' = 2$) found in critical dense polymers $\mathcal{LM}(1, 2)$ [4, 5].

We also discuss how the Y -systems on the strip and cylinder close on *finite* sets of generators. The universality of the Y -system, as presented in Proposition 6.5, is broken by the closure mechanism. The finite systems on the two geometries can nevertheless be described in a uniform way as outlined in Corollary 7.13 and Theorem 7.15 below.

7.1 Closure of the fusion hierarchy on the strip

First, we establish that the fusion hierarchy on the strip closes for fractional λ .

PROPOSITION 7.1 *For $\lambda = \lambda_{p,p'}$ and $m \in \mathbb{N}$, the fusion hierarchy on the strip closes as*

$$\mathbf{D}_0^{m,p'} = [q^m(u_0)q^m(\mu - u_{-1})]^N \mathbf{D}_1^{m,p'-2} + 2(-1)^{p'-p} \left(\prod_{j=0}^{p'-1} s_j(u) s_{j+1}(u - \mu) \right)^{Nm} \mathbf{I}^m. \quad (7.1)$$

A proof of this proposition is given in Appendix F.2.

In terms of the renormalised transfer tangles $\hat{\mathbf{D}}$ defined in (1.13), the fusion closure in equation (7.1) can be written as

$$\hat{\mathbf{D}}_0^{m,p'} = f_0^m f_{p'-2}^m \hat{\mathbf{D}}_1^{m,p'-2} + 2a \mathbf{I}^m \quad (7.2)$$

where a is defined in (1.18) and where it is noted that

$$\hat{\mathbf{D}}_{k+p'}^{m,n} = \hat{\mathbf{D}}_k^{m,n}, \quad f_{k+p'}^m = f_k^m, \quad \nu_{k+p'}^{(n)} = \nu_k^{(n)}, \quad \nu_k^{(p')} = a^2, \quad k \in \mathbb{Z}. \quad (7.3)$$

Combined with the fusion hierarchy derived in Section 6.1, equation (7.2) implies the *functional relations* given in the following theorem. They are expressed in terms of the double-row transfer tangles for which $\hat{\mathbf{D}}_k^{m,1} = s_{2k}(2u-\mu)\mathbf{D}^{m,1}(u+k\lambda)$.

THEOREM 7.2 *For $\lambda = \lambda_{p,p'}$ and $m \in \mathbb{N}$, the double-row transfer tangle on the strip satisfies the functional relation*

$$p' > 2 : \begin{vmatrix} \hat{\mathbf{D}}_0^{m,1} & f_{-1}^m & 0 & 0 & (-1)^{p'} f_0^m \\ f_1^m & \hat{\mathbf{D}}_1^{m,1} & f_0^m & 0 & 0 \\ 0 & f_2^m & \ddots & \ddots & 0 \\ 0 & 0 & \ddots & \hat{\mathbf{D}}_{p'-2}^{m,1} & f_{p'-3}^m \\ (-1)^{p'} f_{p'-2}^m & 0 & 0 & f_{p'-1}^m & \hat{\mathbf{D}}_{p'-1}^{m,1} \end{vmatrix} = 0, \quad p' = 2 : \begin{vmatrix} \hat{\mathbf{D}}_0^{m,1} & f_0^m + f_1^m \\ f_0^m + f_1^m & \hat{\mathbf{D}}_1^{m,1} \end{vmatrix} = 0, \quad (7.4)$$

where non-tangle entries are understood to be multiplied by \mathbf{I}^m .

The functional relations in Theorem 7.2, along with the similar ones on the cylinder (7.25), are among the main results of this paper. We stress that they are valid in the planar algebra and therefore in any representation, for example those described in Section 5.

For $p' = 2$, the functional relation (7.4) is an *inversion identity*. It was investigated in [4] for $p = 1$, $m = 1$ and $\mu = \lambda$ corresponding to critical dense polymers $\mathcal{LM}(1,2)$. For $m = 1$ and $\mu \in \mathbb{C}$, we find

$$\mathbf{D}^{1,1}(u)\mathbf{D}^{1,1}(u + \frac{\pi}{2}) = \left(\frac{[s_0(u)s_1(u-\mu)]^N - [s_1(u)s_2(u-\mu)]^N}{s_0(2u-\mu)} \right)^2 \mathbf{I}. \quad (7.5)$$

For $\lambda = \lambda_{1,2}$ and $m > 1$, the tangle \mathbf{I}^m does not exist in general. An inversion identity nevertheless exists for every m , but only for the corresponding barred transfer tangle (5.2). Recalling from (5.6) that $\bar{\mathbf{I}}^m = \mathbf{I}$, this inversion relation reads

$$\bar{\mathbf{D}}^{m,1}(u)\bar{\mathbf{D}}^{m,1}(u + \frac{\pi}{2}) = \begin{cases} \gamma(u)\gamma(u + \frac{\pi}{2}) \left(\frac{[s_0(u)s_1(u-\mu)]^N - [s_1(u)s_2(u-\mu)]^N}{s_0(2u-\mu)} \right)^2 \mathbf{I}, & m \text{ odd}, \\ 0, & m \text{ even}, \end{cases} \quad (7.6)$$

where

$$\gamma(u) = s_1(2u-\mu) \left(s_0(u)s_1(u)s_1(u-\mu)s_2(u-\mu) \right)^{N(m-1)/2}. \quad (7.7)$$

In the case of critical percolation $\mathcal{LM}(2,3)$, for which $m = 1$ and $\mu = \lambda$, the functional relation for the double-row transfer tangle $\mathbf{D}(u) = \mathbf{D}^{1,1}(u)$ on the strip can be written as

$$\mathfrak{D}(u)\mathfrak{D}(u + \frac{\pi}{3})\mathfrak{D}(u + \frac{2\pi}{3}) = \mathfrak{D}(u) + \mathfrak{D}(u + \frac{\pi}{3}) + \mathfrak{D}(u + \frac{2\pi}{3}) - 2\mathbf{I}, \quad \mathfrak{D}(u) := \frac{\mathbf{D}(u)}{[s_1(u)]^{2N}}. \quad (7.8)$$

The closure of the fusion hierarchy, as described in Proposition 7.1, can be viewed as a *folding* of $\hat{\mathbf{D}}_0^{m,n}$ for $n = p'$ onto a subset of $\{\hat{\mathbf{D}}_k^{m,j}; j, k = 0, \dots, p' - 1\}$. A similar folding property holds for general $n \in \mathbb{N}$ as described by the following proposition.

PROPOSITION 7.3 *Let $n = yp' + j$ with $y \in \mathbb{N}_0$ and $j \in \{0, \dots, p' - 1\}$. Then*

$$\hat{\mathbf{D}}_0^{m,n} = (y+1)a^y \hat{\mathbf{D}}_0^{m,j} + ya^{y-1} \nu_{-1}^{(j+1)} \hat{\mathbf{D}}_{j+1}^{m,p'-j-2}. \quad (7.9)$$

PROOF: This is trivially true for $n = 1, \dots, p' - 1$ and it reduces to (7.2) for $n = p'$. For $n > p'$, it follows recursively in n from the relations

$$\hat{D}_k^{m,n} \hat{D}_{n+k}^{m,1} - f_{n+k}^m f_{n+k-2}^m \hat{D}_k^{m,n-1} = \hat{D}_k^{m,n+1} = \hat{D}_k^{m,1} \hat{D}_{k+1}^{m,n} - f_{k+1}^m f_{k-1}^m \hat{D}_{k+2}^{m,n-1}. \quad (7.10)$$

The second of these relations is obtained by summing over entries of the first column and row in an expansion of the determinant expression in (6.4), and by adding a shift in the spectral parameter. \square

For $p' = 2$, it readily follows from Proposition 7.3 that

$$\hat{D}_0^{m,n} = \begin{cases} (y+1)a^y \hat{D}_0^{m,1}, & n = 2y+1, \\ (y f_0^m + (y+1)f_1^m) f_0^m a^{y-1} \mathbf{I}^m, & n = 2y. \end{cases} \quad (7.11)$$

As already indicated at the beginning of Section 7, for $m > 1$, we stress that (7.11) only makes sense in general with \hat{D} replaced by the barred and renormalised transfer tangle $\hat{\bar{D}}$ and with \mathbf{I}^m replaced by \mathbf{I} .

COROLLARY 7.4 *Let $y \in \mathbb{N}_0$ and $j \in \{0, \dots, p' - 1\}$. With the definition*

$$\mathcal{D}_{\pm}^{(y,j)} := a \hat{D}_0^{m,yp'+j} \pm \nu_{-1}^{(j+1)} \hat{D}_{j+1}^{m,yp'+p'-j-2}, \quad (7.12)$$

the general folding can be expressed as

$$\mathcal{D}_{\pm}^{(y,j)} = (y+1 \pm y) a^y \mathcal{D}_{\pm}^{(0,j)}. \quad (7.13)$$

By taking the appropriate braid limit of (7.1), one finds a closure relation for the braid transfer tangles,

$$\mathbf{F}^{m,p'} = \mathbf{F}^{m,p'-2} + 2(-1)^{p'} \sigma \mathbf{I}^m, \quad \sigma := (-1)^{(Nm+1)p}. \quad (7.14)$$

From (6.5), we have $\mathbf{F}^{m,n} = U_n(\frac{1}{2}\mathbf{F}^{m,1})$ which together with (7.14) implies that

$$T_{p'}(\frac{1}{2}\mathbf{F}^{m,1}) = \epsilon \mathbf{I}^m, \quad \epsilon := (-1)^{p'} \sigma \quad (7.15)$$

where $T_k(x)$ is the k -th Chebyshev polynomial of the first kind and we have used the relation

$$U_k(x) - U_{k-2}(x) = 2T_k(x), \quad k \in \mathbb{N}. \quad (7.16)$$

In determinant form, the closure reads

$$\begin{vmatrix} \mathbf{F}^{m,1} & 1 & 0 & 0 & \sigma \\ 1 & \mathbf{F}^{m,1} & 1 & 0 & 0 \\ 0 & 1 & \ddots & \ddots & 0 \\ 0 & 0 & \ddots & \mathbf{F}^{m,1} & 1 \\ \sigma & 0 & 0 & 1 & \mathbf{F}^{m,1} \end{vmatrix} = 0, \quad (7.17)$$

where the dimension of the matrix is p' . Because we can rewrite the determinant relation in (7.17) as

$$\prod_{k=0}^{p'-1} \left(\mathbf{F}^{m,1} - 2 \cos \frac{(2k+\hat{\epsilon})\pi}{p'} \mathbf{I}^m \right) = 0, \quad \hat{\epsilon} := \frac{1-\epsilon}{2}, \quad (7.18)$$

the eigenvalues of $\mathbf{F}^{m,1}$ in any representation (where \mathbf{I}^m acts as the identity) are of the form $2 \cos \frac{(2k+\hat{\epsilon})\pi}{p'}$ for some integers k . It also follows that the Jordan cells associated to these eigenvalues have rank at most 2, and that the rank is 1 if the eigenvalue $2 \cos \frac{(2k+\hat{\epsilon})\pi}{p'}$ is ± 2 . For $y \in \mathbb{N}_0$ and $j \in \{0, \dots, p' - 1\}$, the general folding property of the set of braid transfer tangles on the strip is given by

$$\mathbf{F}^{m,yp'+j} = U_y(\epsilon) \mathbf{F}^{m,j} + U_{y-1}(\epsilon) \mathbf{F}^{m,p'-j-2} = \epsilon^y (y+1) \mathbf{F}^{m,j} + \epsilon^{y-1} y \mathbf{F}^{m,p'-j-2}. \quad (7.19)$$

7.2 Closure of the fusion hierarchy on the cylinder

The fusion hierarchy on the cylinder closes for fractional λ .

PROPOSITION 7.5 *For $\lambda = \lambda_{p,p'}$ and $m \in \mathbb{N}$, the fusion hierarchy on the cylinder closes as*

$$\mathbf{T}_0^{m,p'} = h_0^m h_{p'-2}^m \mathbf{T}_1^{m,p'-2} + 2\tilde{a} \mathbf{J}^m, \quad (7.20)$$

where \tilde{a} is defined in (1.18), and where \mathbf{J}^m is a u -independent tangle.

The proof of Proposition 7.5 for $m = 1$ is provided in Appendix F.3 where an explicit expression for the tangle \mathbf{J}^1 is given in (F.71). Arguments outlining the proof for general m follow Proposition F.5. It is furthermore observed that for $\lambda = \lambda_{p,p'}$ and $k \in \mathbb{Z}$,

$$\mathbf{T}_{k+p'}^{m,n} = e^{2in\theta} \mathbf{T}_k^{m,n}, \quad h_{k+p'}^m = e^{2i\theta} h_k^m, \quad \tilde{\nu}_{k+p'}^{(n)} = \tilde{\nu}_k^{(n)}, \quad \tilde{\nu}_k^{(p')} = e^{2i\theta} \tilde{a}^2 \quad (7.21)$$

where θ is defined in (1.18) and where it is noted that $e^{2i\theta} \in \{-1, +1\}$.

The Nm -tangle \mathbf{J}^m appearing in Proposition 7.5 can be written in terms of braid transfer tangles. This is done by considering the closure properties of the braid transfer tangles and results in the following proposition where $T_k(x)$ is the k -th Chebyshev polynomial of the first kind.

PROPOSITION 7.6 *For $\lambda = \lambda_{p,p'}$ and $m \in \mathbb{N}$, the tangle \mathbf{J}^m appearing in (7.20) is given by*

$$\mathbf{J}^m = \frac{1}{2}(\tilde{\mathbf{F}}^{m,p'} - \tilde{\mathbf{F}}^{m,p'-2}) = T_{p'}(\frac{1}{2}\tilde{\mathbf{F}}^{m,1}). \quad (7.22)$$

PROOF: Applying the *braid limit evaluator*

$$\mathcal{B}(f(u)) = \lim_{u \rightarrow i\infty} \left(\left(\prod_{i=0}^{m-1} \prod_{j=0}^{p'-1} \frac{e^{i\frac{\pi-\lambda}{2}}}{s_{j-i}(u)} \right)^N f(u) \right) \quad (7.23)$$

to both sides of (7.20), and using

$$\mathcal{B}(\mathbf{T}_0^{m,p'}) = \tilde{\mathbf{F}}^{m,p'}, \quad \mathcal{B}(h_0^m h_{p'-2}^m \mathbf{T}_1^{m,p'-2}) = \tilde{\mathbf{F}}^{m,p'-2}, \quad \mathcal{B}(\tilde{a}) = 1, \quad (7.24)$$

yields the first equality in (7.22). The second equality follows from $\tilde{\mathbf{F}}^{m,n} = U_n(\frac{1}{2}\tilde{\mathbf{F}}^{m,1})$, as given in (6.8), and the relation (7.16). \square

As on the strip, the fusion closure in Proposition 7.5 gives rise to a functional relation which can be written neatly in determinant form. On the cylinder, this expression involves the braid transfer tangle.

THEOREM 7.7 *For $\lambda = \lambda_{p,p'}$ and $m \in \mathbb{N}$, the single-row transfer tangle on the cylinder satisfies the functional relation*

$$\begin{vmatrix} \mathbf{T}_0^{m,1} & h_{-1}^m & 0 & 0 & h_0^m \\ h_1^m & \mathbf{T}_1^{m,1} & h_0^m & 0 & 0 \\ 0 & h_2^m & \ddots & \ddots & 0 \\ 0 & 0 & \ddots & \mathbf{T}_{p'-2}^{m,1} & h_{p'-3}^m \\ h_{p'-2}^m & 0 & 0 & h_{p'-1}^m & \mathbf{T}_{p'-1}^{m,1} \end{vmatrix} = \tilde{a} \begin{vmatrix} \tilde{\mathbf{F}}^{m,1} & 1 & 0 & 0 & e^{-i\theta} \\ 1 & \tilde{\mathbf{F}}^{m,1} & 1 & 0 & 0 \\ 0 & 1 & \ddots & \ddots & 0 \\ 0 & 0 & \ddots & \tilde{\mathbf{F}}^{m,1} & 1 \\ e^{i\theta} & 0 & 0 & 1 & \tilde{\mathbf{F}}^{m,1} \end{vmatrix}, \quad p' > 2, \quad (7.25)$$

$$\begin{vmatrix} \mathbf{T}_0^{m,1} & h_0^m + h_{-1}^m \\ h_0^m + h_1^m & \mathbf{T}_1^{m,1} \end{vmatrix} = \tilde{a} \begin{vmatrix} \tilde{\mathbf{F}}^{m,1} & 1 + e^{-i\theta} \\ 1 + e^{i\theta} & \tilde{\mathbf{F}}^{m,1} \end{vmatrix}, \quad p' = 2, \quad (7.26)$$

where non-tangle entries are understood to be multiplied by \mathbf{I}^m .

The case $(p, p') = (1, 2)$, for which $\theta = \frac{1}{2}Nm\pi$, was investigated in [5] for $m = 1$ corresponding to critical dense polymers $\mathcal{LM}(1, 2)$. For critical percolation $\mathcal{LM}(2, 3)$, the functional relation for the single-row transfer tangle $\mathbf{T} = \mathbf{T}^{1,1}$ on the cylinder can be written as

$$\mathfrak{T}(u)\mathfrak{T}(u + \frac{\pi}{3})\mathfrak{T}(u + \frac{2\pi}{3}) = \mathfrak{T}(u) + \mathfrak{T}(u + \frac{\pi}{3}) + \mathfrak{T}(u + \frac{2\pi}{3}) + i^N(\tilde{\mathbf{F}}^3 - 3\tilde{\mathbf{F}}), \quad \mathfrak{T}(u) := \frac{\mathbf{T}(u)}{[s_1(u)]^N} \quad (7.27)$$

where it is recalled that $\tilde{\mathbf{F}} = \tilde{\mathbf{F}}^{1,1}$.

As in the strip case, the closure of the fusion hierarchy on the cylinder can be viewed as a folding procedure. For general $n \in \mathbb{N}$, this is the content of the following proposition.

PROPOSITION 7.8 *Let $n = yp' + j$ with $y \in \mathbb{N}_0$ and $j \in \{0, \dots, p' - 1\}$. Then*

$$\mathbf{T}_0^{m,n} = e^{i\phi(y,j)} \tilde{a}^{y-1} \left(\tilde{a} U_y(\mathbf{J}^m) \mathbf{T}_0^{m,j} + e^{2i\theta} \tilde{\nu}_{-1}^{(j+1)} U_{y-1}(\mathbf{J}^m) \mathbf{T}_{j+1}^{m,p'-j-2} \right), \quad (7.28)$$

where $U_0(\mathbf{J}^m) = \mathbf{I}^m$ and

$$\phi(y, j) := ((y-1)p' + 2j)y\theta. \quad (7.29)$$

PROOF: This is trivially true for $n = 1, \dots, p' - 1$ and is the content of Proposition 7.5 for $n = p'$. For $n > p'$, it follows recursively in n from the relations

$$\mathbf{T}_k^{m,n} \mathbf{T}_{n+k}^{m,1} - h_{n+k}^m h_{n+k-2}^m \mathbf{T}_k^{m,n-1} = \mathbf{T}_k^{m,n+1} = \mathbf{T}_k^{m,1} \mathbf{T}_{k+1}^{m,n} - h_{k+1}^m h_{k-1}^m \mathbf{T}_{k+2}^{m,n-1}, \quad (7.30)$$

the second of which is obtained by summing over entries of the first column and row in an expansion of the determinant expression in (6.7). \square

For $p' = 2$, it readily follows from Proposition 7.8 that

$$\mathbf{T}_0^{m,n} = \begin{cases} (-1)^{Nmy} \tilde{a}^y U_y(\mathbf{J}^m) \mathbf{T}_0^{m,1}, & n = 2y + 1, \\ \tilde{a}^{y-1} h_0 \left(e^{i\theta} h_1 U_y(\mathbf{J}^m) + h_0 U_{y-1}(\mathbf{J}^m) \right), & n = 2y, \end{cases} \quad (7.31)$$

where the comment following (7.11) about barred transfer tangles on the strip for $m > 1$ applies here too, for $\mathbf{T}^{m,n}$ and \mathbf{J}^m . It is also recalled that results like (7.31) are valid for the corresponding matrix representations for all m .

COROLLARY 7.9 *Let $n = yp' + j$ with $y \in \mathbb{N}_0$ and $j \in \{0, \dots, p' - 1\}$. Then*

$$\tilde{\mathbf{F}}^{m,p'-1} \mathbf{T}_0^{m,n} = e^{i\phi(y,j)} \tilde{a}^{y-1} \left(\tilde{a} \tilde{\mathbf{F}}^{m,yp'+p'-1} \mathbf{T}_0^{m,j} + e^{2i\theta} \tilde{\nu}_{-1}^{(j+1)} \tilde{\mathbf{F}}^{m,yp'-1} \mathbf{T}_{j+1}^{m,p'-j-2} \right). \quad (7.32)$$

PROOF: This follows from multiplying both sides of (7.28) by $\tilde{\mathbf{F}}^{m,p'-1}$ and subsequently using $\tilde{\mathbf{F}}^{m,n} = U_n(\frac{1}{2}\tilde{\mathbf{F}}^{m,1})$ and $\mathbf{J}^m = T_{p'}(\frac{1}{2}\tilde{\mathbf{F}}^{m,1})$ combined with the Chebyshev relation

$$U_{\ell k+k-1}(x) = U_{k-1}(x) U_{\ell}(T_k(x)), \quad k \in \mathbb{N}, \quad \ell \in \mathbb{N}_0. \quad (7.33)$$

\square

COROLLARY 7.10 *Let $y \in \mathbb{N}_0$ and $j \in \{0, \dots, p' - 1\}$. With the definition*

$$\mathcal{T}_{\pm}^{(y,j)} := \tilde{a} e^{-i\phi(y,j)} \mathbf{T}_0^{m,yp'+j} \pm e^{-i\phi(y+1,1)} \tilde{\nu}_{-1}^{(j+1)} \mathbf{T}_{j+1}^{m,yp'+p'-j-2}, \quad (7.34)$$

the general folding can be written as

$$\tilde{\mathbf{F}}^{m,p'-1} \mathcal{T}_{\pm}^{(y,j)} = \tilde{a}^y \left(\tilde{\mathbf{F}}^{m,yp'+p'-1} \pm \tilde{\mathbf{F}}^{m,yp'-1} \right) \mathcal{T}_{\pm}^{(0,j)}. \quad (7.35)$$

For $y \in \mathbb{N}_0$ and $j \in \{0, \dots, p' - 1\}$, the folding of the set of braid transfer tangles on the cylinder is given by

$$\tilde{\mathbf{F}}^{m,yp'+j} = U_y(\mathbf{J}^m) \tilde{\mathbf{F}}^{m,j} + U_{y-1}(\mathbf{J}^m) \tilde{\mathbf{F}}^{m,p'-j-2}. \quad (7.36)$$

7.3 Closure of the Y -systems

For fractional $\lambda = \lambda_{p,p'}$, the Y -system generators (6.15) have the translational symmetry properties

$$\mathbf{d}_{k+p'}^{m,n} = \mathbf{d}_k^{m,n}, \quad \mathbf{t}_{k+p'}^{m,n} = \mathbf{t}_k^{m,n}, \quad k \in \mathbb{Z}. \quad (7.37)$$

PROPOSITION 7.11 *For $\lambda = \lambda_{p,p'}$, $m \in \mathbb{N}$, $y \in \mathbb{N}_0$ and $j \in \{0, \dots, p'-1\}$, the set of Y -system generators on the strip folds as*

$$\mathbf{d}_0^{m,yp'+j} - \mathbf{d}_{j+1}^{m,yp'+p'-j-2} = (2y+1)(\mathbf{d}_0^{m,j} - \mathbf{d}_{j+1}^{m,p'-j-2}) \quad (7.38)$$

where $\mathbf{d}_k^{m,-1} \equiv -\mathbf{I}^m$.

PROOF: For $p' = 2$, the relation follows from $\mathbf{d}_0^{m,2} = \mathbf{d}_1^{m,2}$, itself a consequence of (7.11). For $p' > 2$, the folding rule (7.9) in Proposition 7.3 is used to evaluate the lefthand side of (7.38), and this is done separately in the four cases $j = 0$, $1 \leq j \leq p' - 3$, $j = p' - 2$ and $j = p' - 1$. The expression on the righthand side subsequently follows from relations such as

$$\tilde{\nu}_0^{(j)} \tilde{\nu}_j^{(p'-j)} = a^2 = \tilde{\nu}_{-1}^{(j+2)} \tilde{\nu}_{j+1}^{(p'-j-2)}. \quad (7.39)$$

□

PROPOSITION 7.12 *For $\lambda = \lambda_{p,p'}$, $m \in \mathbb{N}$, $y \in \mathbb{N}_0$ and $j \in \{0, \dots, p'-1\}$, the set of Y -system generators on the cylinder folds as*

$$\mathbf{t}_0^{m,yp'+j} - \mathbf{t}_{j+1}^{m,yp'+p'-j-2} = U_{2y}(\mathbf{J}^m)(\mathbf{t}_0^{m,j} - \mathbf{t}_{j+1}^{m,p'-j-2}) \quad (7.40)$$

where $\mathbf{t}_k^{m,-1} \equiv -\mathbf{I}^m$.

PROOF: The proof is similar to the one of Proposition 7.11, but is now based on the folding properties (7.31) and (7.28), supplemented by the Chebyshev relation

$$U_{2y}(x) = [U_y(x)]^2 - [U_{y-1}(x)]^2, \quad y \in \mathbb{N}_0. \quad (7.41)$$

□

COROLLARY 7.13 *For $\lambda = \lambda_{p,p'}$, $m \in \mathbb{N}$, $y \in \mathbb{N}_0$ and $j \in \{0, \dots, p'-1\}$, the two sets of Y -system generators fold as*

$$\mathbf{y}_0^{m,yp'+j} - \mathbf{y}_{j+1}^{m,yp'+p'-j-2} = U_{2y}(\mathbf{K}^m)(\mathbf{y}_0^{m,j} - \mathbf{y}_{j+1}^{m,p'-j-2}), \quad \mathbf{K}^m = \begin{cases} \mathbf{I}^m, & \mathbf{y} = \mathbf{d}, \\ \mathbf{J}^m, & \mathbf{y} = \mathbf{t}. \end{cases} \quad (7.42)$$

PROOF: This follows readily from $U_{2y}(1) = 2y + 1$. □

PROPOSITION 7.14 *For $\lambda = \lambda_{p,p'}$ and $m \in \mathbb{N}$, the Y -systems close as*

$$\mathbf{y}_0^{m, \lfloor \frac{3p'}{2} \rfloor} = \mathbf{y}_{\lfloor \frac{p'+2}{2} \rfloor}^{m, \lfloor \frac{3p'-3}{2} \rfloor} + U_2(\mathbf{K}^m) \left(\mathbf{y}_0^{m, \lfloor \frac{p'}{2} \rfloor} - \mathbf{y}_{\lfloor \frac{p'+2}{2} \rfloor}^{m, \lfloor \frac{p'-3}{2} \rfloor} \right) \quad (7.43)$$

where \mathbf{K}^m is as in (7.42).

PROOF: The folding property (7.42) implies that the Y -systems close at the minimum value of $\max\{yp' + j, yp' + p' - j - 2\}$, for which $yp' + j \neq yp' + p' - j - 2$, evaluated over $y \in \mathbb{N}$ and $j = \{0, \dots, p' - 1\}$. \square

For p' even, the folding relation

$$\mathbf{y}_0^{m, yp' + \frac{p'-2}{2}} - \mathbf{y}_{p'/2}^{m, yp' + \frac{p'-2}{2}} = U_{2y}(\mathbf{K}^m) \left(\mathbf{y}_0^{m, \frac{p'-2}{2}} - \mathbf{y}_{p'/2}^{m, \frac{p'-2}{2}} \right) \quad (7.44)$$

relates a pair of generators at the same fusion level $n = yp' + \frac{p'}{2} - 1$ and is therefore not suited to close the system. For $p' = 2$, for example, we simply obtain $\mathbf{y}_0^{m,2} = \mathbf{y}_1^{m,2}$. Recalling that $U_2(x) = 4x^2 - 1$, the closure of the Y -system for small p' is given by

$$p' = 2 : \quad \mathbf{y}_0^{m,3} = 4(\mathbf{K}^m)^2 \mathbf{y}_0^{m,1} + 4(\mathbf{K}^m)^2 - \mathbf{I}^m, \quad (7.45)$$

$$p' = 3 : \quad \mathbf{y}_0^{m,4} = \mathbf{y}_2^{m,3} + (4(\mathbf{K}^m)^2 - \mathbf{I}^m) \mathbf{y}_0^{m,1}, \quad (7.46)$$

$$p' = 4 : \quad \mathbf{y}_0^{m,6} = \mathbf{y}_3^{m,4} + (4(\mathbf{K}^m)^2 - \mathbf{I}^m) \mathbf{y}_0^{m,2}, \quad (7.47)$$

$$p' = 5 : \quad \mathbf{y}_0^{m,7} = \mathbf{y}_3^{m,6} + (4(\mathbf{K}^m)^2 - \mathbf{I}^m) (\mathbf{y}_0^{m,2} - \mathbf{y}_3^{m,1}). \quad (7.48)$$

As an immediate consequence of the propositions above, we obtain the following theorem.

THEOREM 7.15 *For $\lambda = \lambda_{p,p'}$ and $m \in \mathbb{N}$, the Y -systems on the strip and cylinder are finite as they close on the sets*

$$\{\mathbf{d}^{m,n}; n = 1, \dots, \lfloor \frac{3p'-2}{2} \rfloor\}, \quad \{\mathbf{t}^{m,n}; n = 1, \dots, \lfloor \frac{3p'-2}{2} \rfloor\}, \quad (7.49)$$

respectively, with relations given by

$$\mathbf{y}_0^{m,n} \mathbf{y}_1^{m,n} = (\mathbf{I}^m + \mathbf{y}_1^{m,n-1}) (\mathbf{I}^m + \mathbf{y}_0^{m,n+1}), \quad n = 1, \dots, \lfloor \frac{3p'-2}{2} \rfloor, \quad (7.50)$$

where $\mathbf{y}_0^{m, \lfloor \frac{3p'}{2} \rfloor}$ is given in (7.43) and where $\mathbf{y} \in \{\mathbf{d}, \mathbf{t}\}$.

To obtain the corresponding finite Y -system for the braid transfer tangles, we first establish the folding property

$$\mathbf{y}^{m, yp' + j} - \mathbf{y}^{m, yp' + p' - j - 2} = U_{2y}(\mathbf{K}^m) (\mathbf{y}^{m,j} - \mathbf{y}^{m, p' - j - 2}), \quad \mathbf{K}^m = \begin{cases} \mathbf{I}^m, & \mathbf{y} = \mathbf{f}, \\ \mathbf{J}^m, & \mathbf{y} = \tilde{\mathbf{f}}, \end{cases} \quad (7.51)$$

using $U_{2y}(\epsilon) = U_{2y}(1)$. This folding relation implies a closure of the Y -system (6.20) similar to the one in Proposition 7.14. However, the simplicity of the braid transfer tangles implies the stronger closure

$$\mathbf{y}^{m,p'} = 2 \mathbf{y}^{m,p'-1} - \mathbf{y}^{m,p'-2} + U_2(\mathbf{K}^m) - \mathbf{I}^m. \quad (7.52)$$

The finite Y -system for the braid transfer tangles is thus given by

$$\mathbf{y}^{m,n} \mathbf{y}^{m,n} = (\mathbf{I}^m + \mathbf{y}^{m,n-1}) (\mathbf{I}^m + \mathbf{y}^{m,n+1}), \quad n = 1, \dots, p' - 1, \quad (7.53)$$

and the closure relation (7.52).

8 Comparison with rational models

In this section, we compare our results for the logarithmic fusion hierarchies, T -systems and Y -systems to those obtained previously for rational models. To this end, we renormalise the (m, n) -fused face operator (3.1) by defining

$$\boxed{\begin{array}{c} (m, n) \\ u \\ \sim \end{array}} := \frac{1}{\eta^{m, n}(u)} \boxed{\begin{array}{c} (m, n) \\ u \end{array}} \quad (8.1)$$

where

$$\eta^{m, n}(u) := (-i)^{mn} \prod_{k=1}^{n-1} \prod_{j=1}^m s_{k-j}(u). \quad (8.2)$$

Recalling the decomposition (3.4) in terms of generalised monoids, the renormalised decomposition coefficients are given by

$$\tilde{\alpha}_a^{m, n}(u) := \frac{\alpha_a^{m, n}(u)}{\eta^{m, n}(u)} = (-i)^{mn} (-1)^{(m+n)a} \left(\prod_{j=1}^a \frac{s_{r-j+1}(0)}{s_j(0)} \right) \left(\prod_{j=0}^{a-1} s_{r-n-j}(-u) \right) \left(\prod_{j=1}^{m-a} s_{-j}(u) \right). \quad (8.3)$$

In terms of the renormalised fused faces (8.1), we define renormalised fused transfer tangles by

$$\begin{aligned} \tilde{D}^{m, n}(u) &:= \underbrace{\left(\begin{array}{ccccc} \boxed{\begin{array}{c} (m, n) \\ \mu - u_{n-1} \\ \sim \end{array}} & \boxed{\begin{array}{c} (m, n) \\ \mu - u_{n-1} \\ \sim \end{array}} & \cdots & \cdots & \boxed{\begin{array}{c} (m, n) \\ \mu - u_{n-1} \\ \sim \end{array}} \\ \boxed{\begin{array}{c} (m, n) \\ u \\ \sim \end{array}} & \boxed{\begin{array}{c} (m, n) \\ u \\ \sim \end{array}} & \cdots & \cdots & \boxed{\begin{array}{c} (m, n) \\ u \\ \sim \end{array}} \end{array} \right)}_N = \left(\frac{1}{\eta^{m, n}(u) \eta^{m, n}(\mu - u_{n-1})} \right)^N D^{m, n}(u) \\ &= (-1)^{Nmn} \left(\prod_{k=0}^{n-2} \frac{1}{\tilde{f}_k^m} \right) D^{m, n}(u) \end{aligned} \quad (8.4)$$

and

$$\tilde{T}^{m, n}(u) := \underbrace{\left(\begin{array}{ccccc} \boxed{\begin{array}{c} (m, n) \\ u \\ \sim \end{array}} & \boxed{\begin{array}{c} (m, n) \\ u \\ \sim \end{array}} & \cdots & \cdots & \boxed{\begin{array}{c} (m, n) \\ u \\ \sim \end{array}} \end{array} \right)}_N = \left(\frac{1}{\eta^{m, n}(u)} \right)^N T^{m, n}(u) = i^{Nm} \left(\prod_{k=0}^{n-2} \frac{1}{h_k^m} \right) T^{m, n}(u). \quad (8.5)$$

Here we have set

$$\tilde{D}_0^{m, 0} \equiv \tilde{f}_{-1}^m I^m, \quad \tilde{D}_0^{m, -1} \equiv 0, \quad \tilde{T}_0^{m, 0} \equiv \tilde{h}_{-1}^m I^m, \quad \tilde{T}_0^{m, -1} \equiv 0 \quad (8.6)$$

and introduced

$$\tilde{f}_k^m = (-1)^{Nm} \left(\prod_{j=0}^{m-1} s_{k-j}(u) s_{k+m-j}(u - \mu) \right)^N, \quad \tilde{h}_k^m := i^{Nm} h_k^m = \left(\prod_{j=0}^{m-1} s_{k-j}(u) \right)^N. \quad (8.7)$$

These renormalised transfer tangles also form fusion hierarchies T -systems and Y -systems, readily obtained from the similar structures satisfied by the original fused transfer tangles. Indeed, we find the fusion hierarchies

$$\tilde{D}_0^{m, n} \tilde{D}_n^{m, 1} = \frac{s_{n-2}(2u - \mu) s_{2n+1}(2u - \mu)}{s_{n-1}(2u - \mu) s_{2n}(2u - \mu)} \tilde{f}_n^m \tilde{D}_0^{m, n-1} + \frac{s_n(2u - \mu) s_{2n-1}(2u - \mu)}{s_{n-1}(2u - \mu) s_{2n}(2u - \mu)} \tilde{f}_{n-1}^m \tilde{D}_0^{m, n+1} \quad (8.8)$$

and

$$\tilde{T}_0^{m, n} \tilde{T}_n^{m, 1} = \tilde{h}_n^m \tilde{T}_0^{m, n-1} + \tilde{h}_{n-1}^m \tilde{T}_0^{m, n+1}. \quad (8.9)$$

The corresponding T -systems are given by

$$\tilde{D}_0^{m,n} \tilde{D}_1^{m,n} = \frac{s_{-1}(2u-\mu)s_{2n+1}(2u-\mu)}{s_{n-1}(2u-\mu)s_{n+1}(2u-\mu)} \tilde{f}_{-1}^m \tilde{f}_n^m \mathbf{I}^m + \frac{[s_n(2u-\mu)]^2}{s_{n-1}(2u-\mu)s_{n+1}(2u-\mu)} \tilde{D}_0^{m,n+1} \tilde{D}_1^{m,n-1} \quad (8.10)$$

and

$$\tilde{T}_0^{m,n} \tilde{T}_1^{m,n} = \tilde{h}_{-1}^m \tilde{h}_n^m \mathbf{I}^m + \tilde{T}_0^{m,n+1} \tilde{T}_1^{m,n-1}, \quad (8.11)$$

while the Y -systems are the same as in Section 6.4. The closure relations for fractional $\lambda = \lambda_{p,p'}$ now read

$$\tilde{D}_0^{m,p'} = \tilde{D}_1^{m,p'-2} + 2(-1)^{p'-p} \tilde{f}_{-1}^m \mathbf{I}^m, \quad \tilde{T}_0^{m,p'} = \tilde{T}_1^{m,p'-2} + 2e^{-i\theta} \tilde{h}_{-1}^m \mathbf{J}^m. \quad (8.12)$$

The fusion hierarchies (8.8)-(8.9) and T -systems (8.10)-(8.11) coincide with those of the (rational) critical A - D - E models, as described in [28], for example. The closure relations (8.12), on the other hand, differ significantly from the closure relations in the rational models. Indeed, in the rational models, the fusion hierarchies truncate at $n = p' - 1$, in the sense that the fused transfer matrices with fusion index $n = p' - 1$ are identically zero. Consequently, the corresponding Y -systems truncate at $n = p' - 2$, so the way in which our Y -systems fold for fractional $\lambda = \lambda_{p,p'}$, as described in Section 7.3, is therefore also new.

9 Conclusion

The (higher fusion level) logarithmic minimal models $\mathcal{LM}(P, P'; n)$ [34, 35] constitute a very large class of $su(2)$ theories describing the critical behaviour of statistical systems with nonlocal degrees of freedom such as generalised polymer systems and generalised percolation processes. In this paper, we have initiated the study of the integrable algebraic structures of the critical fused lattice models $\mathcal{LM}(p, p')_{n \times n}$ [35] realising the general logarithmic minimal models $\mathcal{LM}(P, P'; n)$ described as coset CFTs in [34]. Specifically, we have obtained the fusion hierarchies, T -systems and Y -systems for these models and demonstrated their finite closure both on a strip and on a cylinder. The T -systems and Y -systems are the key to the analytic calculation of non-universal statistical and universal conformal quantities, respectively. The coset construction of the logarithmic minimal models brings these theories within standard schemes for constructing and classifying CFTs based on Lie algebras. The explicit manifestation of the T - and Y -systems further imposes standard integrable algebraic structures on the underlying Yang-Baxter integrable lattice models. The logarithmic minimal models are not rational and not unitary and the accompanying representation theory, with the profusion of reducible yet indecomposable structures, is clearly very intricate. Nevertheless, it is becoming increasingly clear, at least as far as the study of spectra is concerned, that these logarithmic theories are amenable to the standard approaches of mathematical physics as applied to rational CFTs.

The structure of the logarithmic T - and Y -systems we obtain closely mirrors the $su(2)$ T -systems and Y -systems of the (rational) critical RSOS A - D - E models [16, 28, 29]. Remarkably, we find that these functional equations hold for arbitrary coprime integers p, p' and that the underlying structures are related to the Dynkin diagrams of the affine Lie algebras $A_{p'-1}^{(1)}$. Indeed, the determinantal structure of the polynomial functional equations of degree p' is the same [40] as for the CSOS models [41–43]. In contrast, the structure of the T - and Y -systems of rational unitary minimal models are related to Dynkin diagrams of classical Lie algebras. Perhaps it should not be too surprising to see affine Lie algebras enter in the logarithmic setting. After all, it has been argued [59] that, with \mathcal{W} -extended symmetries on the strip or torus, certain aspects of the $n = 1$ theories are in fact encoded by twisted affine coset graphs $A_{p,p'}^{(2)} = A_p^{(2)} \otimes A_{p'}^{(2)} / \mathbb{Z}_2$.

The next stage in this program is to solve the Y -system for the central charges and conformal weights of the logarithmic minimal models in terms of Rogers dilogarithms. Since this system of functional equations closes but does not truncate in the usual way, some new techniques will probably need to be developed. One hope is that, if \mathcal{W} -extended symmetry can be properly incorporated into

the functional equations, then perhaps the associated Y -systems would exhibit the twisted affine coset structure and naturally truncate. In this regard, we stress that the only boundary condition on the strip considered here, namely, the vacuum boundary condition conjugate to the identity operator in the so-called Virasoro picture, in general breaks the \mathcal{W} -extended symmetry. It is clearly of interest to extend the derivation of the logarithmic T - and Y -systems on the strip to more general boundary conditions including \mathcal{W} -symmetric boundary conditions. Lastly, we note that, since the logarithmic minimal models are also exactly solvable off-criticality [60], it should also be possible to obtain both massless (critical) and massive (off-critical) thermodynamic Bethe ansatz equations for these theories with their concomitant implications for the associated relativistic two-particle scattering theories.

Acknowledgments

AMD is supported by the National Sciences and Engineering Research Council of Canada as a post-doctoral fellow. He is also grateful for support from the University of Queensland. JR is supported by the Australian Research Council under the Future Fellowship scheme, project number FT100100774. The authors thank Adam Ong, Yvan Saint-Aubin, Hubert Saleur and Elena Tartaglia for comments and discussions. AMD and JR also thank Jean-Bernard Zuber and the LPTHE at Université Pierre et Marie Curie, where part of this work was done, for their kind hospitality.

Appendices

A Decomposition of fused face operators

Here we recall and prove Proposition 3.1.

PROPOSITION 3.1 *The decomposition of an (m, n) -fused face in terms of generalised monoids is given by*

$$\begin{array}{c} (m, n) \\ \diamond \\ u \end{array} = \sum_{a=0}^r \alpha_a^{m, n} X_a^{m, n}, \quad r = \min(m, n) \quad (\text{A.1})$$

where

$$\frac{\alpha_a^{m, n}}{\alpha_0^{m, n}} = (-1)^{(m+n)a} \left(\prod_{j=1}^a \frac{s_{r-j+1}(0)}{s_j(0)} \right) \left(\prod_{i=0}^{a-1} \frac{s_{n-r+i}(u)}{s_{m-i}(-u)} \right), \quad \alpha_0^{m, n} = \prod_{i=0}^{m-1} \prod_{j=0}^{n-1} s_{i-j+1}(-u). \quad (\text{A.2})$$

PROOF: Because $X_0^{m, n}$ and $X_r^{m, n}$ can only be obtained from the (m, n) -fused face operator by respectively fixing every elementary face operator to \diamond or \diamond , their coefficients $\alpha_0^{m, n}$ and $\alpha_r^{m, n}$ are seen to be given by

$$\alpha_0^{m, n} = \prod_{i=0}^{m-1} \prod_{j=0}^{n-1} s_{i-j+1}(-u), \quad \alpha_r^{m, n} = \prod_{i=0}^{m-1} \prod_{j=0}^{n-1} s_{j-i}(u). \quad (\text{A.3})$$

This is correctly reproduced by (A.2), with the usual convention $\prod_{j=1}^0 f(j) = 1$. The coefficients $\alpha_a^{m, n}$ for $a = 1, \dots, r-1$ are found recursively by using the following three relations. The first one of these relations,

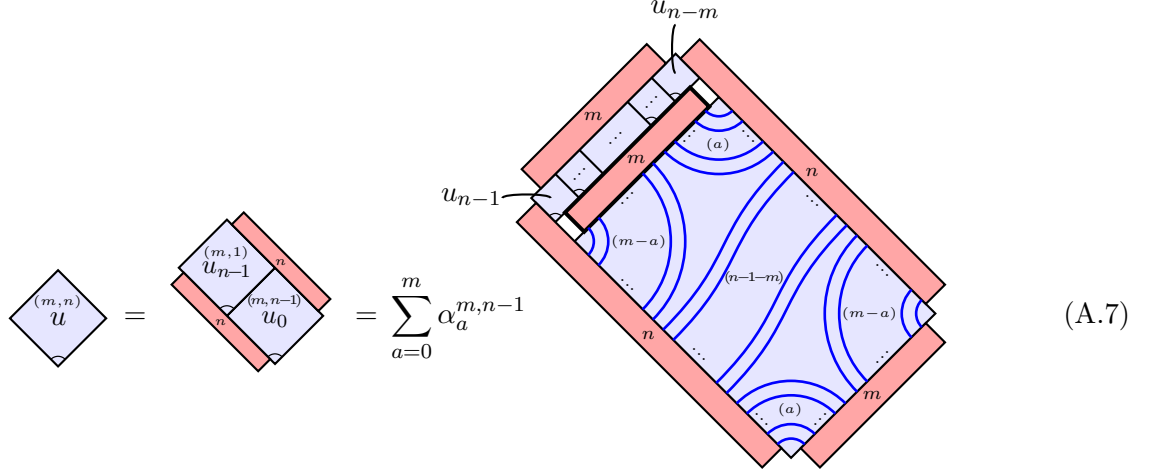
$$\alpha_a^{m, n}(u) = \alpha_{r-a}^{n, m}(\lambda - u), \quad (\text{A.4})$$

stems from the crossing relation and allows one to relate a coefficient $\alpha_a^{m,n}$ with $m \leq n$ to a coefficient $\alpha_a^{m',n'}$ with $m' \geq n'$. The other two relations,

$$\alpha_a^{m,n} = \alpha_a^{m,n-1} \prod_{j=n-m}^{n-m+a-1} s_j(u) \prod_{k=n-m+a}^{n-1} s_{1-k}(-u) \quad (m < n), \quad (\text{A.5})$$

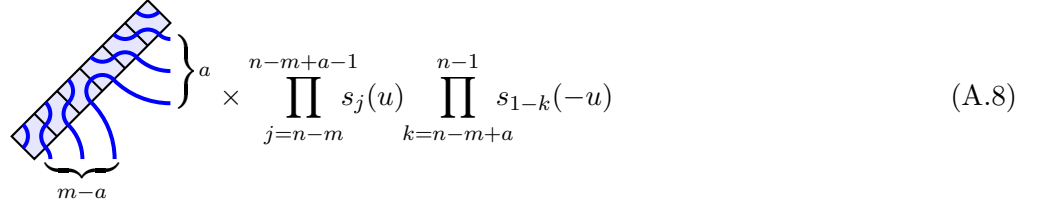
$$\alpha_a^{n,n} = (\alpha_a^{n,n-1} + \alpha_{a-1}^{n,n-1}) \prod_{j=0}^{a-1} s_j(u) \prod_{k=a}^{n-1} s_{1-k}(-u) \quad (0 < a < n), \quad (\text{A.6})$$

are proven diagrammatically in the following. For $m < n$, we have



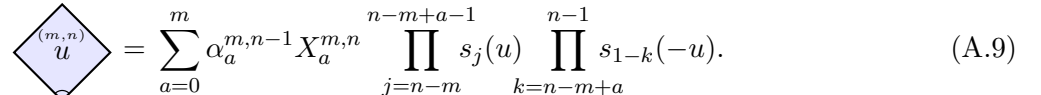
$$(\text{A.7})$$

where we have used (3.16) to reverse the order of the spectral parameters appearing in the upper-left column of elementary face operators. The push-through properties now allow us to remove the projector P_m drawn with a thicker boundary. It subsequently follows that only a single configuration in the decomposition of the array of elementary face operators appearing in the upper-left part of the previous diagram gives a nonzero contribution, namely



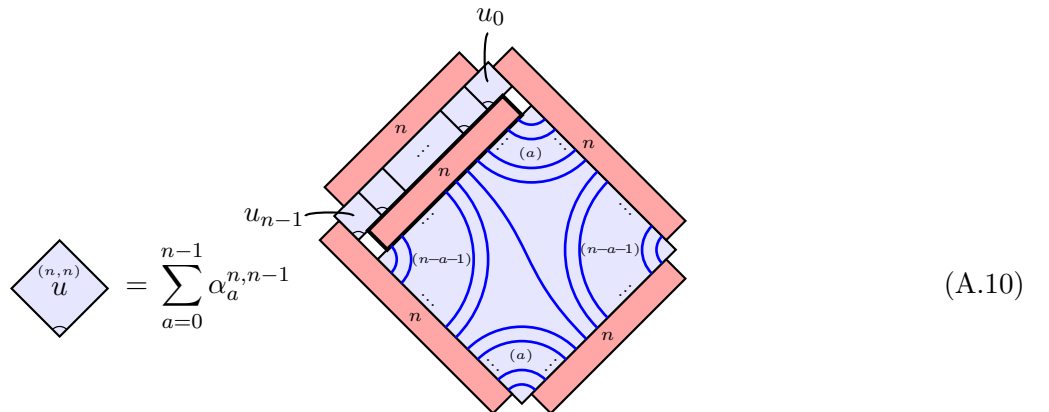
$$(\text{A.8})$$

and subsequently



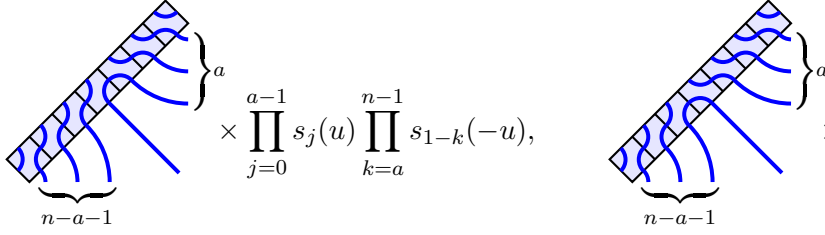
$$(\text{A.9})$$

This completes the proof of (A.5). For $m = n$, we have




$$(\text{A.10})$$

After removing the P_n projector indicated by a thick boundary, we now have two contributing configurations, namely



$$\times \prod_{j=0}^{a-1} s_j(u) \prod_{k=a}^{n-1} s_{1-k}(-u), \quad \times \prod_{j=0}^a s_j(u) \prod_{k=a+1}^{n-1} s_{1-k}(-u). \quad (\text{A.11})$$

It follows that



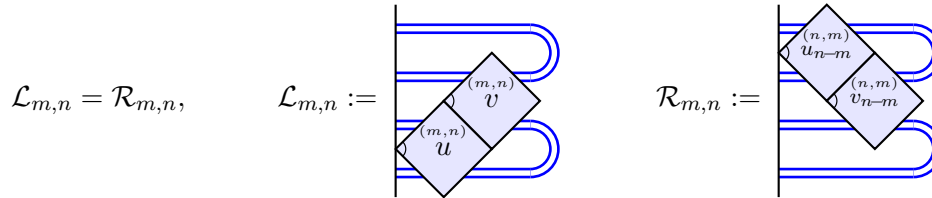
$$= \sum_{a=0}^{n-1} \alpha_a^{n,n-1} \left(X_a^{n,n} \prod_{j=0}^{a-1} s_j(u) \prod_{k=a}^{n-1} s_{1-k}(-u) + X_{a+1}^{n,n} \prod_{j=0}^a s_j(u) \prod_{k=a+1}^{n-1} s_{1-k}(-u) \right)$$

$$= \alpha_0^{n,n} X_0^{n,n} + \alpha_n^{n,n} X_n^{n,n} + \sum_{a=1}^{n-1} X_a^{n,n} (\alpha_a^{n,n-1} + \alpha_{a-1}^{n,n-1}) \prod_{j=0}^{a-1} s_j(u) \prod_{k=a}^{n-1} s_{1-k}(-u), \quad (\text{A.12})$$

where we used (A.3) to establish the last equality. This completes the proof of (A.6). As already announced, the coefficients $\alpha_a^{m,n}$ for $a = 1, \dots, r-1$ now follow recursively. \square

B Boundary Yang-Baxter equations for fused face operators

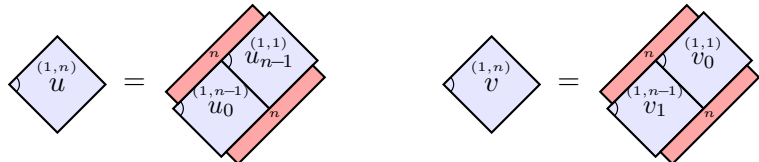
First, we note in (3.14) that the left BYBE is obtained from the right BYBE by rotating the diagram by 180° while simultaneously mapping $u \rightarrow u_{n-m}$ and $v \rightarrow v_{n-m}$. The objective of this appendix is then to show that



$$\mathcal{L}_{m,n} = \mathcal{R}_{m,n}, \quad \mathcal{L}_{m,n} := \text{Diagram}, \quad \mathcal{R}_{m,n} := \text{Diagram} \quad (\text{B.1})$$

We refer to this equation as $\text{BYBE}_{m,n}$. Note that the special case $\text{BYBE}_{1,1}$ is identical to the second relation in (2.23). Following the ideas of [29], the proof for general m, n is done in two steps. First, a recursion in n will show that $\text{BYBE}_{1,n}$ results from the YBE, $\text{BYBE}_{1,n-1}$ and $\text{BYBE}_{1,1}$. A second recursion, in m , will show that the YBE, $\text{BYBE}_{m-1,n}$ and $\text{BYBE}_{1,n}$ imply $\text{BYBE}_{m,n}$.

First recursion: $\text{BYBE}_{1,n}$ We start by writing



$$\text{Diagram} = \text{Diagram}, \quad \text{Diagram} = \text{Diagram} \quad (\text{B.2})$$

where we have used (3.16) to establish the second equality. In the diagrammatic representation of $\mathcal{L}_{1,n}$, we remove the two unnecessary projectors and add an extra tile,

$$\mathcal{L}_{1,n} = \frac{1}{\eta(w)} \quad w = v - u - (n-2)\lambda, \quad \eta(w) = \prod_{i=0}^{n-2} s_i(w). \quad (\text{B.3})$$

In fact, an extra $(1, n-1)$ -fused face with arbitrary spectral parameter w can be added because, after it is decomposed as in (3.15) in terms of two diagrams, one can show using the push-through properties that (i) the two projectors can be removed, and (ii) the second term is zero. The particular choice for w in (B.3) allows us to use the YBE and the (assumed) BYBE. At every step, the required identity is indicated above the equality sign, and the boxes to be changed are specified by thick boundaries. We thus find

$$\begin{aligned} \mathcal{L}_{1,n} &= \frac{1}{\eta(w)} \quad \xrightarrow{\text{YBE}} \frac{1}{\eta(w)} \quad \xrightarrow{\text{BYBE}_{1,1}} \frac{1}{\eta(w)} \\ &\xrightarrow{\text{BYBE}_{1,n-1}} \frac{1}{\eta(w)} \quad \xrightarrow{\text{YBE}} \frac{1}{\eta(w)} = \mathcal{R}_{1,n} \end{aligned} \quad (\text{B.4})$$

which is the required result.

Second recursion: BYBE_{m,n} This time, we write

$$\diamond_{(m,n)}^u = \text{diamond with } u_{-1}^{(m-1,n)} \text{ and } u_0^{(1,n)} \text{ faces} \quad (\text{B.5})$$

and use the similar expansion for the v -dependent face operator. As before, we add a new face operator, this time with parameter $w = u + v + (n-2)\lambda$ and function $\tilde{\eta}(w) = \prod_{j=0}^{m-2} s_{-j}(w)$, remove unnecessary

projectors and find

$$\begin{aligned}
\mathcal{L}_{m,n} &= \text{Diagram 1} = \frac{1}{\tilde{\eta}(w)} \text{Diagram 2} \\
&\stackrel{\text{BYBE}_{1,n}}{=} \frac{1}{\tilde{\eta}(w)} \text{Diagram 3} \stackrel{\text{YBE}}{=} \frac{1}{\tilde{\eta}(w)} \text{Diagram 4} \\
&\stackrel{\text{YBE}}{=} \frac{1}{\tilde{\eta}(w)} \text{Diagram 5} \stackrel{\text{BYBE}_{m-1,n}}{=} \frac{1}{\tilde{\eta}(w)} \text{Diagram 6} = \mathcal{R}_{m,n}.
\end{aligned} \tag{B.6}$$

This concludes the proof.

C Effective projectors

Here we recall and prove Proposition 4.1.

PROPOSITION 4.1 *For λ generic, the transfer tangles can be expressed in terms of effective projectors as*

$$D_0^{m,n} = \text{Diagram 1} \quad T_0^{m,n} = \text{Diagram 2} \tag{C.1}$$

PROOF: For the proof on the strip, we use induction to establish a more general relation, namely

$$\mathbf{G}^{m,n}(u, v) := \text{Diagram 1} = \text{Diagram 2} \quad (\text{C.2})$$

and note that $\mathbf{G}^{m,n}(u, u_1 - \mu) = \mathbf{D}^{m,n}(u)$. The choice of face operators ensures that the propagation of half-arcs from push-through properties is towards the right within the top n layers and towards the left within the bottom n layers (\rightleftarrows). Since $Q_1 = P_1$ and $Q_2 = P_2$, the relation (C.2) is trivially true for $n = 1, 2$.

The first step in building the induction is to modify the first form in (C.2) using (2.42),

$$\mathbf{G}^{m,n}(u, v) = \text{Diagram 3} - \frac{s_{n-1}(0)}{s_n(0)} \text{Diagram 4} \quad (\text{C.3})$$

One readily recognizes that the first tangle contains $\mathbf{G}^{m,n-1}(u_1, v_0)$ as a sub-tangle, and by the induction assumption, the full tangle satisfies

$$\text{Diagram 5} = \text{Diagram 6} \quad (\text{C.4})$$

As for the second term in (C.3), the push-through properties and property (2.46) of the projectors

allow one to remove the leftmost P_{n-1} projector. The ensuing term can then be written as

$$\begin{aligned}
& -\frac{s_{n-1}(0)}{s_n(0)} \left[\text{Diagram 1} \right] = -\frac{s_{n-1}(0)}{s_n(0)} [q^m(u_1)q^m(-v_{n-3})]^N \left[\text{Diagram 2} \right] \\
& = -[q^m(u_1)q^m(-v_{n-3})]^N \mathbf{G}^{m,n-2}(u_2, v_0) \quad (\text{C.5})
\end{aligned}$$

The diagrams represent lattice paths on a grid. Diagram 1 is a 4x4 grid with a red vertical bar on the left labeled $n-1$. The top two rows are labeled with $(1,m)$ and v values, and the bottom two rows with $(m,1)$ and u values. Blue loops connect the left and right sides of the grid. Diagram 2 is a similar 4x4 grid with a red vertical bar on the left labeled $n-1$, but with different labels and a more complex loop structure.

where property (2.48) was used at the last step. Again, the induction assumption implies that this can be written in terms of effective projectors. One now applies the same evaluation technique to the second form in (C.2), this time using the recursive definition (4.14) for effective projectors. This yields the exact same result as for the first form of $\mathbf{G}^{m,n}(u, v)$, thereby completing the proof of (C.2). The proposition for $\mathbf{T}_0^{m,n}$ is verified similarly. \square

D Cabled link states and lattice paths

The dimensions of the linear spans $V_{N,m}^d$ and $\tilde{V}_{N,m}^d$ can be determined by establishing bijections to certain families of (generalised Dyck) lattice paths. We first consider the situation on the cylinder.

PROPOSITION D.1 *For $N, m \in \mathbb{N}$ and $d \in \mathbb{N}_0$ subject to (5.12), the number of linearly independent m -cabled link states on N nodes with d defects on the cylinder is given by*

$$\dim \tilde{V}_{N,m}^d = \binom{N}{\frac{Nm-d}{2}}_m. \quad (\text{D.1})$$

PROOF: We first establish a bijection between the canonical basis of cabled link states and a class of N -tuples of integers. The number of link states is subsequently found by counting these N -tuples.

To every node of a cabled link state in the canonical basis of $\tilde{V}_{N,m}^d$, we assign an integer

$$x_i \in \{+1, -1\}, \quad i = 1, \dots, Nm, \quad (\text{D.2})$$

setting $x_i = -1$ if the loop segment tied to the i -th node connects to another node by moving toward the left, and $+1$ otherwise, that is, if the emanating loop segment moves to the right or happens to be a defect. Because for every $\ell \in \{0, \dots, N-1\}$, two nodes i, j with $\ell m + 1 \leq i < j \leq (\ell + 1)m$ only can be linked via the back of the cylinder, the sequence of integers x_i must be of the form

$$\underbrace{\underbrace{(-1) \dots (-1)}_{\frac{m-y_1}{2}} \underbrace{(+1) \dots (+1)}_{\frac{m+y_1}{2}}}_{m} \underbrace{\underbrace{(-1) \dots (-1)}_{\frac{m-y_2}{2}} \underbrace{(+1) \dots (+1)}_{\frac{m+y_2}{2}}}_{m} \dots \underbrace{\underbrace{(-1) \dots (-1)}_{\frac{m-y_N}{2}} \underbrace{(+1) \dots (+1)}_{\frac{m+y_N}{2}}}_{m}, \quad (\text{D.3})$$

where

$$y_k \in \{-m, -m+2, \dots, m\}, \quad k = 1, \dots, N. \quad (\text{D.4})$$

By construction, we have

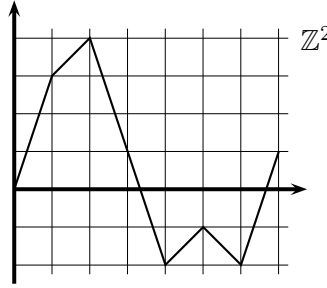
$$y_k = x_{(k-1)m+1} + x_{(k-1)m+2} + \cdots + x_{km} \quad (\text{D.5})$$

and

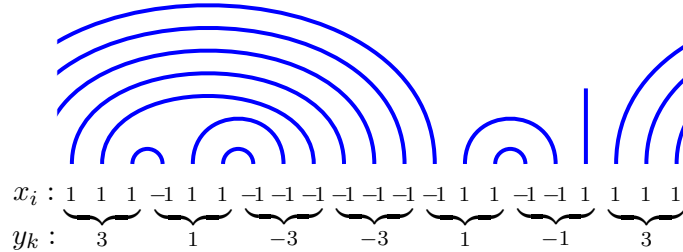
$$\sum_{k=1}^N y_k = \sum_{i=1}^{Nm} x_i = d. \quad (\text{D.6})$$

Since the structure of link states disallows half-arcs arching over defects, the association of the N -tuple (y_1, \dots, y_N) to the link state we started out with is clearly an invertible map. Indeed, the sequence x_1, \dots, x_{Nm} associated to the N -tuple decomposes into alternating subsequences consisting exclusively of (-1) 's or $(+1)$'s. There are two possible scenarios. (i) If there is only one such subsequence, it must consist of $(+1)$'s and all associated nodes give rise to defects. (ii) If instead there is more than one subsequence, there must be an even number of them, and the leftmost (-1) in every subsequence of (-1) 's must be linked to the $(+1)$ to its immediate left. Ignoring these pairs of connected nodes, the remaining shorter sequence of x 's also decomposes into alternating subsequences of (-1) 's or $(+1)$'s, respectively, and we repeat iteratively the steps following (i) or (ii). The half-arcs produced in these subsequent iterations will thus arch over already produced half-arcs. The last step in this procedure is the first (and only) time option (i) is applied and is reached when the sequence of x 's has been reduced to d $(+1)$'s. Note that this last step is only executed if $d > 0$. By construction, the ensuing link state is the one we started out with. We have thus established a bijection between the canonical basis of cabled link states in $\tilde{V}_{N,m}^d$ and the set $Y_{N,m}^d$ of N -tuples of integers, $(y_1, \dots, y_N) \in Y_{N,m}^d$, subject to (D.4) and (D.6).

These N -tuples can be used to characterise a family of lattice paths in \mathbb{Z}^2 , where the path associated to $(y_1, y_2, \dots, y_N) \in Y_{N,m}^d$ starts at the origin and ends at (N, d) , with steps $(1, y_1), (1, y_2), \dots, (1, y_N)$ along the way. We thus have a bijection between cabled link states on the cylinder and the corresponding family of lattice paths labeled by the elements of $Y_{N,m}^d$. Illustrating this bijection, the path $(3, 1, -3, -3, 1, -1, 3) \in Y_{7,3}^1$ is depicted as



and corresponds to the link state



To determine the cardinality of the set $Y_{N,m}^d$ and hence the dimension of $\tilde{V}_{N,m}^d$, we relax the parameters of the space of tuples and thus let $Y_{n,m}^d$ denote the set of n -tuples of integers (y_1, \dots, y_n) subject to

$$y_k \in \{-m, -m+2, \dots, m\}, \quad \sum_{k=1}^n y_k = d, \quad n, \frac{1}{2}(nm - |d|), |d| \in \mathbb{N}_0, \quad m \in \mathbb{N}. \quad (\text{D.7})$$

From the lattice path interpretation, the cardinalities of the sets $Y_{n,m}^d$ are easily seen to satisfy the recursive relations

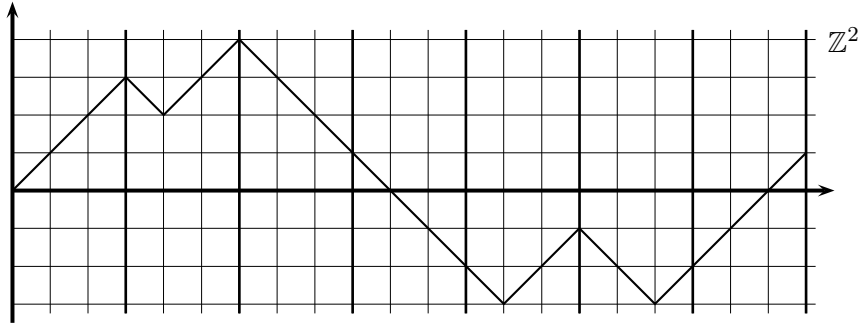
$$|Y_{n,m}^d| = \sum_{i=-m, -m+2, \dots, m} |Y_{n-1,m}^{d+i}|, \quad |Y_{0,m}^d| = \delta_{d,0}, \quad (\text{D.8})$$

and it is straightforward to verify from the definition (5.17) that

$$|Y_{n,m}^d| = \binom{n}{\frac{nm-d}{2}}_m \quad (\text{D.9})$$

satisfies (D.8). \square

A refinement of the y -paths used in the proof of Proposition D.1 is obtained by using the x -parameters instead to define the steps. The corresponding lattice path thus ends at (nm, d) , with steps $(1, x_1), (1, x_2), \dots, (1, x_{nm})$ along the way. For instance, the x -path refinement of the y -path in the example above is given by



PROPOSITION D.2 For $N, m \in \mathbb{N}$ and $d \in \mathbb{N}_0$ subject to (5.12), the number of linearly independent m -cabled link states on N nodes with d defects on the strip is given by

$$\dim V_{N,m}^d = \binom{N}{\frac{Nm-d}{2}}_m - \binom{N}{\frac{Nm-d-2}{2}}_m. \quad (\text{D.10})$$

PROOF: The result trivially holds for $d = Nm$. For $d < Nm$, let $\tilde{C}_{N,m}^d$ denote the linear span of the set of cabled link states on the cylinder with loop segments crossing the virtual boundary. The number of linearly independent cabled link states on the strip is then given by

$$\dim V_{N,m}^d = \dim \tilde{V}_{N,m}^d - \dim \tilde{C}_{N,m}^d. \quad (\text{D.11})$$

There is a simple bijection between the canonical basis of $\tilde{C}_{N,m}^d$ and that of $\tilde{V}_{N,m}^{d+2}$. A link state in the basis of $\tilde{C}_{N,m}^d$ contains at least one half-arc crossing the virtual boundary. By identifying the top one and cutting it into two defects, we produce a unique link state in the basis of $\tilde{V}_{N,m}^{d+2}$. Noting that every link state in the basis of $\tilde{V}_{N,m}^{d+2}$ contains at least two defects, the inverse map follows by replacing the left- and rightmost defects of a given link state in $\tilde{V}_{N,m}^{d+2}$ by a half-arc linking the corresponding two nodes via the back of the cylinder, thereby producing a unique link state in the basis of $\tilde{C}_{N,m}^d$. This bijection implies that $\dim \tilde{C}_{N,m}^d = \dim \tilde{V}_{N,m}^{d+2}$ and hence (D.10). \square

In terms of x -sequences, the cabled link states on the strip are characterised as on the cylinder, but with the additional constraint that only nonnegative partial sums can appear,

$$\sum_{i=1}^t x_i \geq 0, \quad \forall t \in \{1, \dots, Nm\}. \quad (\text{D.12})$$

Viewed as a refined lattice path, an x -path can thus not extend under the horizontal axis. In terms of y -sequences, this constraint translates into

$$\mathfrak{h}_s \geq 0, \quad \mathfrak{h}_{s-1} + \mathfrak{h}_s \geq m, \quad s = 1, \dots, N \quad (\text{D.13})$$

where the height \mathfrak{h}_s after s steps is defined by

$$\mathfrak{h}_0 := 0, \quad \mathfrak{h}_s := \sum_{k=1}^s y_k, \quad s = 1, \dots, N. \quad (\text{D.14})$$

The corresponding y -paths are those in $Y_{N,m}^d$ that do not extend below the horizontal axis and for which every pair of consecutive heights sum to m or more. For $m = 2$, the y -paths on the strip are the generalised Riordan paths discussed in [35]. In this case, (D.12) implies that these lattice paths cannot remain at height 0 for two (or more) consecutive steps.

E Fusion hierarchies

E.1 On the strip

Here we recall and prove Proposition 6.1.

PROPOSITION 6.1 *On the strip, the fusion hierarchy for $m, n \in \mathbb{N}$ is given by*

$$\begin{aligned} D_0^{m,n} D_n^{m,1} &= \frac{s_n(2u - \mu)s_{2n-1}(2u - \mu)}{s_{n-1}(2u - \mu)s_{2n}(2u - \mu)} D_0^{m,n+1} \\ &\quad + \frac{s_{n-2}(2u - \mu)s_{2n+1}(2u - \mu)}{s_{n-1}(2u - \mu)s_{2n}(2u - \mu)} [q^m(u_n)q^m(\mu - u_{n-1})]^N D_0^{m,n-1} \end{aligned} \quad (\text{E.1})$$

where $q^m(u)$ is defined in (1.11).

PROOF: Equation (E.1) will be obtained after applying planar transformations to the tangle $D_0^{m,n+1}$. For arbitrary n , this requires studying diagrams with many layers of $(m, 1)$ - and $(1, m)$ -fused faces. We start by noting that the annihilating property (2.46) of the WJ projectors allows us to write the left and right boundaries of $D_0^{m,n+1}$ as

$$D_0^{m,n+1} = \frac{1}{\alpha_L} \left(\text{left part} \right) + \frac{1}{\alpha_R} \left(\text{right part} \right) \quad (\text{E.2})$$

where the functions

$$\alpha_L^{\diamond} = \prod_{i=0}^{n-1} s_0(-v_i) = \prod_{j=n}^{2n-1} s_j(2u - \mu), \quad \alpha_R^{\diamond} = \prod_{i=0}^{n-1} s_0(v_i) = \prod_{j=n}^{2n-1} s_{-j}(\mu - 2u) \quad (\text{E.3})$$

are such that the configuration with all diamond face operators given by \diamond has weight 1. The order of the spectral parameters in the diamond boxes in (E.2) ensures that half-arc propagation in the bulk and boundary of the transfer tangle is of the form $\curvearrowright \rightleftharpoons \curvearrowleft$. Also, (E.2) holds for all $v \in \mathbb{C}$, but setting

$$v := \mu - 2u - (2n - 1)\lambda \quad (\text{E.4})$$

will permit the use of the YBE below. Repeating the argument used in (4.10) to write $\mathbf{D}^{m,n}(u)$ with a single projector, we reexpress $\mathbf{D}_0^{m,n+1}$ as

$$\alpha_L \diamond \alpha_R \mathbf{D}_0^{m,n+1} = \begin{array}{c} \begin{array}{c} \text{Diagram with diamond boxes } -v_0, -v_1, \dots, -v_{n-1} \text{ on the left and } v_0, v_1, \dots, v_{n-1} \text{ on the right, connected by a central vertical strip of boxes labeled } n+1. \end{array} \end{array} \quad (\text{E.5})$$

Transforming P_{n+1} using its recursive definition (2.42) yields two terms, the first of which is

$$\begin{array}{c} \text{Diagram similar to (E.5) but with a central vertical strip of boxes labeled } n \text{ instead of } n+1. \end{array} \quad (\text{E.6})$$

$$= \eta(u, \mu) D_0^{m,n} D_n^{m,1}, \quad (\text{E.7})$$

where at the first equality, P_n projectors have been reinserted to produce the (m, n) -fused faces inversion identity and where (3.11) was used at the last equality, with the ensuing factor

$$\eta(u, \mu) = g^{n,1} (2u + (2n+1)\lambda - \mu) = \left(\prod_{i=n+1}^{2n} s_i(2u - \mu) \right) \left(\prod_{j=n-1}^{2n-2} s_{-j}(\mu - 2u) \right). \quad (\text{E.8})$$

The second term in the decomposition of $\alpha_L \alpha_R D_0^{m,n+1}$ is

$$- \frac{s_n(0)}{s_{n+1}(0)} \quad (\text{E.9})$$

and the next step is to expand the leftmost P_n projector in a linear combination of elementary tangles. Except for the one with n horizontal strands, all connectivities have half-arcs propagating as $\curvearrowright \rightleftharpoons \curvearrowleft$ and are annihilated by the second projector by property (2.46). As a consequence, this leftmost projector can be removed.

Then, using the identity

$$\begin{array}{c} \text{diamond with } u \text{ and a loop below} \end{array} = s_2(-u) \begin{array}{c} \text{diamond with two vertical lines and a loop below} \end{array} \quad (\text{E.10})$$

and property (2.46) of P_n , it follows that

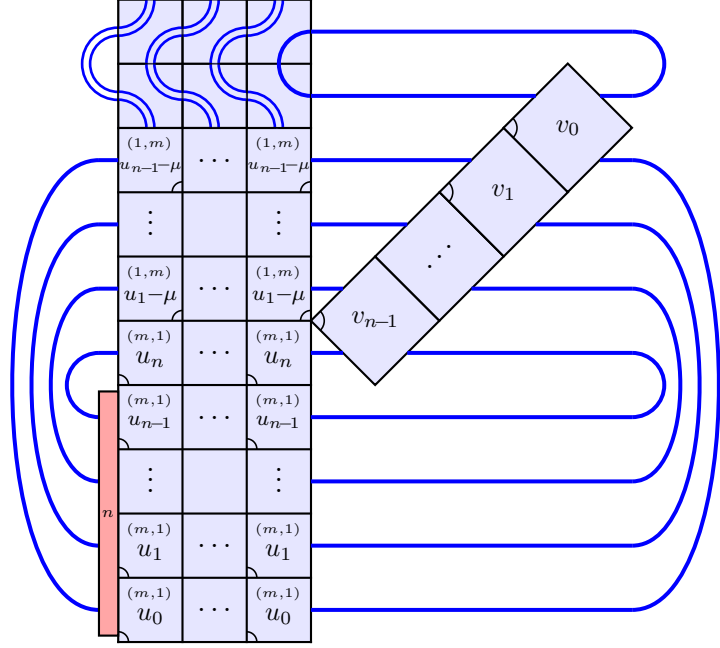
$$\begin{array}{c} \text{diamond with } -v_0, -v_1, \dots, -v_{n-1} \text{ and a loop below} \end{array} = \gamma_L \begin{array}{c} \text{diamond with wavy lines and a loop below} \end{array} \quad \gamma_L = s_{2-n}(\mu-2u) \prod_{j=n}^{2n-2} s_{-j}(\mu-2u) \quad (\text{E.11})$$

and that the tangle (E.9) can be reexpressed as

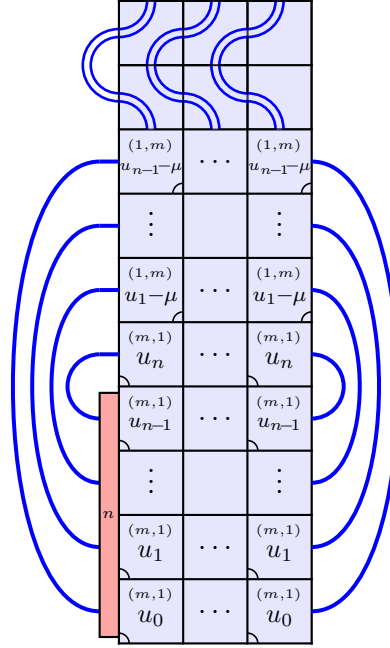
$$-\frac{s_n(0)}{s_{n+1}(0)} \begin{array}{c} \text{Diagram 1: A central grid of boxes with labels } (1,m), (m,1), u_{n+1-\mu}, \dots, u_{n-1}, u_n, u_{n-1}, \dots, u_1, u_0 \text{ and blue strands forming loops. A diamond with } -v_0, -v_1, \dots, -v_{n-1} \text{ is on the left and a diamond with } v_0, v_1, \dots, v_{n-1} \text{ is on the right.} \end{array}$$

$$= -\frac{s_n(0)}{s_{n+1}(0)} \gamma_L \begin{array}{c} \text{Diagram 2: Similar to Diagram 1, but the left diamond is replaced by a vertical stack of boxes with labels } (1,m), (m,1), u_{n+1-\mu}, \dots, u_{n-1}, u_n, u_{n-1}, \dots, u_1, u_0 \text{ and the right diamond is replaced by a vertical stack of boxes with labels } (1,m), (m,1), u_{n+1-\mu}, \dots, u_{n-1}, u_n, u_{n-1}, \dots, u_1, u_0. \end{array}$$

$$= -\frac{s_n(0)}{s_{n+1}(0)} \gamma_L [q^m(\mu - u_{n-1})]^N$$



$$= -\frac{s_n(0)}{s_{n+1}(0)} \gamma_L \gamma_R [q^m(\mu - u_{n-1})]^N$$



(E.12)

$$\begin{aligned}
&= -\frac{s_n(0)}{s_{n+1}(0)} \gamma_L \gamma_R [q^m(u_n) q^m(\mu - u_{n-1})]^N \\
&\quad \text{Diagram: A grid of boxes with labels } (1,m), (m,1), u_{n-1}-\mu, u_1-\mu, u_{n-2}, u_0 \text{ and blue wavy lines. A red vertical bar labeled } n \text{ is on the left.} \\
&= -\gamma_L \gamma_R [q^m(u_n) q^m(\mu - u_{n-1})]^N \mathbf{D}_0^{m,n-1}
\end{aligned} \tag{E.13}$$

One should note that in (E.12), the idea underlying (E.11) was used for the right boundary, with

$$\gamma_R = s_{2n+1}(2u - \mu) \prod_{j=n+1}^{2n-1} s_j(2u - \mu), \tag{E.14}$$

and that property (2.47) of the WJ projectors was used at the last equality. Finally,

$$\alpha_L^\diamond \alpha_R^\diamond \mathbf{D}_0^{m,n+1} = \eta(u, \mu) \mathbf{D}_0^{m,n} \mathbf{D}_n^{m,1} - \gamma_L \gamma_R [q^m(u_n) q^m(\mu - u_{n-1})]^N \mathbf{D}_0^{m,n-1} \tag{E.15}$$

which leads to (E.1) after simplifications of the trigonometric functions. As a final remark, we note that all the arguments go through for $n = 1$ as well, with the final result given by (E.15) with $\mathbf{D}_0^{m,0}$ replaced by \mathbf{I}^m . \square

E.2 On the cylinder

Here we recall and prove Proposition 6.2.

PROPOSITION 6.2 *On the cylinder, the fusion hierarchy for $m, n \in \mathbb{N}$ is given by*

$$\mathbf{T}_0^{m,n} \mathbf{T}_n^{m,1} = \mathbf{T}_0^{m,n+1} + h_n^m h_{n-2}^m \mathbf{T}_0^{m,n-1}, \tag{E.16}$$

where h_k^m is defined in (1.16).

PROOF: We use the form (4.10) for $\mathbf{T}_0^{m,n+1}$ and rewrite the projector using (2.42) to obtain

$$\begin{aligned}
\mathbf{T}_0^{m,n+1} &= \text{Diagram 1} - \frac{s_n(0)}{s_{n+1}(0)} \text{Diagram 2} \\
&\quad \text{Diagram 1: Grid with labels } (m,1), u_n, u_{n-1}, u_1, u_0 \text{ and blue wavy lines. Red vertical bar labeled } n \text{ on the left.} \\
&\quad \text{Diagram 2: Similar grid with blue wavy lines. Red vertical bar labeled } n \text{ on the left.}
\end{aligned} \tag{E.17}$$

The first term is readily recognised as $\mathbf{T}_0^{m,n} \mathbf{T}_n^{m,1}$. For the second term, we expand the rightmost projector in connectivities and find that only the identity connectivity contributes nontrivially. All other connectivities have half-arcs that push through towards the left and are annihilated when reaching the leftmost projector. The second term can then be written as

$$\begin{aligned}
& -\frac{s_n(0)}{s_{n+1}(0)} \begin{array}{c} \text{Diagram 1: A grid of } (m,1) \text{ projectors } u_n, \dots, u_n \text{ in the top row, } u_{n-1}, \dots, u_{n-1} \text{ in the next row, and } u_1, \dots, u_1 \text{ in the bottom row. A red vertical bar labeled } n \text{ is on the left. Blue arcs connect the top and bottom of the grid.} \end{array} = -\frac{s_n(0)}{s_{n+1}(0)} [q^m(u_n)]^N \begin{array}{c} \text{Diagram 2: Similar grid to Diagram 1, but with blue arcs connecting the projectors in a more complex pattern.} \end{array} \\
& = -[q^m(u_n)]^N \begin{array}{c} \text{Diagram 3: A grid of } (m,1) \text{ projectors } u_{n-2}, \dots, u_{n-2} \text{ in the top row, } u_1, \dots, u_1 \text{ in the next row, and } u_0, \dots, u_0 \text{ in the bottom row. A red vertical bar labeled } n-1 \text{ is on the left.} \end{array} = -h_n^m h_{n-2}^m \mathbf{T}_0^{1,n-1} \quad (\text{E.18})
\end{aligned}$$

as required. Note that property (2.48) of the WJ projectors was used at the second equality and

$$[q^m(u_n)]^N = h_n^m h_{n-2}^m \quad (\text{E.19})$$

at the last one. \square

F Closure of the fusion hierarchies

F.1 Preliminaries

For every integer $n \geq 2$ and all $\lambda \in \pi(\mathbb{R} \setminus \mathbb{Z})$, the fusion hierarchy equations of Section 6 (proved above in Appendix E) express (m, n) -fused transfer tangles in terms of products and sums of (m, n') -fused transfer tangles with $n' < n$. In this appendix, we show that, for fractional $\lambda = \lambda_{p,p'}$, the fusion hierarchy closes both on the strip and cylinder, and find that the (m, p') -fused transfer tangle can be expressed as a linear combination of (m, n') -fused transfer tangles with $n' < p'$. For convenience, in the remainder of this appendix, we parameterise p' as

$$p' = \ell + 1. \quad (\text{F.1})$$

As will soon become evident, the fusion closure is made possible by properties specific to fractional values of λ . One such property is that the local Boltzmann weights satisfy

$$s_{i+\ell+1}(u) = (-1)^{\ell+1-p} s_i(u), \quad s_{\ell+1}(0) = 0 \quad (\text{F.2})$$

from which it follows that the following four properties hold:

- (a) $\boxed{u_\ell} = (-1)^{\ell+1-p} \boxed{u_{-1}}$
- (b) $P_{\ell+1}$ does not exist.
- (c) $\boxed{\ell} = 0$.

(d) The recursive definition of P_ℓ in terms of $P_{\ell-1}$ can be simplified to

$$\boxed{\ell} = \boxed{\ell-1} \mid - \beta \begin{array}{c} \boxed{\ell-1} \\ \vdots \\ \boxed{\ell-1} \end{array} \quad (F.3)$$

Even though $P_{\ell+1}$ is singular, the limits (4.17) of the transfer tangles $\mathbf{D}_k^{m,\ell+1}$ and $\mathbf{T}_k^{m,\ell+1}$ still exist for $m < p$ and can for example be defined in terms of effective projectors, as explained in Section 4.2. Here the closure relations will be shown using only diagrammatic objects which are well defined for $\lambda = \lambda_{p,\ell+1}$. Indeed, the starting points of the proofs will be $\mathbf{D}_0^{m,\ell} \mathbf{D}_\ell^{m,1}$ and $\mathbf{T}_0^{m,\ell} \mathbf{T}_\ell^{m,1}$ instead of $\mathbf{D}_0^{m,\ell+1}$ and $\mathbf{T}_0^{m,\ell+1}$. Equations (7.1) and (7.20) are just concise rewritings of the results we obtain, using the fusion hierarchy equations (6.1) and (6.6). For simplicity, we will first prove the closure for $m = 1$ and then generalise to $m > 1$. For $m = 1$, the tangles $\mathbf{D}_0^{1,\ell} \mathbf{D}_\ell^{1,1}$ and $\mathbf{T}_0^{1,\ell} \mathbf{T}_\ell^{1,1}$ will be written in terms of columns of elementary face operators, to which projectors are glued, of the form

$$\begin{array}{c} \boxed{u_\ell} \\ \boxed{u_{\ell-1}} \\ \vdots \\ \boxed{u_1} \\ \boxed{u_0} \end{array} \mid \ell = \begin{array}{c} \boxed{u_\ell} \\ \boxed{u_0} \\ \boxed{u_1} \\ \vdots \\ \boxed{u_{\ell-1}} \end{array} \mid \ell \quad (F.4)$$

Because

$$\begin{array}{c} \boxed{u_\ell} \\ \boxed{u_0} \end{array} \mid = (-1)^{\ell+1-p} q^1(u) \begin{array}{c} \boxed{u_\ell} \\ \boxed{u_0} \end{array} \mid \quad (F.5)$$

going from one form to the other in (F.4) reverses the order of half-arc propagation for the full column of faces, from \leftarrow to \rightarrow . This property will play a key role in the following.

We conclude these preliminaries with the following lemma.

LEMMA F.1 For $\lambda = \lambda_{p,\ell+1}$, the $(\ell+2)$ -tangle defined by

$$\boxed{\ell} := \begin{array}{c} \boxed{\ell} \\ \vdots \\ \boxed{\ell} \end{array} + (-1)^p \begin{array}{c} \boxed{\ell} \\ \vdots \\ \boxed{\ell} \end{array} \quad (F.6)$$

satisfies

$$\begin{array}{c} \boxed{\ell} \end{array} \mid = -\beta \begin{array}{c} \boxed{\ell} \\ \vdots \\ \boxed{\ell-1} \end{array} \mid \quad \begin{array}{c} \boxed{\ell} \end{array} \mid = (-1)^{p+1} \beta \begin{array}{c} \boxed{\ell-1} \\ \vdots \\ \boxed{\ell} \end{array} \mid \quad (F.7)$$

PROOF: To prove the first relation in (F.7), we examine the two contributions coming from the expansion (F.6) and write the lefthand side as $X_1 + (-1)^p X_2$. For X_1 , using (F.3), we expand the rightmost projector and find

$$X_1 = \begin{array}{c} \text{Diagram 1} \\ \ell \quad \ell \end{array} = \begin{array}{c} \text{Diagram 2} \\ \ell \quad \ell-1 \end{array} - \beta \begin{array}{c} \text{Diagram 3} \\ \ell \quad \ell-1 \quad \ell-1 \end{array} = \begin{array}{c} \text{Diagram 4} \\ \ell \end{array} - \beta \begin{array}{c} \text{Diagram 5} \\ \ell \quad \ell-1 \end{array} \quad (\text{F.8})$$

where the two horizontal loop segments in blue represent a total of $\ell - 2$ links. For X_2 , in the expansion of the rightmost projector, only a single connectivity survives,

$$\underbrace{(-1)^{\ell-1} \frac{s_1(0)}{s_\ell(0)}}_{=(-1)^{p+1}} \begin{array}{c} \vdots \\ \text{Diagram 6} \\ \vdots \end{array} \quad (\text{F.9})$$

and this yields

$$X_2 = \begin{array}{c} \text{Diagram 7} \\ \ell \quad \ell \end{array} = (-1)^{p+1} \begin{array}{c} \text{Diagram 8} \\ \ell \end{array} \quad (\text{F.10})$$

Two terms cancel out in $X_1 + (-1)^p X_2$ and this concludes the proof of the first identity. The second identity in (F.7) is obtained by a left-right reflection of the first, with the factor of $(-1)^p$ arising due to the relative sign in (F.6). \square

One should note that the proofs in this appendix are for general fractional $\lambda = \lambda_{p,\ell+1}$ and require planar calculations involving arrays of face operators whose heights can go up to $2(\ell + 1)$. Vertical dots are usually included to indicate high columns, but in some cases this would make the diagrams cumbersome, and planar computations are then reported for some large column height instead. The previous proof is an example where this reporting technique has been employed.

F.2 On the strip

PROPOSITION F.2 *For $m = 1$, the fusion hierarchy on the strip closes as*

$$\mathbf{D}_0^{1,\ell+1} = [q^1(u_0)q^1(\mu - u_{-1})]^N \mathbf{D}_1^{1,\ell-1} + 2(-1)^{\ell+1-p} \left(\prod_{j=0}^{\ell} s_j(u) s_{j+1}(u - \mu) \right)^N \mathbf{I}. \quad (\text{F.11})$$

PROOF: The proof of (F.11) is based on a set of recursion relations to be constructed in the following. First, we write down the relations and describe the objects they link together, but postpone their technically involved proofs till the end. The fusion closure we set out to prove is thus given by

$$\begin{aligned} \frac{s_{2\ell}(2u-\mu)s_{\ell-1}(2u-\mu)}{s_{2\ell-1}(2u-\mu)s_\ell(2u-\mu)} \mathbf{D}_0^{1,\ell} \mathbf{D}_\ell^{1,1} &= [q^1(u_{-1})q^1(\mu - u_{-2})]^N \mathbf{D}_0^{1,\ell-1} + [q^1(u_0)q^1(\mu - u_{-1})]^N \mathbf{D}_1^{1,\ell-1} \\ &+ 2(-1)^{\ell+1-p} \left(\prod_{j=0}^{\ell} s_j(u) s_{j+1}(u - \mu) \right)^N \mathbf{I}. \end{aligned} \quad (\text{F.12})$$

Because no $P_{\ell+1}$ appears in this expression, all objects are well defined. It is also straightforward to show that (F.12) and (6.1) imply (F.11).

The first step is to prove that the following identity holds,

$$s_{2\ell}(2u-\mu)s_{\ell-1}(2u-\mu)\mathbf{D}_0^{1,\ell}\mathbf{D}_\ell^{1,1} = s_{2\ell-1}(2u-\mu)s_\ell(2u-\mu)\mathbf{A}, \quad (\text{F.13})$$

where the tangle \mathbf{A} is defined as

The proof of (F.13) is rather technical and given below.

The next step is to establish recursion relations between two (new) families of objects, \mathbf{A}_r and $\mathbf{D}_{k,r}^{1,\ell-1}$, $r = 0, \dots, N$, for which $\mathbf{A} = \mathbf{A}_0$ and $\mathbf{D}_k^{1,\ell} = \mathbf{D}_{k,0}^{1,\ell}$ are special cases. The new lower index r indicates that the r leftmost columns of boxes are removed from the diagrammatic definition of \mathbf{A}_0 and $\mathbf{D}_{k,0}^{1,\ell}$ and replaced by r vertical strands. The left boundary is then displaced toward the right to act as the left boundary for the reduced diagram of face operators which is composed of $N - r$ columns, that is,

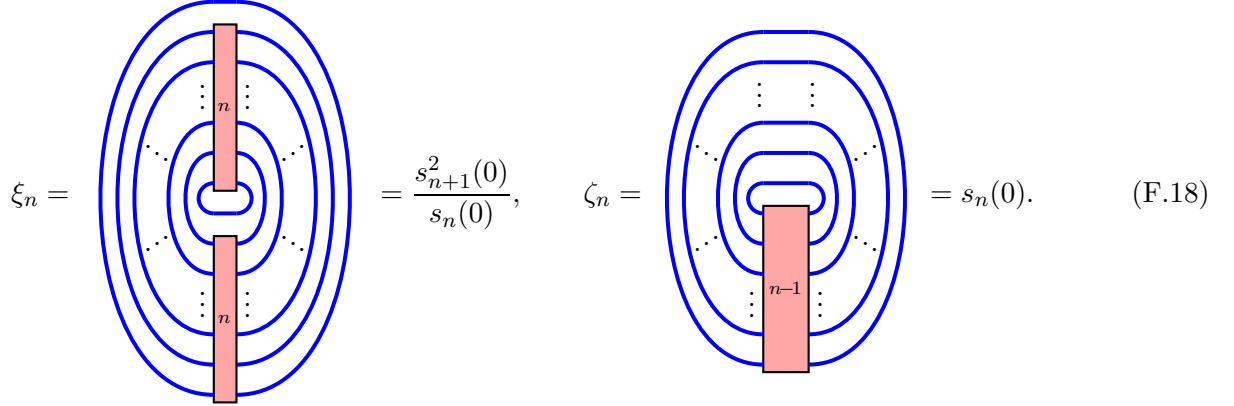
By summing over configurations of face operators in the first column of \mathbf{A}_r , we will find, in (F.26) – (F.50),

$$\begin{aligned} \mathbf{A}_r = & \mathbf{A}_{r+1} \left(\prod_{j=0}^{\ell} s_j(u) s_{j+1}(u-\mu) \right) \\ & + [q^1(u_0)q^1(\mu-u_{-1})]^{N-r} \left(\mathbf{D}_{1,r}^{1,\ell-1} - \mathbf{D}_{1,r+1}^{1,\ell-1} s_\ell(u) s_{\ell-1}(u-\mu) \prod_{j=1}^{\ell-2} s_j(u) s_{j+1}(u-\mu) \right) \\ & + [q^1(u_{-1})q^1(\mu-u_{-2})]^{N-r} \left(\mathbf{D}_{0,r}^{1,\ell-1} - \mathbf{D}_{0,r+1}^{1,\ell-1} s_{\ell-1}(u) s_\ell(u-\mu) \prod_{j=0}^{\ell-3} s_j(u) s_{j+1}(u-\mu) \right). \end{aligned} \quad (\text{F.16})$$

For $r = N$, it is straightforward to show that

$$\mathbf{A}_N = \xi_\ell \mathbf{I} = \frac{s_{\ell+1}^2(0)}{s_\ell(0)} \mathbf{I} = 0, \quad \mathbf{D}_{k,N}^{1,\ell-1} = \zeta_\ell \mathbf{I} = s_\ell(0) \mathbf{I} = (-1)^{\ell-p} \mathbf{I}, \quad (\text{F.17})$$

where, in general, for $n \in \mathbb{N}$ and λ generic,



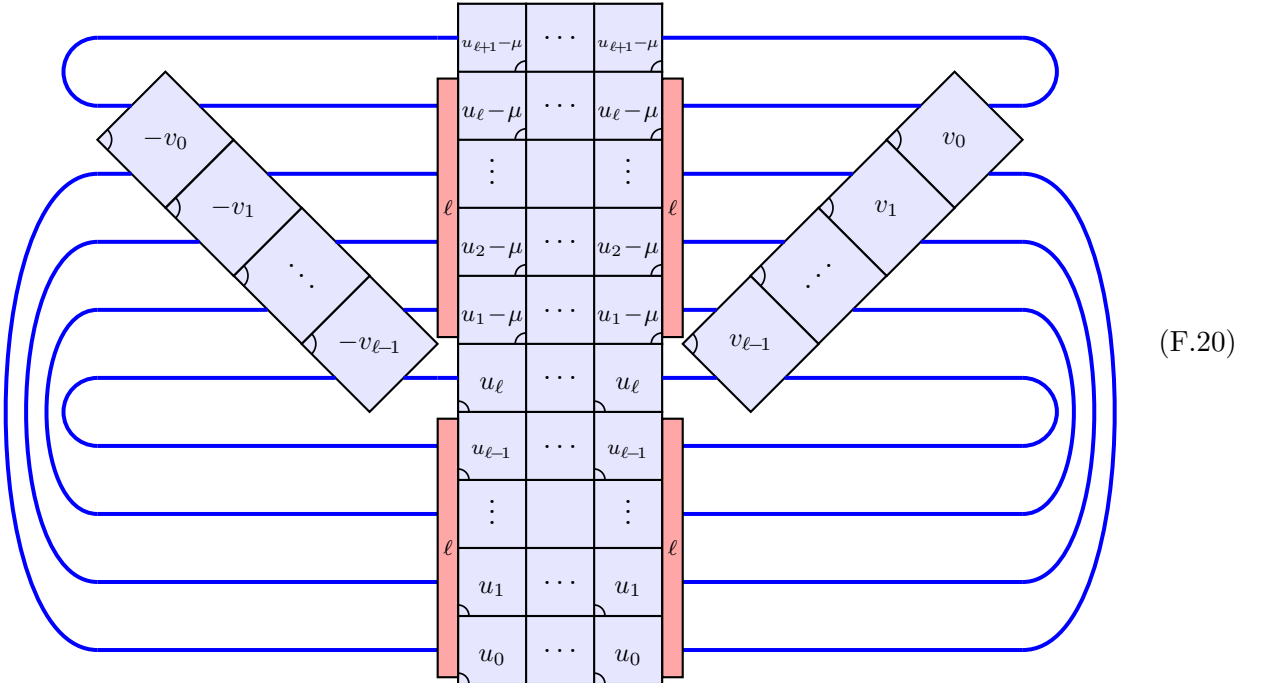
$$\xi_n = \frac{s_{n+1}^2(0)}{s_n(0)}, \quad \zeta_n = s_n(0). \quad (\text{F.18})$$

The recursion relation (F.16) allows us to write an equality tying \mathbf{A} , $\mathbf{D}_0^{1,\ell-1}$ and $\mathbf{D}_1^{1,\ell-1}$ with \mathbf{A}_N , $\mathbf{D}_{0,N}^{1,\ell-1}$ and $\mathbf{D}_{1,N}^{1,\ell-1}$ which reads, after simplification,

$$\mathbf{A} - [q^1(u_{-1})q^1(\mu - u_{-2})]^N \mathbf{D}_0^{1,\ell-1} - [q^1(u_0)q^1(\mu - u_{-1})]^N \mathbf{D}_1^{1,\ell-1} = 2(-1)^{\ell+1-p} \left(\prod_{j=0}^{\ell} s_j(u) s_{j+1}(u - \mu) \right)^N \mathbf{I}. \quad (\text{F.19})$$

With (F.13), this concludes the proof of (F.11). The remaining technical computations are the proofs of (F.13) and (F.16), which are done in the next two paragraphs.

Proof of equation (F.13) We start with the form (E.6) for $\eta(u, \mu) \mathbf{D}_0^{1,\ell} \mathbf{D}_\ell^{1,1}$,



$$(\text{F.20})$$

where three new P_ℓ projectors have been added. This is permitted by push-through properties and the annihilation property (2.46) of the projectors. Diamond face operators are then expanded as

$$\text{Diagram (F.21)} \quad (F.21)$$

$$\text{Diagram (F.22)} \quad (F.22)$$

where α_L^\diamond and α_R^\diamond are obtained by setting $n = \ell$ in (E.3). This gives four terms, three of which are zero. For example, the term corresponding to $\alpha_L^\diamond \alpha_R^\diamond$ is

$$\text{Diagram (F.23)} \quad (F.23)$$

A single connectivity now contributes to the lower-left P_ℓ projector,

$$\text{Diagram (F.24)} \quad (F.24)$$

while all the others have half-arcs that propagate and are annihilated by the remaining P_ℓ projector. Up to the factor $(-1)^{p+1}[q^1(u_\ell)]^N$, this gives

$$= [q^1(\mu - u_{\ell-1})]^N \quad (\text{F.25})$$

which is zero due to property (c) given in Section F.1. Similarly, the tangles corresponding to $\alpha_L^\diamond \alpha_R^\diamond$ and $\alpha_L^\diamond \alpha_R^\diamond$ are also zero, because half-arcs propagate all the way around the tangle, $\curvearrowright \rightleftharpoons \curvearrowleft$, and are annihilated by the last P_ℓ projector. The only contribution to $\eta(u, \mu) \mathcal{D}_0^{1, \ell} \mathcal{D}_\ell^{1, 1}$ is $\alpha_L^\diamond \alpha_R^\diamond \mathbf{A}$, with \mathbf{A} defined in (F.14), and this simplifies to (F.13).

Proof of equation (F.16) In the computations to follow, only the $L := N - r$ columns of boxes will be considered, while the r identity strands located on the left simply act as spectators. These will therefore be omitted from the diagrams in our planar computations. We start by expanding, in \mathbf{A}_r , the bottom ℓ elementary faces in the leftmost column of face operators,

$$= s_\ell(u) \prod_{j=0}^{\ell-1} s_{1-j}(-u) \underbrace{\quad}_{x_1} + s_{1-\ell}(-u) \prod_{j=0}^{\ell-1} s_j(u) \underbrace{\quad}_{x_2} + \prod_{j=0}^{\ell} s_j(u) \underbrace{\quad}_{x_3} \quad (\text{F.26})$$

where the last tangle is defined in (F.6). We thus write

$$\mathbf{A}_r = \mathbf{B}_1 + \mathbf{B}_2 + \mathbf{B}_3 \quad (\text{F.27})$$

and set out to study each term individually. For B_1 ,

$$\begin{aligned}
 & B_1 = x_1 \\
 & = x_1(-1)^{p+1}
 \end{aligned}
 \tag{F.28}$$

The diagrams consist of two vertically stacked grids of blue squares. Each grid has 4 columns and 12 rows. The top grid has red vertical bars at columns 1, 3, 5, 7, 9, and 11. The bottom grid has red vertical bars at columns 1, 3, 5, 7, 9, and 11, but with a different connectivity pattern for the blue arcs. Blue arcs connect the top and bottom rows of the grids, with some arcs passing through the red bars. The labels $u_{\ell+1}-\mu$, $u_{\ell}-\mu$, $u_2-\mu$, $u_1-\mu$, u_{ℓ} , $u_{\ell-1}$, u_1 , and u_0 are placed in specific squares. The label ℓ is placed in the red bars. The label $B_1 = x_1$ is to the left of the top diagram, and $= x_1(-1)^{p+1}$ is to the left of the bottom diagram. The label (F.28) is to the right of the bottom diagram.

where the P_{ℓ} projector at the bottom left of the tangle has been replaced by its only contributing connectivity (F.9) and all the other projectors (except two) have been removed using push-through

properties and property (2.46) of the projectors. Then,

$$\begin{aligned}
 & \mathbf{B}_1 = x_1(-1)^{p+1} [q^1(\mu - u_{-2})]^L \\
 & = x_1 [q^1(\mu - u_{-1})]^L [q^1(u_0)]^{L-1}
 \end{aligned}
 \tag{F.29}$$

where this time, the P_ℓ projector has been replaced by a left-right reflection of the connectivity (F.9). The next step is to use (F.3) on the remaining projector, and this yields two tangles,

$$\mathbf{B}_1 = x_1 [q^1(\mu - u_{-1})]^L [q^1(u_0)]^{L-1} (\mathbf{M}_1 + \mathbf{M}_2). \quad (\text{F.30})$$

The first one is

$$\mathbf{M}_1 = \begin{array}{c} \begin{array}{|c|c|c|c|} \hline u_{\ell-1}-\mu & \dots & \dots & u_{\ell-1}-\mu \\ \hline \vdots & & & \vdots \\ \hline u_2-\mu & \dots & \dots & u_2-\mu \\ \hline u_1-\mu & \dots & \dots & u_1-\mu \\ \hline \vdots & & & \vdots \\ \hline u_{\ell-2} & \dots & \dots & u_{\ell-2} \\ \hline \vdots & & & \vdots \\ \hline u_1 & \dots & \dots & u_1 \\ \hline u_0 & \dots & \dots & u_0 \\ \hline \end{array} \end{array} \quad (\text{F.31})$$

while the second one is

$$\mathbf{M}_2 = -\beta \begin{array}{c} \begin{array}{|c|c|c|c|} \hline \vdots & & & \vdots \\ \hline u_{\ell-1}-\mu & \dots & \dots & u_{\ell-1}-\mu \\ \hline \vdots & & & \vdots \\ \hline u_2-\mu & \dots & \dots & u_2-\mu \\ \hline u_1-\mu & \dots & \dots & u_1-\mu \\ \hline \vdots & & & \vdots \\ \hline u_{\ell-2} & \dots & \dots & u_{\ell-2} \\ \hline \vdots & & & \vdots \\ \hline u_1 & \dots & \dots & u_1 \\ \hline u_0 & \dots & \dots & u_0 \\ \hline \end{array} \end{array} \quad (\text{F.32})$$

$$= (-1)^{p+1} \begin{array}{c} \begin{array}{|c|c|c|c|} \hline u_{\ell-1}-\mu & \dots & \dots & u_{\ell-1}-\mu \\ \hline \vdots & & & \vdots \\ \hline u_2-\mu & \dots & \dots & u_2-\mu \\ \hline u_1-\mu & \dots & \dots & u_1-\mu \\ \hline & u_{\ell-2} & \dots & u_{\ell-2} \\ \hline & \vdots & & \vdots \\ \hline & u_1 & \dots & u_1 \\ \hline & u_0 & \dots & u_0 \\ \hline \end{array} \\ \text{Diagram with blue arcs connecting the left and right sides of the grid, and a red vertical bar labeled } \ell-1 \text{ in the middle column.} \end{array} \quad (\text{F.33})$$

where at the last step we replaced the leftmost $P_{\ell-1}$ projector by its unique contributing connectivity,

$$\underbrace{(-1)^{\ell-2} \frac{s_1(0)}{s_{\ell-1}(0)}}_{=(-1)^p \beta^{-1}} \begin{array}{c} \vdots \\ \text{Diagram of two crossing blue arcs} \\ \vdots \end{array} \quad (\text{F.34})$$

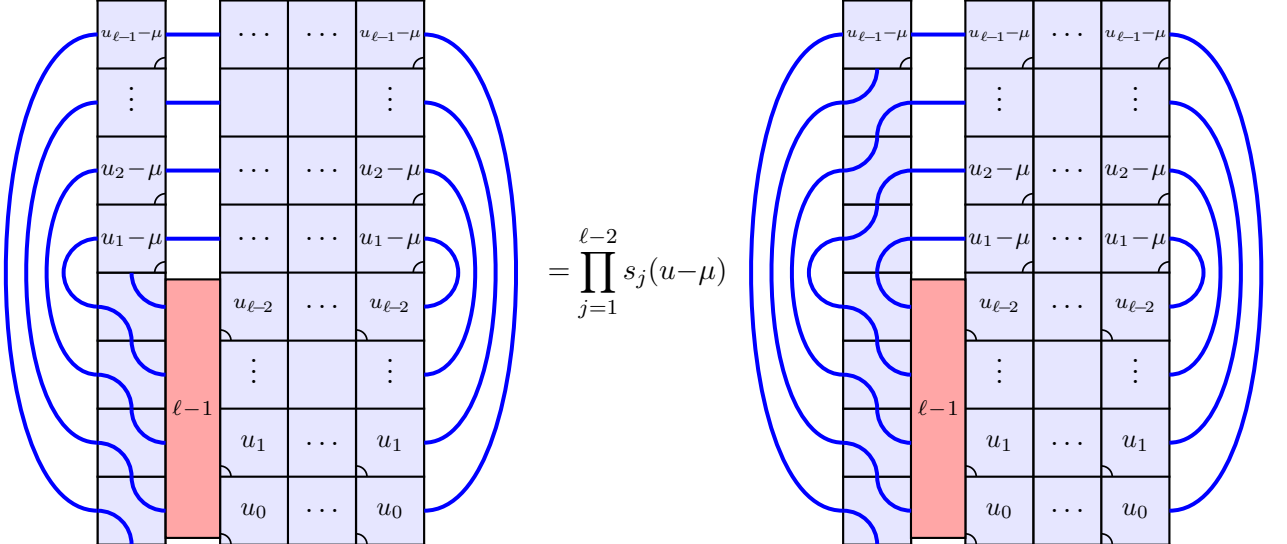
A final form for \mathbf{B}_1 is obtained after making two remarks. The first one is that an extra projector can be added at no cost in the resulting tangles of both (F.31) and (F.33),

$$\mathbf{M}_1 = \begin{array}{c} \begin{array}{|c|c|c|c|} \hline u_{\ell-1}-\mu & \dots & \dots & u_{\ell-1}-\mu \\ \hline \vdots & & & \vdots \\ \hline u_2-\mu & \dots & \dots & u_2-\mu \\ \hline u_1-\mu & \dots & \dots & u_1-\mu \\ \hline & u_{\ell-2} & \dots & u_{\ell-2} \\ \hline & \vdots & & \vdots \\ \hline & u_1 & \dots & u_1 \\ \hline & u_0 & \dots & u_0 \\ \hline \end{array} \\ \text{Diagram with blue arcs and two red vertical bars labeled } \ell-1 \text{ in the first two columns.} \end{array} \quad \mathbf{M}_2 = \begin{array}{c} \begin{array}{|c|c|c|c|} \hline u_{\ell-1}-\mu & \dots & \dots & u_{\ell-1}-\mu \\ \hline \vdots & & & \vdots \\ \hline u_2-\mu & \dots & \dots & u_2-\mu \\ \hline u_1-\mu & \dots & \dots & u_1-\mu \\ \hline & u_{\ell-2} & \dots & u_{\ell-2} \\ \hline & \vdots & & \vdots \\ \hline & u_1 & \dots & u_1 \\ \hline & u_0 & \dots & u_0 \\ \hline \end{array} \\ \text{Diagram with blue arcs and two red vertical bars labeled } \ell-1 \text{ in the first two columns, with different arc connectivity than } \mathbf{M}_1. \end{array} \quad (\text{F.35})$$

A particular linear combination of these gives $\mathbf{D}_{0,r}^{1,\ell-1}$, that is

$$\mathbf{D}_{0,r}^{1,\ell-1} = \mathbf{M}_1 \prod_{j=0}^{\ell-2} s_{1-j}(-u) + \mathbf{M}_2 \prod_{j=0}^{\ell-2} s_j(u). \quad (\text{F.36})$$

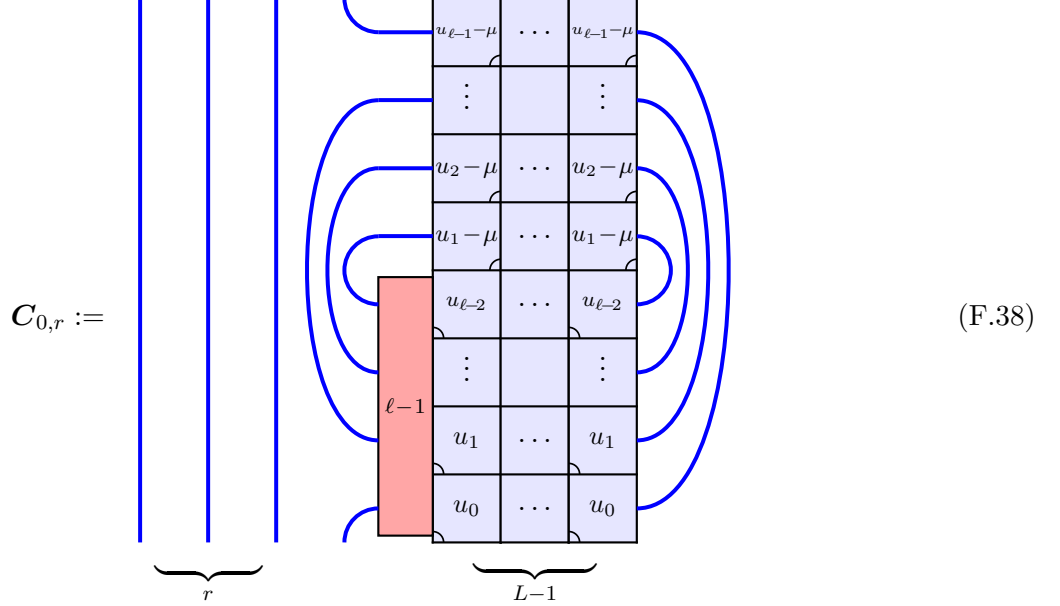
The other remark is that



$$= \prod_{j=1}^{\ell-2} s_j(u-\mu) \left(s_{\ell-1}(\mu-u) \mathbf{D}_{0,r+1}^{1,\ell-1} + s_{\ell-2}(\mu-u) \mathbf{C}_{0,r} \right) \quad (\text{F.37})$$

$$= \prod_{j=1}^{\ell-2} s_j(\mu-u) \times \left(s_{\ell-1}(\mu-u) \mathbf{D}_{0,r+1}^{1,\ell-1} + s_{\ell-2}(\mu-u) \mathbf{C}_{0,r} \right) \quad (\text{F.37})$$

where



$$\mathbf{C}_{0,r} := \text{Diagram} \quad (\text{F.38})$$

Putting these results together, we find

$$\mathbf{B}_1 = [q^1(u_{-1})q^1(\mu-u_{-2})]^L \left(\mathbf{D}_{0,r}^{1,\ell-1} - \beta s_{\ell-1}(u) \left(\prod_{j=0}^{\ell-3} s_j(u) s_{j+1}(u-\mu) \right) [s_{\ell-1}(u-\mu) \mathbf{D}_{0,r+1}^{1,\ell-1} - s_{\ell-2}(u-\mu) \mathbf{C}_{0,r}] \right). \quad (\text{F.39})$$

The same ideas are used for \mathbf{B}_2 , which in the end reads

$$\mathbf{B}_2 = [q^1(u_0)q^1(\mu-u_{-1})]^L \left(\mathbf{D}_{1,r}^{1,\ell-1} - \beta \mathbf{C}_{1,r} s_{\ell}(u) s_{\ell+1}(u-\mu) \prod_{j=1}^{\ell-2} s_j(u) s_{j+1}(u-\mu) \right) \quad (\text{F.40})$$

where $\mathbf{C}_{1,r} := \mathbf{C}_{0,r}(u+\lambda)$.

For B_3 , we proceed to sum over the remaining ℓ face operators of the leftmost column,

$$\begin{array}{|c|} \hline u_\ell \\ \hline u_{\ell-1} \\ \hline \vdots \\ \hline u_1 \\ \hline u_0 \\ \hline \end{array} = s_{\ell+1}(u-\mu) \prod_{j=0}^{\ell-1} s_{-j}(\mu-u) \begin{array}{|c|} \hline \text{blue wavy lines} \\ \hline \end{array} + s_\ell(\mu-u) \prod_{j=1}^{\ell} s_j(u-\mu) \begin{array}{|c|} \hline \text{blue wavy lines} \\ \hline \end{array} + (-1)^p \prod_{j=1}^{\ell+1} s_j(u-\mu) \begin{array}{|c|} \hline \text{blue wavy lines} \\ \hline \end{array} \quad (\text{F.41})$$

This leads to the separate contributions

$$B_3 = B_4 + B_5 + B_6 \quad (\text{F.42})$$

which are tackled independently. Using the same arguments as before, one finds

$$B_4 = -\beta s_{\ell-1}(u) s_{\ell+1}(u-\mu) \left(\prod_{j=0}^{\ell-3} s_j(u) s_{j+1}(u-\mu) \right) [q^1(u_{-1}) q^1(\mu-u_{-2})]^L (D_{0,r+1}^{1,\ell-1} - \beta C_{0,r}) \quad (\text{F.43})$$

and also

$$B_5 = 0. \quad (\text{F.44})$$

This last equality results from

$$\begin{array}{|c|} \hline \text{blue wavy lines} \\ \hline \end{array} = (-1)^{p+1} \begin{array}{|c|} \hline \text{blue wavy lines} \\ \hline \end{array} = \beta \begin{array}{|c|} \hline \text{blue wavy lines} \\ \hline \end{array} = \beta \begin{array}{|c|} \hline \text{blue wavy lines} \\ \hline \end{array} = 0 \quad (\text{F.45})$$

where, in order, we replaced the top P_ℓ by the connectivity (F.9), used (F.7) and property (2.47) of the projectors. Finally, to compute B_6 , we use the identity

$$\begin{array}{|c|} \hline \text{blue wavy lines} \\ \hline \end{array} = (-1)^p \begin{array}{|c|} \hline \text{blue wavy lines} \\ \hline \end{array} + \begin{array}{|c|} \hline \text{blue wavy lines} \\ \hline \end{array} + (-1)^p s_3(0) \begin{array}{|c|} \hline \text{blue wavy lines} \\ \hline \end{array} + \begin{array}{|c|} \hline \text{blue wavy lines} \\ \hline \end{array} \quad (\text{F.46})$$

whose proof will be the topic of the paragraph below. This separates the computation of B_6 into the four parts

$$B_6 = B_7 + B_8 + B_9 + B_{10}, \quad (\text{F.47})$$

each of which can be computed using the techniques presented earlier. This yields

$$\mathbf{B}_7 = \left(\prod_{j=0}^{\ell} s_j(u) s_{j+1}(u-\mu) \right) \mathbf{A}_{r+1}, \quad \mathbf{B}_8 = 0, \quad (\text{F.48})$$

$$\mathbf{B}_9 = s_3(0) s_{\ell-1}(u) s_{\ell}(u-\mu) \left(\prod_{j=0}^{\ell-3} s_j(u) s_{j+1}(u-\mu) \right) [q^1(u_{-1}) q^1(\mu-u_{-2})]^L (\mathbf{D}_{0,r+1}^{1,\ell-1} - \beta \mathbf{C}_{0,r}), \quad (\text{F.49})$$

$$\mathbf{B}_{10} = (-1) s_{\ell}(u) s_{\ell+1}(u-\mu) \left(\prod_{j=1}^{\ell-2} s_j(u) s_{j+1}(u-\mu) \right) [q^1(u_0) q^1(\mu-u_{-1})]^{2L} (\mathbf{D}_{1,r+1}^{1,\ell-1} - \beta \mathbf{C}_{1,r}). \quad (\text{F.50})$$

Combining (F.27), (F.39), (F.40), (F.42)-(F.44) and (F.47)-(F.50), one finds that the coefficients of $\mathbf{C}_{0,r}$ and $\mathbf{C}_{1,r}$ cancel out and that the final result for \mathbf{A}_r indeed is given by (F.16). The only missing piece of the puzzle is the proof of equation (F.46).

Proof of equation (F.46) We write the lefthand side as

$$= \text{[Diagram 1]} + \text{[Diagram 2]} + (-1)^p \text{[Diagram 3]} + (-1)^p \text{[Diagram 4]} \quad (\text{F.51})$$

By virtue of property (c) given in Section F.1, the last term is readily seen to be zero. The first term is not and expands as

$$= \text{[Diagram 1]} - \beta \text{[Diagram 2]} = \text{[Diagram 3]} - \beta \text{[Diagram 4]} \quad (\text{F.52})$$

$$\begin{aligned}
&= \text{Diagram 1} + (-1)^p \beta \text{Diagram 2} = \text{Diagram 3} + (-1)^p \beta \text{Diagram 4} \quad (\text{F.53})
\end{aligned}$$

For the second term,

$$\begin{aligned}
&\text{Diagram 5} = (-1)^{p+1} \text{Diagram 6} = (-1)^{p+1} \text{Diagram 7} + (-1)^p \beta \text{Diagram 8} \quad (\text{F.54})
\end{aligned}$$

$$\begin{aligned}
&= (-1)^{p+1} \text{Diagram 9} + \text{Diagram 10} = (-1)^{p+1} \text{Diagram 11} + \text{Diagram 12} \quad (\text{F.55})
\end{aligned}$$

Finally, the last term in (F.51) is the longest to compute,

(F.56)

Both diagrams on the right can be simplified,

(F.57)

and

(F.58)

Two connectivities contribute to the remaining $P_{\ell-1}$ projector in the second tangle of (F.58),

$$\begin{array}{c} \text{---} \\ \text{---} \\ \vdots \\ \text{---} \end{array} \quad \text{and} \quad \underbrace{(-1)^{\frac{s_{\ell-2}(0)}{s_{\ell-1}(0)}}}_{= (-1)^{\frac{s_3(0)}{s_2(0)}}} \quad \begin{array}{c} \text{---} \\ \text{---} \\ \vdots \\ \text{---} \end{array} \quad \begin{array}{c} \text{---} \\ \text{---} \\ \vdots \\ \text{---} \end{array} \quad (F.59)$$

yielding

(F.60)

Adding up all these contributions gives (F.46), as already announced. \square

PROPOSITION F.3 *On the strip, the fusion hierarchy for $m \in \mathbb{N}$ closes as*

$$D_0^{m,\ell+1} - [q^m(u_0)q^m(-u_{-2})]^N D_1^{m,\ell-1} = 2(-1)^{\ell+1-p} \left(\prod_{j=0}^{\ell} s_j(u) \right)^{2Nm} \mathbf{I}^m, \quad (\text{F.61})$$

where $q^m(u)$ is defined in (1.11).

OUTLINE OF THE PROOF: The generalisation from $m = 1$ to $m > 1$ is almost straightforward, so we will only give an outline of the steps of the proof without repeating the diagrammatic arguments. Because, as discussed in Section 5, the tangles $\mathbf{D}_k^{m,n}$ are in the subalgebra $FTL_{N,m}(\beta)$, it suffices to prove that (F.61) is satisfied with \mathbf{D} replaced by $\bar{\mathbf{D}}$, see (5.2). Now, the two transfer tangles $\bar{\mathbf{D}}_0^{m,\ell}$ and $\bar{\mathbf{D}}_0^{1,\ell}$, seen as elements of $TL_{Nm}(\beta)$, are quite similar. The only distinction is that, in $\bar{\mathbf{D}}_0^{m,\ell}$, columns of face operators have their spectral parameters shifted by an integer multiple of λ , and thus appear as

$$\begin{array}{c}
\textcolor{blue}{\boxed{u_{\ell+i}}} \\
\vdots \\
\textcolor{blue}{\boxed{u_{1+i}}} \\
\textcolor{blue}{\boxed{u_i}} \\
\textcolor{blue}{\boxed{u_{\ell-i}}} \\
\vdots \\
\textcolor{blue}{\boxed{u_{1-i}}} \\
\textcolor{blue}{\boxed{u_{-i}}}
\end{array}
\quad \left(\begin{array}{l} \ell \\ \ell \end{array} \right)
\tag{F.62}$$

for some $i \in \{0, \dots, m-1\}$. The proof of Proposition F.4 can be adjusted and now involves modified versions of \mathbf{A}_r , $\mathbf{D}_{k,r}^{m,\ell-1}$, $\mathbf{C}_{0,r}$ and $\mathbf{C}_{1,r}$ with varying spectral parameters. In the end, by summing over

configurations of the leftmost column of face operators in \mathbf{A}_r , one finds a recursion relation relating these objects from which (F.61) stems after simplifications.

F.3 On the cylinder

In Proposition F.4 below, we prove Proposition 7.5 for $m = 1$, recalling that λ is assumed fractional, $\lambda = \lambda_{p,p'}$, and that p' is parametrised as $p' = \ell + 1$.

PROPOSITION F.4 *On the cylinder, the fusion hierarchy for $m = 1$ closes as*

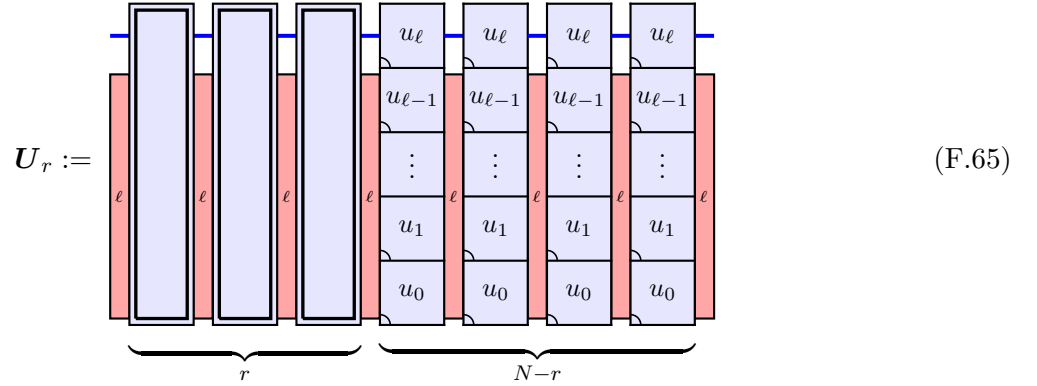
$$\mathbf{T}_0^{m,\ell+1} = h_0^1 h_{\ell-1}^1 \mathbf{T}_1^{m,\ell-1} + 2i^{N(\ell+1-p)} \left(\prod_{j=0}^{\ell} h_j^1 \right) \mathbf{J}^1 \quad (\text{F.63})$$

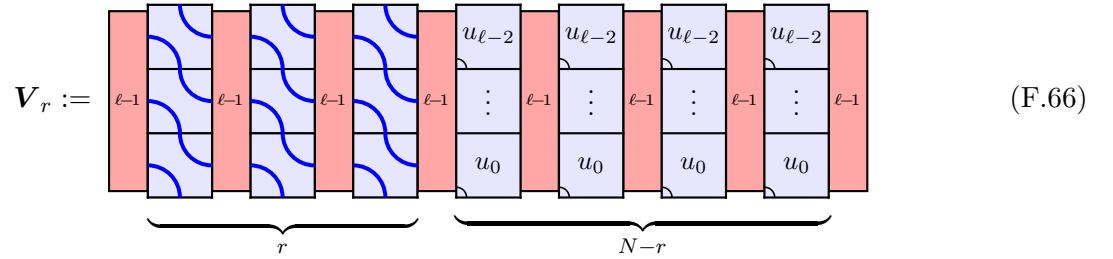
where \mathbf{J}^1 is a u -independent tangle.

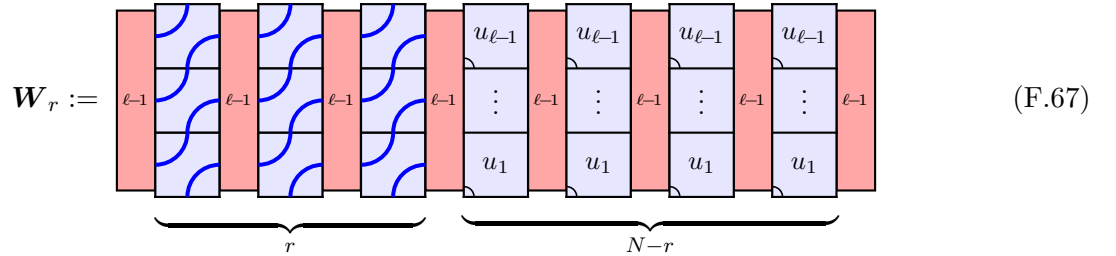
PROOF: The fusion closure we set out to prove is

$$\mathbf{T}_0^{1,\ell} \mathbf{T}_\ell^{1,1} = h_\ell^1 h_{\ell-2}^1 \mathbf{T}_0^{1,\ell-1} + h_0^1 h_{\ell-1}^1 \mathbf{T}_1^{1,\ell-1} + 2i^{N(\ell+1-p)} \left(\prod_{j=0}^{\ell} h_j^1 \right) \mathbf{J}^1, \quad h_k^1 = [-i s_k(u)]^N \quad (\text{F.64})$$

which, from (6.6), is equivalent to (F.63). For every $r \in \{0, \dots, N\}$, we introduce the three new objects \mathbf{U}_r , \mathbf{V}_r and \mathbf{W}_r defined as







$$= (-\beta)^r [s_\ell(u) s_{2-\ell}(-u)]^{N-r-1} \quad (F.73)$$

The final step is to rewrite the remaining P_ℓ projector using (F.3). This gives

$$\mathbf{X}_1 = (-\beta)^r [s_\ell(u) s_{2-\ell}(-u)]^{N-r-1} (\mathbf{Z}_1 - \beta \mathbf{Z}_2) \quad (F.74)$$

where

$$\begin{aligned} \mathbf{Z}_1 = & \quad \text{Diagram: A grid of blue squares with white circles. Red vertical bars of height 4 are placed at columns 2, 4, 6, and 8. The first bar is labeled \ell-1, and the last is labeled \ell-1. To the right of the last bar is a 3x3 grid of blue squares with white circles, labeled with u_{\ell-2}, u_{\ell-2}, u_{\ell-2} in the top row, \vdots, \vdots, \vdots in the middle row, and u_0, u_0, u_0 in the bottom row.} \\ = & \quad \text{Diagram: A sequence of red vertical bars of height 4, labeled \ell-1, followed by a 3x3 grid of blue squares with white circles, labeled with u_{\ell-2}, u_{\ell-2}, u_{\ell-2} in the top row, \vdots, \vdots, \vdots in the middle row, and u_0, u_0, u_0 in the bottom row.} \\ & = \frac{\mathbf{V}_r - \mathbf{V}_{r+1} \prod_{i=0}^{\ell-2} s_i(u)}{\prod_{k=0}^{\ell-2} s_{1-k}(-u)} \quad (F.75) \end{aligned}$$

and

$$\mathbf{Z}_2 = \quad \text{Diagram: A grid of blue squares with white circles. Red vertical bars of height 4 are placed at columns 2, 4, 6, and 8. The first bar is labeled \ell-1, and the last is labeled \ell-1. To the right of the last bar is a 3x3 grid of blue squares with white circles, labeled with u_{\ell-2}, u_{\ell-2}, u_{\ell-2} in the top row, \vdots, \vdots, \vdots in the middle row, and u_0, u_0, u_0 in the bottom row. Blue lines connect the right side of the last red bar to the left side of the 3x3 grid.} \quad (F.76)$$

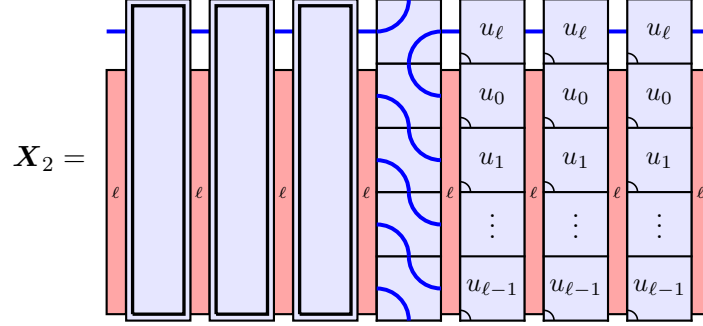
To proceed further, we note that the $P_{\ell-1}$ projector drawn with thicker boundaries in (F.76) has only one contributing connectivity, (F.34), and this allows us to write

$$\mathbf{Z}_2 = (-1)^p \beta^{-1} \quad \text{Diagram: A sequence of red vertical bars of height 4, labeled \ell-1, followed by a 3x3 grid of blue squares with white circles, labeled with u_{\ell-2}, u_{\ell-2}, u_{\ell-2} in the top row, \vdots, \vdots, \vdots in the middle row, and u_0, u_0, u_0 in the bottom row.} = (-1)^p \beta^{-1} \mathbf{V}_{i+1}. \quad (F.77)$$

Together, these rewritings of \mathbf{Z}_1 and \mathbf{Z}_2 yield

$$s_\ell(u) \left(\prod_{i=0}^{\ell-1} s_{1-i}(-u) \right) \mathbf{X}_1 = (-\beta)^r [s_\ell(u) s_{2-\ell}(-u)]^{N-r} \left(\mathbf{V}_r - \mathbf{V}_{r+1} \beta s_{\ell-1}(u) \prod_{j=0}^{\ell-3} s_j(u) \right). \quad (F.78)$$

For \mathbf{X}_2 , the same calculation is done by first reversing the order of the spectral parameters using (F.4), such that



Then, with arguments similar to the ones above, we find

$$s_{1-\ell}(-u) \left(\prod_{i=0}^{\ell-1} s_i(u) \right) \mathbf{X}_2 = ((-1)^{p+1} \beta)^r [s_0(u) s_{1-\ell}(-u)]^{N-r} \left(\mathbf{W}_r - \mathbf{W}_{r+1} (-1)^p \beta s_\ell(u) \prod_{j=1}^{\ell-2} s_j(u) \right). \quad (\text{F.79})$$

Combining equations (F.72), (F.78) and (F.79) completes the proof of equation (F.68). \square

PROPOSITION F.5 *On the cylinder, the fusion hierarchy for $m \in \mathbb{N}$ closes as*

$$\mathbf{T}_0^{m,\ell} \mathbf{T}_\ell^{m,1} - h_\ell^m h_{\ell-2}^m \mathbf{T}_0^{m,\ell-1} - h_0^m h_{\ell-1}^m \mathbf{T}_1^{m,\ell-1} = 2i^{Nm(\ell+1-p)} \left(\prod_{j=0}^{\ell} h_j^m \right) \mathbf{J}^m, \quad (\text{F.80})$$

where \mathbf{J}^m is a u -independent tangle and h_j^m is defined in (1.16).

OUTLINE OF THE PROOF: For $m > 1$, the generalisation turns out to be straightforward albeit tedious. Following the discussion in Section 5, it suffices to prove (F.80) with \mathbf{T} replaced by $\bar{\mathbf{T}}$, see (5.3). As tangles, $\bar{\mathbf{T}}_0^{m,n}, \bar{\mathbf{T}}_0^{1,n} \in \mathcal{EPTL}_{Nm}(\alpha, \beta)$ are very similar, with the difference that rows of face operators in $\bar{\mathbf{T}}_0^{m,n}$ have spectral parameters shifted by an integer multiple of λ and appear as



for some $i \in \{0, \dots, m-1\}$. The steps in the proof of Proposition F.4 are then repeated: Summing over configurations of a single column of face operators produces a recursion relation relating adapted versions of \mathbf{U}_r , \mathbf{V}_r and \mathbf{W}_r , eventually leading to (F.80).

References

- [1] P.A. Pearce, J. Rasmussen, J.-B. Zuber, *Logarithmic minimal models*, J. Stat. Mech. (2006) P11017, arXiv:hep-th/0607232.
- [2] H.N.V. Temperley, E.H. Lieb, *Relations between the ‘percolation’ and ‘colouring’ problem and other graph-theoretical problems associated with regular planar lattices: Some exact results for the ‘percolation’ problem*, Proc. Roy. Soc. **A322** (1971) 251–280.
- [3] V.F.R. Jones, *Planar algebras I*, arXiv:math.QA/9909027.

- [4] P.A. Pearce, J. Rasmussen, *Solvable critical dense polymers*, J. Stat. Mech. (2007) P02015, arXiv:hep-th/0610273.
- [5] P.A. Pearce, J. Rasmussen, S.P. Villani, *Solvable critical dense polymers on the cylinder*, J. Stat. Mech. (2010) P02010, arXiv:0910:4444 [hep-th].
- [6] P.A. Pearce, J. Rasmussen, S. Villani, *Infinitely extended Kac table of solvable critical dense polymers*, J. Phys. A: Math. Theor. **46** (2013) 175202, arXiv:1210.8301 [math-ph].
- [7] A. Morin-Duchesne, P.A. Pearce, J. Rasmussen, *Modular invariant partition function of critical dense polymers*, Nucl. Phys. **B874** (2013) 312–357, arXiv:1303.4895 [hep-th].
- [8] S.R. Broadbent, J.M. Hammersley, *Percolation processes I. Crystals and mazes*, Proc. Camb. Phil. Soc. **53** (1957) 629–641.
- [9] A.A. Belavin, A.M. Polyakov, A.B. Zamolodchikov, *Infinite conformal symmetry in two-dimensional quantum field theory*, Nucl. Phys. **B241** (1984) 333–380.
- [10] A. Gainutdinov, D. Ridout, I. Runkel (Guest Editors), *Special issue on logarithmic conformal field theory*, J. Phys. A: Math. Theor. **46** (2013) Number 49.
- [11] G.E. Andrews, R.J. Baxter, P.J. Forrester, *Eight-vertex SOS model and generalized Rogers-Ramanujan-type identities*, J. Stat. Phys. **35** (1984) 193–266.
- [12] P.J. Forrester, R.J. Baxter, *Further exact solutions of the eight-vertex SOS model and generalizations of the Rogers-Ramanujan identities*, J. Stat. Phys. **38** (1985) 435–472.
- [13] V.V. Bazhanov, N. Reshetikhin, *Critical RSOS models and conformal field theory*, Int. J. Mod. Phys. **A4** (1989) 115–142.
- [14] P.A. Pearce, A. Klümper, *Finite-size corrections and scaling dimensions of solvable lattice models: An analytic method*, Phys. Rev. Lett. **66** (1991) 974–977.
- [15] A. Klümper, P.A. Pearce, *Analytic calculation of scaling dimensions: Tricritical hard squares and critical hard hexagons*, J. Stat. Phys. **64** (1991) 13–76.
- [16] A. Klümper, P.A. Pearce, *Conformal weights of RSOS lattice models and their fusion hierarchies*, Physica A **183** (1992) 304–350.
- [17] R.J. Baxter, *The inversion relation method for some two-dimensional exactly solved models in lattice statistics*, J. Stat. Phys. **28** (1982) 1–41.
- [18] D.L. O’Brien, P.A. Pearce, R.E. Behrend, *Surface free energies and surface critical behavior of the ABF models with fixed boundaries*, in Statistical Models, Yang-Baxter Equation and Related Topics, Tianjin, China (1996), arXiv:cond-mat/9511081.
- [19] D.L. O’Brien, P.A. Pearce, *Surface free energies, interfacial tensions and correlation lengths of the ABF models*, J. Phys. A: Math. Gen. **30** (1997) 2353–2366.
- [20] I. Krichever, O. Lipan, P. Wiegmann, A. Zabrodin, *Quantum integrable models and discrete classical Hirota equations*, Commun. Math. Phys. **188** (1997) 267–304, arXiv:hep-th/9604080.
- [21] A.B. Zamolodchikov, *On the thermodynamic Bethe ansatz equations for reflection less ADE scattering theories*, Phys. Lett. **B253** (1991) 391–394.
- [22] A.B. Zamolodchikov, *Thermodynamic Bethe ansatz for RSOS scattering theories*, Nucl. Phys. **B358** (1991) 497–523.

- [23] A. Kuniba, T. Nakanishi, J. Suzuki, *Functional relations in solvable lattice models I: functional relations and representation theory*, Int. J. Mod. Phys. **A9** (1994) 5215–5266, arXiv:hep-th/9309137.
- [24] A. Kuniba, T. Nakanishi, J. Suzuki, *Functional relations in solvable lattice models II*, Int. J. Mod. Phys. **A9** (1994) 5267–5312, arXiv:hep-th/9310060.
- [25] A. Kuniba, T. Nakanishi, *Spectra in conformal field theories from the Rogers dilogarithm*, Mod. Phys. Lett. **A7** (1992) 3487–3494, arXiv:hep-th/9206034.
- [26] F. Ravanini, R. Tateo, A. Valleriani, *Dynkin TBA's*, Int. J. Mod. Phys. **A8** (1993) 1707–1728, arXiv:hep-th/9207040.
- [27] A. Kuniba, T. Nakanishi, J. Suzuki, *T-systems and Y-systems in integrable systems*, J. Phys. A: Math. Theor. **44** (2011) 103001, arXiv:1010.1344 [hep-th].
- [28] C.H.O. Chui, C. Mercat, P.A. Pearce, *Integrable boundaries and universal TBA functional equations*, Prog. Math. Phys. **23** (2002) 391–413, arXiv:hep-th/0108037.
- [29] R.E. Behrend, P.A. Pearce, D.L. O'Brien, *Interaction-round-a-face models with fixed boundary conditions: the ABF fusion hierarchy*, J. Stat. Phys. **84** (1996) 1–48, arXiv:hep-th/9507118.
- [30] D.L. O'Brien, P.A. Pearce, S.O. Warnaar, *Analytic calculation of conformal partition functions: Tricritical hard squares with fixed boundary conditions*, Nucl. Phys. **B501** (1997) 773–799.
- [31] P. Goddard, A. Kent, D. Olive, *Virasoro algebras and coset space models*, Phys. Lett. **B152** (1985) 88–92.
- [32] P. Goddard, A. Kent, D. Olive, *Unitary representations of the Virasoro and super-Virasoro algebras*, Commun. Math. Phys. **103** (1986) 105–119.
- [33] C. Ahn, S.-W. Chung, S.-H. Tye, *New parafermion, SU(2) coset and N = 2 superconformal field theories*, Nucl. Phys. **B365** (1991) 191–240.
- [34] P.A. Pearce, J. Rasmussen, *Coset construction of logarithmic minimal models: branching rules and branching functions*, J. Phys. A: Math. Theor. **46** (2013) 355402, arXiv:1305.7304 [hep-th].
- [35] P.A. Pearce, J. Rasmussen, E. Tartaglia, *Logarithmic superconformal minimal models*, arXiv:1312.6763 [hep-th].
- [36] J. Rasmussen, *Logarithmic limits of minimal models*, Nucl. Phys. **B701** (2004) 516–528, arXiv:hep-th/0405257.
- [37] J. Rasmussen, *Jordan cells in logarithmic limits of conformal field theories*, Int. J. Mod. Phys. **A22** (2007) 67–82, arXiv:hep-th/0406110.
- [38] J.H. Conway, *An enumeration of knots and links and some of their algebraic properties*, in Computational Problems in Abstract Algebra, J. Leech (Ed.), Pergamon Press (1970) 329–358.
- [39] L.H. Kauffman, S. Lins, *Temperley-Lieb recoupling theory and invariant 3-manifolds*, Princeton University Press (1994).
- [40] P.A. Pearce, *Row transfer matrix functional equations for A-D-E lattice models*, Int. J. Mod. Phys. **A7** Suppl. 1B (1992) 791–804.
- [41] P.A. Pearce, K.A. Seaton, *Solvable hierarchy of cyclic solid-on-solid lattice models*, Phys. Rev. Lett. **60** (1988) 1347–1350.

- [42] A. Kuniba, T. Yajima, *Local state probabilities for solvable restricted solid-on-solid models A_n , D_n , $D_n^{(1)}$ and $A_n^{(1)}$* , J. Stat. Phys. **52** (1988) 829–883.
- [43] P.A. Pearce, K.A. Seaton, *Exact solution of cyclic solid-on-solid lattice models*, Ann. Phys. **193** (1989) 326–366.
- [44] P. Fendley, N. Read, *Exact S -matrices for supersymmetric sigma models and the Potts model*, J. Phys. A: Math. Gen. **35** (2002) 10675–10704, arXiv:hep-th/0207176.
- [45] P. Zinn-Justin, *Combinatorial point for fused loop models*, Commun. Math. Phys. **272** (2007) 661–682, arXiv:math-ph/0603018.
- [46] P. Martin, H. Saleur, *On an algebraic approach to higher dimensional statistical mechanics*, Commun. Math. Phys. **158** (1993) 155–190, arXiv:hep-th/9208061.
- [47] J.J. Graham, G.I. Lehrer, *The representation theory of affine Temperley-Lieb algebras*, Enseign. Math. **44** (1998) 173–218.
- [48] R.M. Green, *On representations of affine Temperley-Lieb algebras*, CMS Conf. Proc. **24** (1998) 245–261.
- [49] K. Erdmann, R.M. Green, *On representations of affine Temperley-Lieb algebras, II*, Pac. J. Math. **191** (1999) 243–274, arXiv:math/9811017.
- [50] P.P. Martin, *Potts models and related problems in statistical mechanics*, Ser. Adv. Stat. Mech. **5**, World Scientific, Singapore (1991).
- [51] D. Ridout, Y. Saint-Aubin, *Standard modules, induction and the Temperley-Lieb algebra*, arXiv:1204.4505 [math-ph].
- [52] R.J. Baxter, *Exactly solved models in statistical mechanics*, Academic Press, London (1982).
- [53] V.F.R. Jones, *Index of subfactors*, Invent. Math. **72** (1983) 1–25.
- [54] H. Wenzl, *Hecke algebras of type A_n and subfactors*, Invent. Math. **92** (1988) 349–384.
- [55] P.A. Pearce, J. Rasmussen, P. Ruelle, *Integrable boundary conditions and \mathcal{W} -extended fusion in the logarithmic minimal models $\mathcal{LM}(1, p)$* , J. Phys. A: Math. Theor. **41** (2008) 295201, arXiv:0803.0785 [hep-th],
- [56] J. Rasmussen, *Classification of Kac representations in the logarithmic minimal models $\mathcal{LM}(1, p)$* , Nucl. Phys. **B853** (2011) 404–435, arXiv:1012.5190 [hep-th].
- [57] A. Morin-Duchesne, Y. Saint-Aubin, *The Jordan structure of two dimensional loop models*, J. Stat. Mech. (2011) P04007, arXiv:1101.2885 [math-ph].
- [58] A. Morin-Duchesne, Y. Saint-Aubin, *Jordan cells of periodic loop models*, J. Phys. A: Math. Theor. **46** (2013) 494013, arXiv:1302.5483 [math-ph].
- [59] P.A. Pearce, J. Rasmussen, *Coset graphs in bulk and boundary logarithmic minimal models*, Nucl. Phys. **B846** (2011) 616–649, arXiv:1010.5328 [hep-th].
- [60] P.A. Pearce, K.A. Seaton, *Off-critical logarithmic minimal models*, J. Stat. Mech. (2012) P09014, arXiv:1207.0259 [hep-th].